ENERGY UTILIZATION FROM DISPOSED BRINE OF DESALINATION PLANTS USING PRESSURE RETARDED OSMOSIS

BY

WAQAS AKRAM

A Thesis Presented to the
DEANSHIP OF GRADUATE STUDIES

KING FAHD UNIVERSITY OF PETROLEUM & MINERALS

DHAHRAN, SAUDI ARABIA

In Partial Fulfillment of the
Requirements for the Degree of

MASTER OF SCIENCE

In

Mechanical Engineering

MAY, 2014

KING FAHD UNIVERSITY OF PETROLEUM & MINERALS
DHAHRAN, SAUDI ARABIA

DEANSHIP OF GRADUATE STUDIES

This thesis, written by **Waqas Akram** under the direction of his thesis advisor and approved by his thesis committee, has been presented to and accepted by the Dean of Graduate Studies, in partial fulfillment of the requirements for the degree of **MASTER OF SCIENCE** in **MECHANICAL ENGINEERING**.

Thesis Committee

Thesis Advisor
Dr. Mostafa H. Sharqawy

Member
Dr. Syed M. Zubair

Department Chairman
Dr. Zuhair M. Gasem

Member
Dr. Mohamed A. Antar

Dean of Graduate Studies
Dr. Salam A. Zummo

21/5/15
Date

Dedicated to my parents, my brothers, my sister and my teachers

ACKNOWLEDGEMENTS

I begin with the name of Allah, the most Beneficent, the most Merciful. May Allah bestow peace on our beloved Prophet Mohammed (*peace and blessings of Allah be upon him*), and his family. First and the foremost, I am grateful to Allah (*subhanahu wa-ta'ala*) that by His grace and bounty, I am able to write my thesis and indeed without His help; I would not have been able to complete this work. I ask sincerity in all my deeds from Allah (*subhanahu wa-ta'ala*) and I quote the following verse of the Holy Quran:

"Say, my prayer, my offering, my life and my death are for Allah, the Lord of all the world" (Surat Al-'An'am, verse 162)

I would like to express deepest gratitude to my family, and especially to my parents. Their persistent prayers and constant support have always given me the strength to accomplish goals throughout my life. No words can express my gratitude to them, but I pray to Allah to bless them and reward them.

Acknowledgements are due to *King Fahd University of Petroleum and Minerals* which gave me the opportunity to pursue a graduate degree and also for all the support I received in carrying out this research. I am also grateful to the *Center for Clean Water and Clean Energy* at *KFUPM* (Project # R13-CW-10) and *MIT* for its support during this research.

Special appreciation goes to my mentor, Dr. Mostafa H. Sharqawy for teaching me the way of research, his keen support whenever I needed assistance, his patience over my shortcomings and his constant encouragement. I would like to thank my committee members, Dr. Syed M. Zubair and Dr. Mohamed A. Antar for their useful discussions and involvement during the development of this work.

I sincerely thank my seniors Muhammad Usama Siddiqui and Dr. Bilal Qureshi for all the help they provided through the course of this work. Not forgotten, special thanks to Osama Hasan, Amir Hamza and Osman Kaleem for their immense dedication whenever I needed them. Last but not the least, I am very grateful to all my colleagues in the Mechanical Engineering department for making my time in ME graduate room memorable.

TABLE OF CONTENTS

LIST OF TABLES

LIST OF FIGURES

ABSTRACT (ENGLISH)

NAME:	Waqas Akram
TITLE:	Energy Utilization from Disposed Brine of Desalination Plants Using Pressure Retarded Osmosis
MAJOR FIELD:	MECHANICAL ENGINEERING
DATE OF DEGREE:	MAY 2014

Desalination plants discharge brine which is at higher salinity than the feed water. Diluting this brine by mixing it with the feed water will reduce the environmental hazards associated with the high salt concentration of the disposed brine. In addition, energy can be generated if the diluting process is performed in a reversible manner. Pressure retarded osmosis (PRO) is a process in which water permeates through a semi permeable membrane from the low hydrostatic pressure stream (feed solution) to the higher hydrostatic pressure stream (draw solution) due to the osmotic pressure difference. This increases the volume flow rate of the pressurized draw stream and energy is obtained by depressurizing the draw stream through a hydro turbine. In the present work, PRO process is used as an energy recovery device (ERD) for MSF and RO desalination plants. A steady state model is developed for MSF process to perform energy and exergy analyses. The energy analysis evaluates the performance of the desalination plant and determines the streams of mass and energy while the exergy analysis reveals the components that are responsible for greatest losses. A steady state, 2-D, computational

model is developed for PRO process using the solution diffusion and Fick's diffusion models. Parallel- and counter-flow PRO configurations are investigated under different operating conditions with and without the effect of concentration polarization. It is found that the maximum power produced from the rejected brine (salinity 70 g/kg) of MSF desalination plant when mixing with a feed water (salinity 46.5 g/kg) is 0.017 kWh/m^3. On the other hand, the maximum power produced from the rejected brine (salinity 64 g/kg) of RO desalination plant when mixing with a feed water (salinity 45 g/kg) is 0.022 kWh/m^3. These amounts of the generated energy from the rejected brine are very small when compared with the pumping power required which doesn't make it feasible. Therefore it is not recommended to use PRO process to recover energy from the rejected brine of desalination plants. However, it was found that there is a high potential of energy generation if the brine is mixed with waste water (salinity of 5 g/kg) which suggests that waste water plants should be built near to desalination plants to utilize this option. On the other hand, novel PRO multi-stage and multi-pass configurations are proposed for increasing the power output. As compared with single stage PRO system, a 4% more power is obtained using multi-stage PRO system and an increase of 132% is achieved using multi-pass PRO system.

ABSTRACT (ARABIC)

ملخص الرسالة

الاسم: وقاص اكرم

عنوان الرسالة: انتاج الطاقة من المحلول الملحي المراد التخلص منه في محطة تحلية المياه باستخدام تقنية ضغط التناضح العكسي

التخصص العام : الهندسة الميكانيكية

تأريخ التخرج: 1435 هـ - (مايو 2014 م)

ينتج عن محطات تحلية مياه البحر محلول ملحي والذي يعتبر تركيزه اعلى من مياه البحر المغذية لهذه المحطات. ان تمييع هذا المحلول الملحي عن طريق خلطها مع مياه البحر ذات التركيز الملحي الأقل سوف تقلل من المخاطر البيئية فيما لو تم التخلص من المحلول الملحي ذو التركيز الملحي العالي مباشرة دون خلطه. ومن الجدير بالذكر انه يمكن توليد الطاقة من عملية التمييع هذه إذا تم تنفيذها بطريقة انعكاسية. ان الهدف من هذه الرسالة تحقيق الاستفادة من نظام ضغط التناضح العكسي (بي ار او) والذي يمكن استخدامه كجهاز استعادة الطاقة المهدره في محطات التحلية. في الجزء الأول من هذه الرسالة، تم تطوير نموذج تحليلي مفصل لنظام تحلية المياه متعدد المراحل (ام اس اف) ودراسه محطة تحلية الجبيل (ام اس اف) للتعرف على المكونات المسؤولة عن أكبر خسارة في النظام. في الجزء الثاني من العمل، تم تطوير نموذج تحليلي مفصل لنظام (بي ار او) للتحقيق في إمكانية إنتاج الطاقة باستخدام مجموعة مختلفة من تكوينات (بي ار او). كما تم استخدام نموذج (بي ار او) أيضا لتحليل (بي ار او) كجهاز استعادة الطاقة لمحطات تحلية المياه (بي ار) و (ام اس اف). صافي كمية الطاقة المنتجة هي 9 كيلو واط وذلك في حالة محطات تحلية المياه (ار او)، بينما تنتج محطة تحلية المياه (ام اس اف) مقدار أقل بكثير مقارنة بمقدار الطاقة

المطلوبة للضخ. ولهذا تم اقتراح عدم استعمال (بي ار او) كَ (أي ار دي) في محطات تحلية المياه (ام اس اف). علاوة على ذلك، تم استخدام مغذيات مختلفة وبيانات التراكيز وذلك لتقدير الإنتاجية المحتملة من الطاقة باستخدام نظام (بي ار او). أقصى طاقة محتملة يمكن الوصول اليها باستخدام مياه البحر المالحة مع المياه العذبة. تم لاقتراح ترتيبات جديدة لل (بي ار او) متعدد المراحل ومتعدد السريان وذلك للحصول على أقصى إنتاجية للطاقة. عندما تمت مقارنة نظام (بي ار او) مفرد المرحلة، وجد أن هنالك زيادة بمقدار 4% في الطاقة الناتجة عند استخدام نظام (بي ار او) متعدد المراحل، وأيضا هنالك زيادة بنسبة 132% في الطاقة المنتجة عند استخدام نظام (بي ار او) متعدد السريان. وعلاوة على ذلك، التصاميم المعدلة، ومتعددة المراحل، ومتعددة التمرير-بي ار او تم اقتراحها للحصول على اقصى انتاجية للطاقة.

CHAPTER 1

INTRODUCTION

Global water demand continues to increase while fresh water sources are unchanging and becoming scarcer due to population growth and economic development. In 2010, 25% of the world population lived in areas under severe water crisis and this percentage is expected to increase to 55 % by the year of 2050 [1]. Yet water is the most abundant element on the earth. Three fourth of the total earth's surface is covered by water but only few percent of that is suitable for human use. Less than one percent is fresh water accessible for human use in the form of groundwater, rivers, and lakes, but most of the fresh water is in the form of glaciers. About 97% of the water is in oceans which contain high proportions of salts. In order to convert saline water into fresh water useful for drinking or agriculture, desalination technologies are being employed. Desalination is a process for producing fresh water from saline water.

One of the first references to the desalination was by Greek philosopher Aristotle who wrote about seawater desalination in 320 BC. Since then scientists and researchers are experimenting with many techniques in quest for new sources of fresh water. By the

midst of twentieth century, commercial desalination plants began to be installed in various part of the world, most of these installation were thermal desalination.

There are about 17,000 desalination plants worldwide with global daily capacity of 78.8 million m^3/day [2]. Figure 1.1 represents the global cumulative installed desalination plants during the last two decades (1994 to 2013). As shown in the figure, the number of installed desalination plants has been almost doubled in the last two decades. The representation of the global cumulative installed capacity for the last twenty years is shown in Figure 1.2. It can be seen that the global installed capacity has been increased four times from 1994 to 2013.

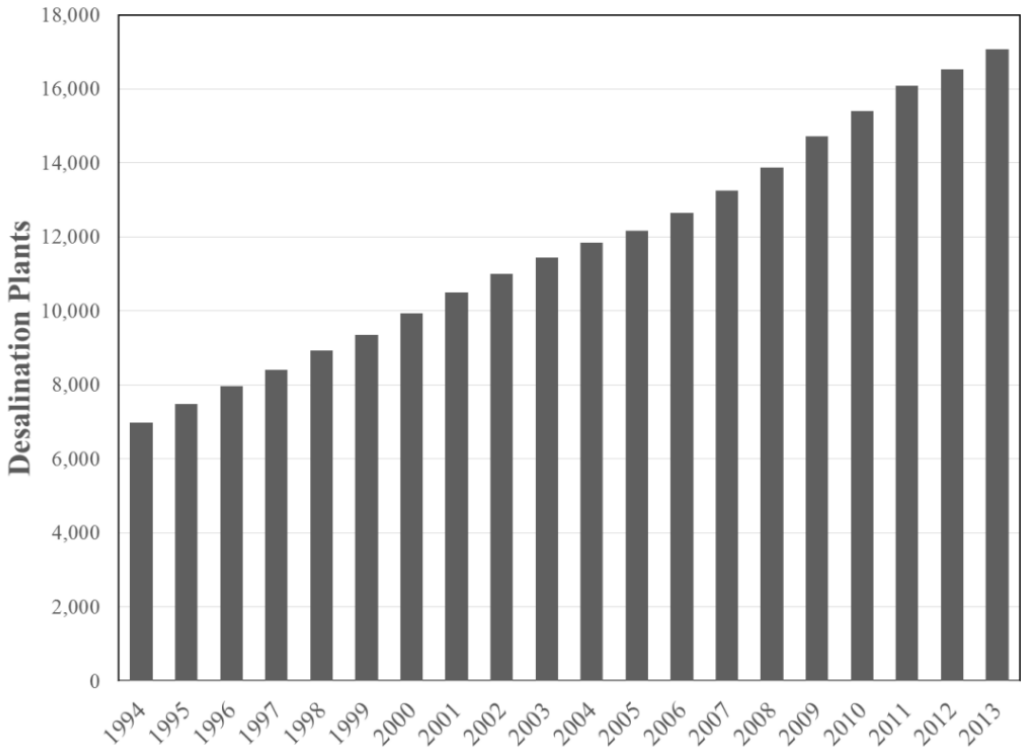

Figure 1.1: Global cumulative installed number of desalination plants (data from [2])

The Middle East and North Africa (MENA) is the largest desalination market in the world which constitutes more than 48% of the total desalinated water [2]. Saudi Arabia is leading the worldwide production for desalinated water with a share of 33% of the installed capacity in MENA region and 16% of the global installed capacity. The desalination production capacity of Saudi Arabia has been doubled since the year 2000. Currently, the total desalinated water in Saudi Arabia is about 12.7 million m^3/day [2]. Figure 1.3 represents the increase in installed capacity in Saudi Arabia for the period of 2000 to 2013.

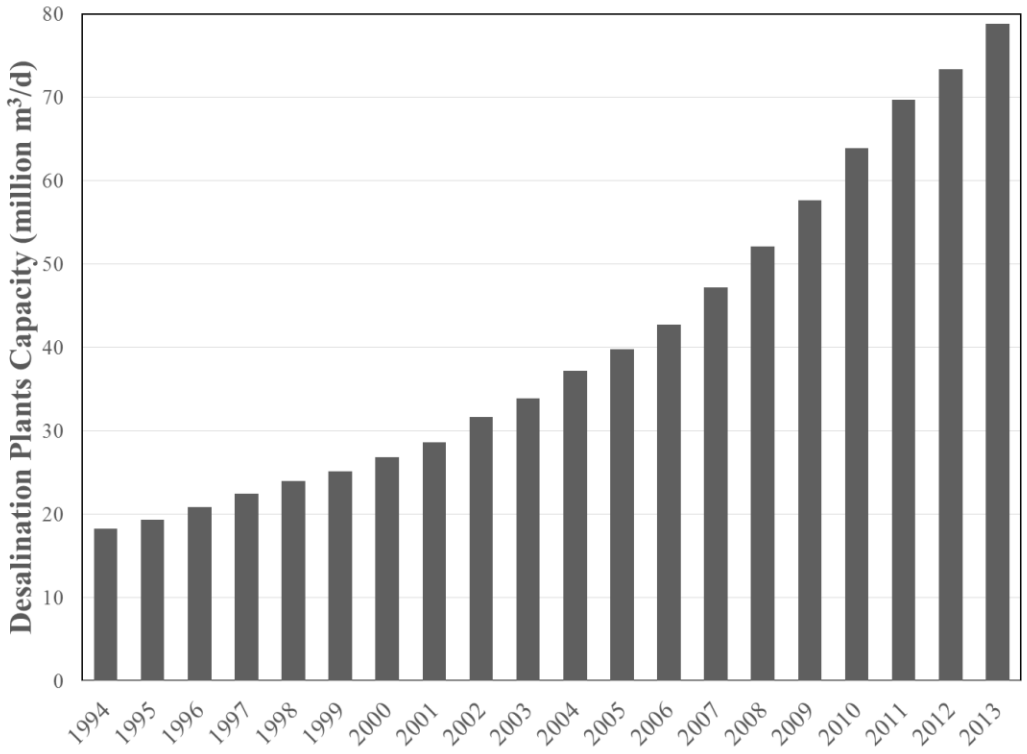

Figure 1.2: Global cumulative installed desalination capacity (data from [2])

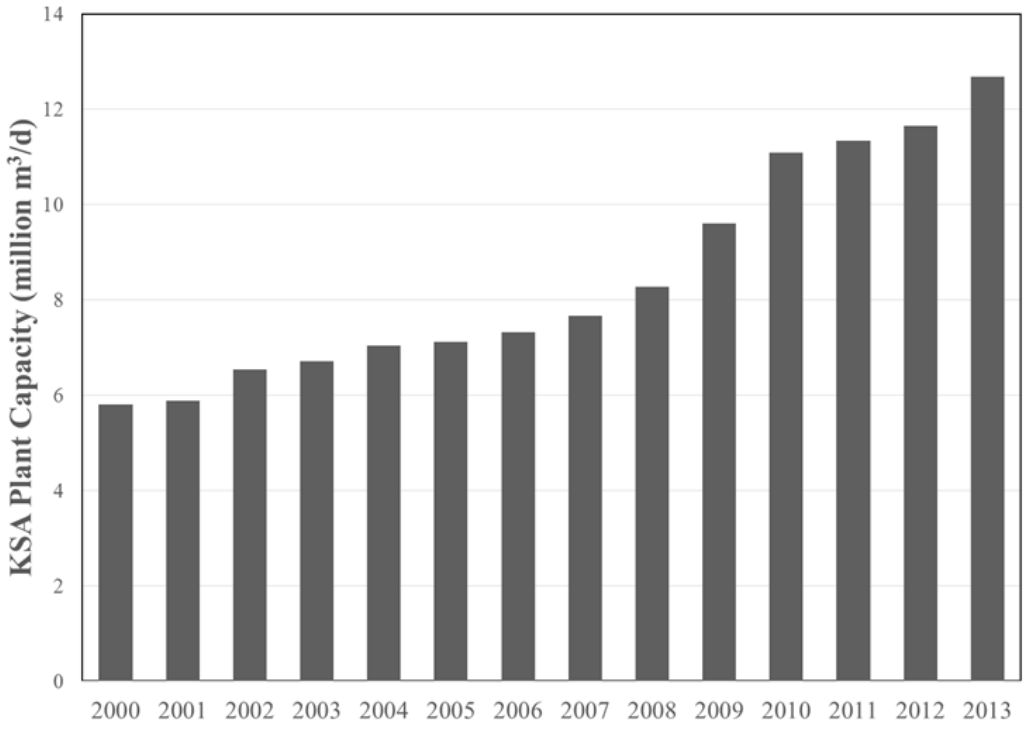

Figure 1.3: Cumulative installed desalination capacity in Kingdom of Saudi Arabia (data from [2])

The major desalination plants employed either membrane and/or thermal desalination processes. Reverse osmosis, the prominent membrane process, accounts for sixty three percent (63%) of the total world installed capacity. The thermal desalination technologies such as multistage flash (MSF) accounts for 23%, and multi effect distillation (MED) has a share of 8% in total installed capacity in the world. Figure 1.4 shows the share of desalination technologies in total worldwide installed capacity.

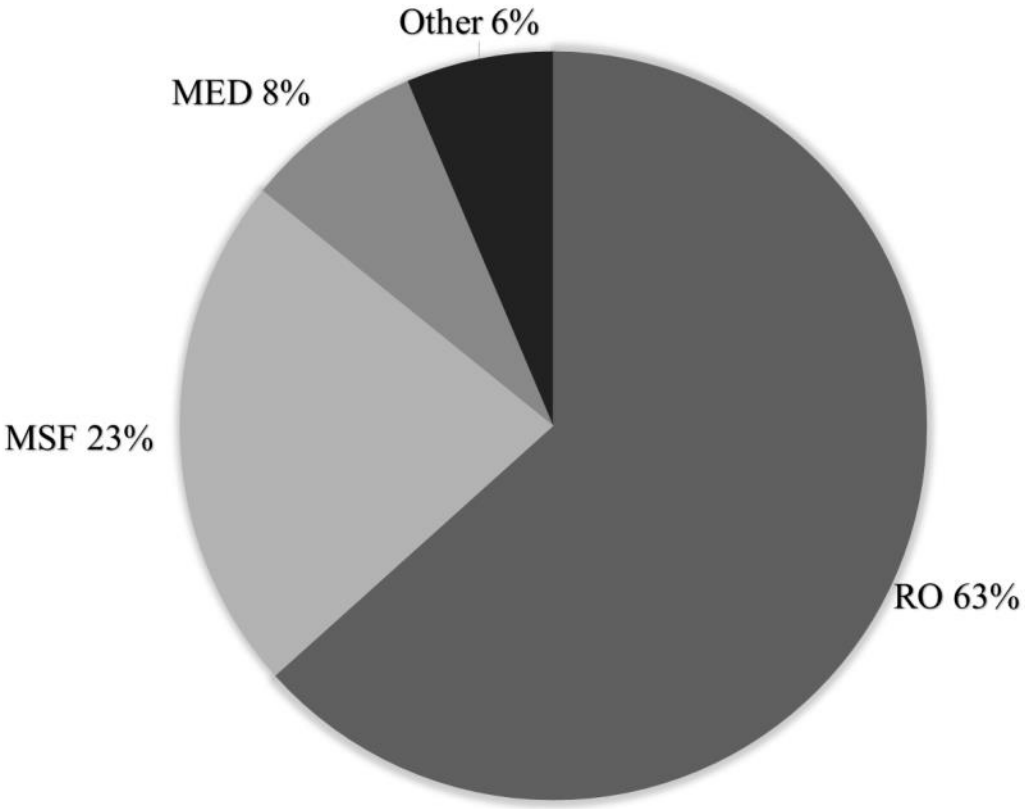

Figure 1.4: Total worldwide installed desalination capacity by technology (data from [2])

Figure 1.5 shows the cumulative installed membrane and thermal capacity over the period of last two decades, the currently installed membrane capacity is 49.9 million m^3/day while thermal desalination plants produced 23.8 million m^3/day of desalinated water [2]. Figure 1.6 represents the annual new installed capacity of different technologies for the period of twenty years, with the reverse osmosis leading overall.

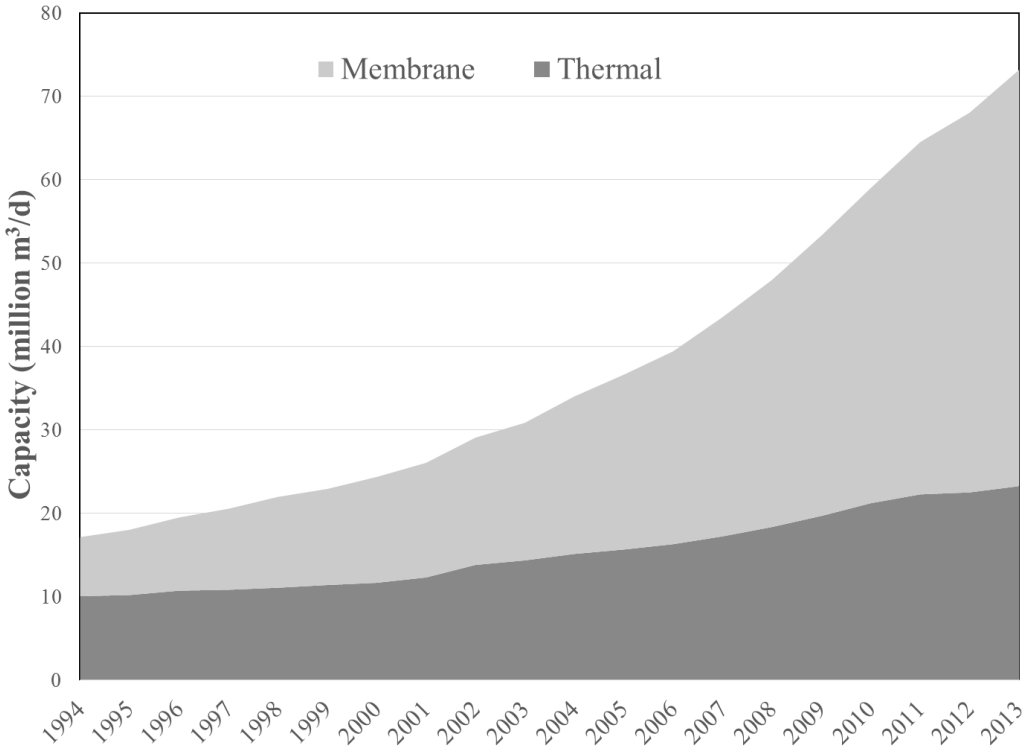

Figure 1.5: Global cumulative installed membrane and thermal capacity (data from [2])

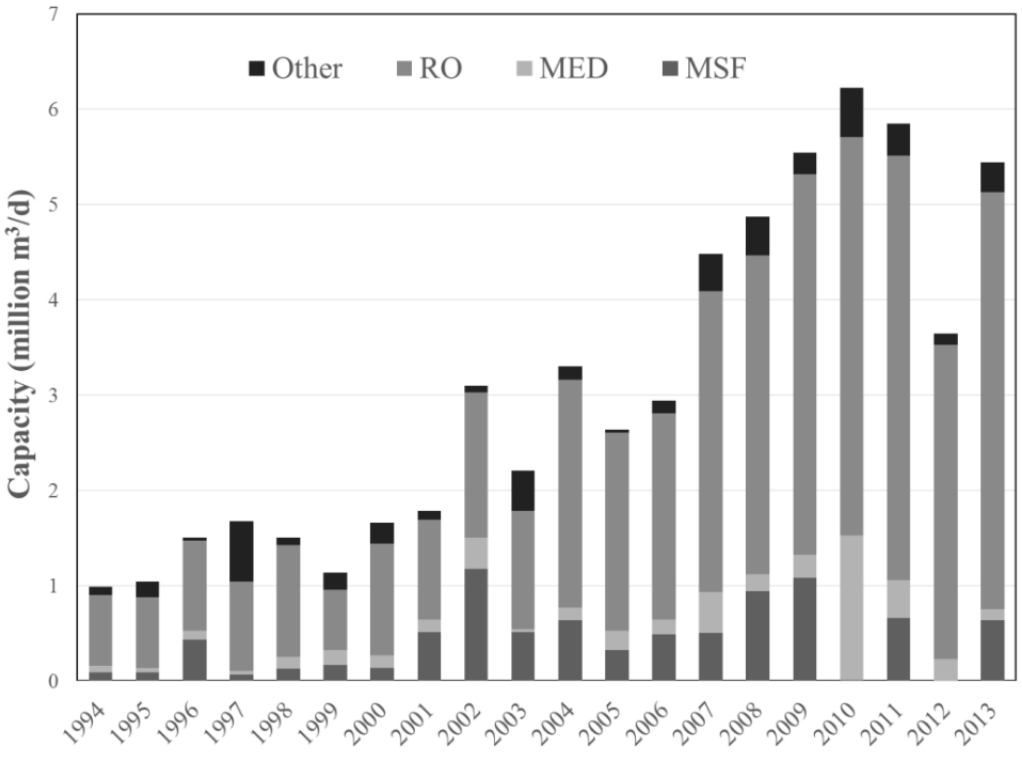

Figure 1.6: Annual installed capacity by technology (data from [2])

Thermal desalination has been extensively used for large scale production of fresh water. Over the years the thermal desalination capacity is decreasing but it still has a major share due to large presences in Middle East and North Africa (MENA) region. About thirty percent (30%) of the global water production is produced by thermal desalination processes while this percentage reaching 52% in MENA region. Multistage flash desalination (MSF) is still the dominating technology within thermal desalination processes. The MSF process accounts more than 80% percent within thermal desalination plant in MENA and Saudi Arabia, while in the entire desalination industry its contribution in producing fresh water is about 23% [2].

Figure 1.7 represents the percentage installed capacity in Saudi Arabia, with the major share of reverse osmosis (49%), whereas the multistage flash (MSF) accounts for 38 % and about ten percent (10%) is produced by multi effect distillation (MED).

The Saudi Arabia obtains 70% of its drinking water supply from desalination plants. The largest capacity MSF plant is in Shoaiba, Saudi Arabia with a water capacity of 880,300 m^3/day which started production in 2009. Currently, the world largest hybrid (MSF-RO) desalination plant is being built in Ras Al-khair, Saudi Arabia with a water capacity of 1,025,000 m^3/day [2].

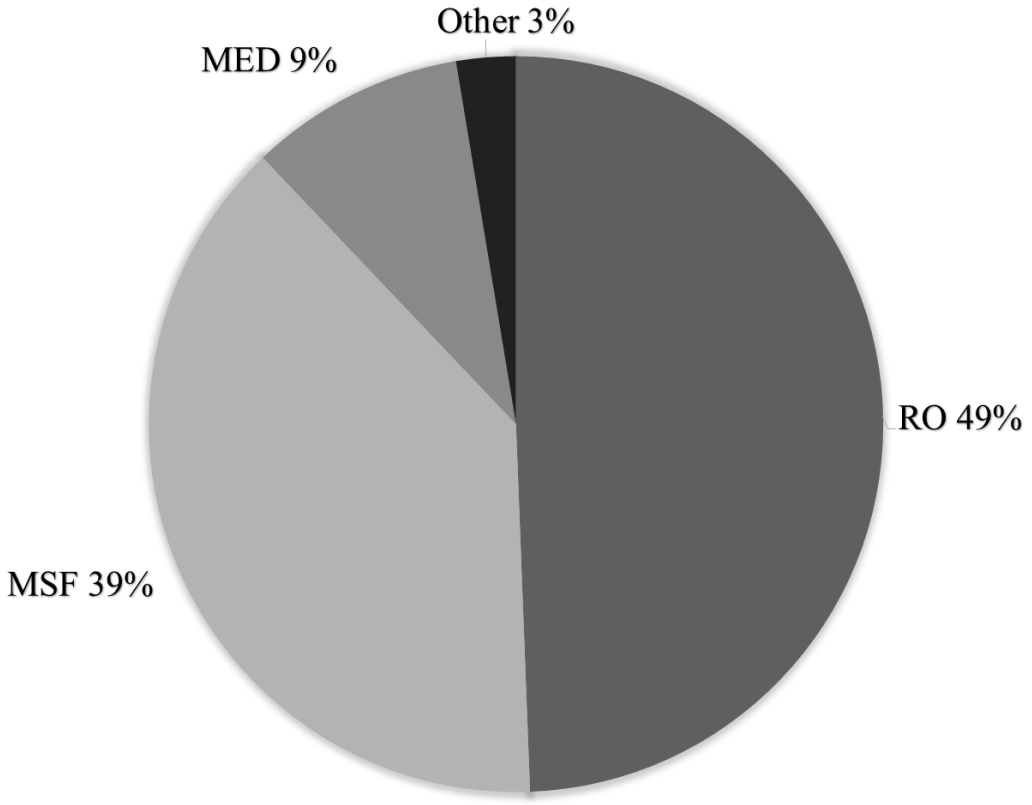

Figure 1.7: Saudi Arabia's installed desalination capacity by technology (data from [2])

Desalination technologies require significant amount of energy, membrane desalination processes requires only electrical energy while the thermal desalination processes require both thermal and electrical energy. Membrane desalination technologies consume 3 to 5 kWh per m^3 of desalinated water and no thermal energy is needed, while the thermal desalination plants consume about 80 kWh/m^3 of thermal energy and 2.5-3.5 kWh/m^3 of electrical energy [3]. The total energy demand of desalination approximately 75.2 TWh/ year [4], while in the MENA region the annual electricity demand for desalination is expected to rise to 122 TWh by the year 2030, almost three times from the energy requirement in the year 2007 [5].

Despite many benefits of the desalination technologies, there are some concerns rises over its potential harmful effect on the environment. Key issues are the brine and chemicals rejection, the thermal energy dissipation with the brine, and the emissions of greenhouse gases. All desalination plants reject brine which is at a higher salinity and higher temperature than the supplied feed water. This brine is usually discharged back to the feed water source. The rejected brine discharged to the sea has the ability to change the concentration, alkalinity and the temperature of the seawater and could results in long-term changes in species compositions and abundance in the discharge site. One of the major economic and environmental challenge to the desalination industry is the handling of the rejected brine. It is estimated that, for every 1 m^3 of desalinated water, an equivalent amount is generated as reject brine. The cost of brine disposal ranges from 5% to 33% of the total cost of desalination, while for the disposal cost of inland desalination plant is higher than the plants disposing brine into the sea [6–8]

Energy has always been an important issue all over the world. Global energy demand is increasing rapidly due to the global population growth and industrialization. Recent studies predict that the global energy consumption is expected to rise about 56% from 5.52×10^{11} MJ to 8.65×10^{11} MJ between 2010 and 2040 [9,10]. The necessity of environmentally sustainability has shifted the global trend of power generation from the fossil fuels to the renewable green energy.

Among many renewable energy sources, the osmotic power has a high potential and receiving remarkable attention recently. Osmotic energy is the energy generated when waters with different salt concentration are mixed together. The concept of harvesting the energy generated from mixing two water of different salinities was first reported by Pattle [11]. The estimation of global energy potential from all renewable energy sources is 10,000 TWh/year whereas the estimated potential of global energy from osmotic power is about 1,700 TWh/year [12].

Different methods have been proposed to generate energy by mixing two streams of different salt concentration, including pressure retarded osmosis (PRO), reverse electro dialysis (RED), vapor compression, and hydrocratic generation. The concept of pressure retarded osmosis process was first purposed by Sidney Loeb in 1975 [13]. In pressure retarded osmosis, pure water permeates through a semi permeable membrane from the low hydrostatic pressure stream to the higher hydrostatic pressure stream due to the osmotic pressure difference. This increases the volume flow rate of the pressurized draw stream and energy is obtained by depressurizing the draw stream through a hydro turbine.

The energy produced using pressure retarded osmosis is clean and non–polluting as it does not produce any greenhouse gases and will also help in reducing dependency on fossil fuels. The PRO process can be used as an energy recovery device in desalination plants. The rejected brine from desalination plants can be used in PRO with the lower salinity stream to produce energy. Diluting this brine will reduce the environmental hazards and risk to marine life, associated with the discharged high salt concentration brine.

1.1 OBJECTIVES OF PRESENT WORK

The objective of this study is to investigate the utilization of the pressure retarded osmosis system as an energy recovery device in thermal and membrane desalination plants. The following details shows how this objective can be approached.

- Develop a detailed mathematical model for multistage flash (MSF) desalination process :
    - *Section 2.3 covers the detailed mathematical modeling required for energy and exergy analyses of multistage flash desalination plants.*
- Validate the MSF model using available data in literature
    - *Section 2.4.1 covers the model validation with the plant data of Jubail desalination plant* [14] *and with the case study reported in* [15].
- Perform an exergy analysis of MSF desalination plant.
    - *Section 2.4 covers the detailed exergy analysis of MSF desalination plant*
- Develop a mathematical model of pressure retarded osmosis (PRO)
    - *Section 3.3 covers the modeling of pressure retarded osmosis.*
- Validate the PRO model using experimental data reported in [16]
    - *Section 3.4.1 covers the validation of mathematical model with the experimental data reported in literature.*
- Investigate PRO as an energy recovery device (ERD) for MSF and RO desalination plants

- *Section 4.1 and 4.2 covers the analysis of PRO as an energy recovery device for MSF and RO desalination plants respectively*.

- Investigate the potential power production using PRO
  - *Section 4.3 covers the potential of power production using different combination of PRO configurations.*
- Investigate different designs of multistage PRO systems for maximizing power output.
  - *Chapter 5 covers the analyses of new designs proposed for PRO systems*

CHAPTER 2

MULTISTAGE FLASH DESALINATION

2.1 LITERATURE REVIEW

Modeling of thermal desalination technologies is important for improvement of the system design, process parameters, control and operation of the thermal plants. Several studies related to the modeling of multistage flash (MSF) desalination have been presented by researchers [15,17–24]. The governing equations of the mathematical model are based on mass balances, energy balances, and heat transfer equations.

Analysis of MSF process can be performed by simple or detailed mathematical models. The simple models, focused on obtaining closed form equations to quickly estimate the process parameters, i.e., performance ratio and heat transfer area. There are some correlations and short-cut techniques are summarized by Dessouky and Ettouney [15] which can be used to provide quick estimates of system characteristics of MSF plant. Mutaz and Soliman [25] presented a simple steady state method for MSF desalination plant. Instead of solving mass and energy balances for all stages, they selected few stages and performed calculations for quick estimation of the thermal performance.

Darwish [17] developed a simple mathematical model to determine various system characteristics of MSF desalination plant including brine circulation flow rate, the performance ratio and heat transfer area. The results from his analysis indicate that the circulation ratio decrease with the increase in flashing range and performance ratio increases with the increase of number of stages. The main drawback of simple models is their inability to capture or provide an accurate representation for entire performance of the system. Accordingly, the simple model must be used for only quick estimation of the MSF processes. Therefore, detailed analysis is required for accurate thermal calculations and feasible studies of MSF plants.

The detailed mathematical model takes into consideration the dependence of the thermophysical properties on temperature and salinity for various streams. The models solve iteratively the mass balances, mass salt balances, energy balances and heat transfer equations for each flashing stage of the MSF system. These also include correlations for evaluation for the physical properties, stage dimensions, thermodynamic losses and heat transfer coefficients.

Dessouky *et al*. [18] developed a detailed steady state mathematical model for the analysis of MSF process with brine circulation. The model assumes constant heat transfer area for all stages. It also incorporates the effect of temperature and concentration on the thermophysical properties of water and vapor, losses to the surroundings, the effect of fouling factors, and presence of non-condensable gases on the rate of heat transfer. The results obtained from the model were compared with six different MSF plants. They also investigated the effect of different operating conditions on the system performance

including performance ratio, specific heat transfer area (heat transfer area per unit water production), and specific cooling water flow rate (cooling water flow rate per unit water production).

Rosso *et al*. [19] developed a steady state mathematical model to analyze the MSF desalination process. This model is based on a detailed physiochemical representation of the process, and accounts for the geometry of the stages, the variation of physical properties of water with temperature and salinity, heat transfer and role of fouling. They investigated the effect of number of stages, steam temperature, and intake seawater temperature on the thermal performance of the MSF plant

Husain *et al*. [20] conducted a steady state and transient simulations for MSF plant using a commercial software SPEEDUP [26]. They developed a rigorous steady state model and solved it using FORTRAN based on the tridiagonal matrix formulation. They performed an analysis for MSF desalination plant with a water production capacity of 14,500 m^3/hr.

Baig *et al*. [21] analyzed a once through MSF desalination system using a detailed steady state mathematical model to investigate plant performance characteristics. They incorporated the fouling effect in the modeling and concluded that fouling has a significant effect in decreasing the overall heat transfer coefficient. In addition, they performed a sensitivity analysis of the system and found out that the brine inlet and outlet temperatures, number of stages, top brine temperature and fouling resistances are the

most influential parameters which affect the water production rate of the MSF desalination system.

ElMoudir *et al*. [22] pointed out the difficulties encountered while the developing process modeling of MSF plant, especially when the plant is old. They developed Excel spreadsheets for MSF process modeling and used them to determine the faulty operating conditions of an operating plant. They also emphasized that the fouling is an important factor in calculation of heat transfer area of the plant.

Khan [27] established a mathematical model by incorporating the thermal losses and considering a constant heat transfer area as a practical approach. These model equations were applicable to all stage to stage calculations. Shafaghat *et al*. [28] used a simple mathematical model to design an efficient MSF desalination plant supplied by a 42 MW power plant. The process model included mass and energy balances, heat transfer equations, physical properties correlations, and temperature losses due to the boiling point elevation. The designed MSF desalination plant has 24 flashing stages with constant heat transfer area and production capacity of 2480 m^3/day.

Jabbar *et al*. [23] analyzed the performance of large scale brine circulation MSF plant (50,000 to 75,000 m^3/d) by using a detailed mathematical model. The analysis focused on evaluation of weir loading, dimensions of tube bundles, demister length, stage dimensions, temperature, and flow rate profiles. Iterative procedure (Newton's method) was used to solve the model equations. These values were compared with ten different MSF plants located in the Middle East. The results indicated that the specific heat

transfer decreases with the increase of top brine temperature while it increases with the increase in production capacity, and top brine temperature has small effect of stage dimensions.

Darwish *et al*. [29] studied the major steps which the MSF process went through during its development over the period of four decades. In addition they presented the specific design features of modern MSF plant and investigated the effect of operating parameters on the system performance of MSF desalination plant.

Dessouky *et al*. [30] summarized the present and future developments of MSF processes. They compared the performances of different MSF configurations including once through, brine circulation, and brine mixing. They found that the performance ratio of MSF with brine mixing is higher than the other systems, but its performance is limited by maximum salinity value imposed. They stated that the seasonal variation of intake seawater temperature has almost no effect on MSF brine circulation.

Helal and Odeh [31] conducted a comparative study of MSF once through and MSF brine circulation to determine an optimal design where the total heat transfer area is minimum, and to check the possibility of adopting once through design over brine circulation for large scale desalination plants. They concluded that the once through design does not have a significant effect on the heat transfer area. However, it will require 70% more chemicals than the brine circulation MSF design for same operating conditions. In addition, they found that the once through design will only be favorable if the number of stages are 40 or more.

Hawaidi and Mujtaba [32] developed the detailed mathematical process model for MSF brine circulation to investigate the brine heater fouling variation effect, with different seawater temperature, on plant performance, brine streams flow rate, and steam flow rate for fixed fresh water output under fixed steam temperature. They performed the optimization of MSF plant and provided the optimized operating parameters. The results indicate that increasing the fouling by 90%, the overall heat transfer coefficient decreases and consequently lowers the top brine temperature which decrease the fresh water production by 5%.

Jawad and Ezzeghni [33] performed an optimization process of once through MSF plant. They used a similar mathematical model as earlier presented by Helal [34] with constraints of the existing plant and used a simple mixer to maintain the temperature on input feed water at 28 ^{0}C in all seasons. They modified Helal's model [34] by taking into account variations of average temperature due to boiling point elevation in winter. By using the mathematical model, optimal operating conditions were obtained for different water production capacities. In addition, optimum performance is ensured if the parameters are maintained. Their results show that the plant capacity can be increased by 10 % at inlet feed temperatures of 14 and 28 °C. The optimized plant performance is more or less unaffected by changing the plant productivity at constant feed water temperature, but a little decrease in the plant performance has occurred in winter period, which is attributed to the effect of boiling point elevation increase as a result of brine mixing. The higher capacities of 55 million gallon per day at 28 °C and 54.8 at 14 °C are achieved at TBT of 114 °C

Helal [34] used a mathematical model developed by Soliman [24] for steady state performance calculations of MSF by assuming constant heat transfer coefficient, boiling point elevation, and specific heat capacity of brine solution. He performed the uprating of three MSF desalination plants of Umm Al Nasr by maximizing the gained output ratio (GOR) which is achieved by increasing Top Brine Temperature and steam flow rate subject to all design and operation constraints. The maximum rated capacity achieved at top brine temperature of 113.6 °C which was 12% more than the targeted 8.5 million gallon per day. To make sure constant supply of 8.5mgd water excessive scale formation should not be permissible in the plant.

Marcovecchio *et al* [35] optimized a hybrid desalination plant including MSF and RO. They used the MSF model developed eariler by Helal [34] which included the geometric design of each stage, brine velocity on pre-heater, number of tubes in the preheater and total heat transfer coefficient as an optimization variable for the system.

It is important to mention that there are some assumptions were considered by most of the researchers which idealizes the whole process such as using an average temperature for thermophysical properties, and modeling the seawater properties as an ideal mixture of pure water and sodium chloride salt, which may lead to significant deviations in the analysis of thermal desalination systems. Therefore, it is necessary to use correct representation of seawater properties for accurate thermo-economic analysis of thermal desalination systems. Sharqawy *et al*. [36] provided the most updated correlations for seawater properties, including density, boiling point elevation, specific enthalpy etc. which include the variation of temperature and salinity of streams.

The increasing attention in energy conservation has resulted in increasing use of exergy analysis as a useful diagnostic tool in design, optimization and improvement of the thermal systems. Exergy analysis allocates the irreversibilities of the system and identifies components that are responsible for greatest losses in the system. Many researchers have performed exergy analysis of seawater desalination technologies including multi stage flash (MSF), multi effect distillation (MED), reverse osmosis (RO), mechanical and thermal vapor compression (MVC & TVC), and humidification and dehumidification (HDH) systems.

Kempton *et al*. [37] conducted a second law analysis of three desalination technologies: Multistage Flash (MSF), Multi effect distillation (MED) and Reverse osmosis (RO). The analysis performed was based on the published plant data from MSF and RO facilities and experimental data for MED. They concluded that the RO is most exergetic efficient (30.1%) followed by MED (14.27%) while the MSF has exergy efficiency of 7.73%.

Mistry *et al*. [38] conducted second law analysis for different desalination technologies including MED, MSF, RO, and Humidification-Dehumidification system (HDH). They concluded the second law efficiency of these technologies are 5.9%, 2.9%, 31.9% and 2.4% respectively.

Al-sulaiman and Ismail [39] presented a simple scheme to quantify exergy losses and applied it to three larger MSF desalination process located in Saudi Arabia (Alkhobar II, Jubail II and Shuaibah). They found that these plants are highly irreversible with an

exergetic efficiency ranging from 1.12 to 10.38% and the exergy losses are directly proportional to the top brine temperature of the system.

Hamed *et al*. [40] performed an exergy analysis of Saline Water Conversion Corporation (SWCC) MSF desalination plants in Khobar, Jeddah, Jubail and Khafji, Saudi Arabia. They used the operational data of these plants for energy and exergy analyses for performance evaluation purpose of these plants. They found that the exergetic efficiencies of these plants ranged between 4.3 to 6.7% and all components of the plant, particularly the flashing chambers and brine heater contribute to the major exergy losses.

Kahraman and Cengel [14] performed an exergy analysis of a large scale MSF desalination plant in Saudi Arabia. They assumed an ideal mixture model of pure water and sodium chloride salt to present and calculate thermodynamic properties of seawater. This model was initially suggested by Cerci [41]. They concluded that the MSF desalination plant has second law efficiency of 4.2% and the largest exergy destruction occurs in MSF (by 78%). The exergy destruction in brine heater accounts for 8% of the total while 5.3% of the total exergy is destroyed in the pumps. The same plant was later analyzed by Sharqawy *et al*. [42] using the most up to-date correlations for exergy and flow exergy which covers both physical and chemical exergy of seawater streams. They determined that the MSF has second law efficiency of 7.65% which differs about 80% with the Kahraman and Cengel [14] reported values. They also concluded that the largest exergy destruction (75.54%) occurred in the flashing chambers and the next largest component of exergy destroyed is the brine heater with 10.5% of total exergy destroyed.

Pumps accounts for 5.5% while the remainder of the exergy is destroyed during the disposal of different streams into the environment.

In most of the previous studies of the MSF desalination plant was analyzed as a single unit. Nafey *et al* [43] examined a detailed second law analysis of a 5000 m^3/d MSF desalination plant and concluded that the exergetic efficiency of the system is 1.83%. They also calculated the exergy destruction and exergetic efficiency of each flashing stage, showing the potential of improvement and enhancement through reducing exergy destruction. Using the same concept, Wehshahi *et al*. [44] conducted a detailed exergy analysis of an existing 3800 m^3/h MSF desalination plant using the latest published seawater properties by Sharqawy *et al*. [42]. The input data for exergy analysis is taken from IPSEpro software [45]. The second law efficiency of the plant computed is 5.82%. They also found that about 65% of the exergy destruction occurs in MSF and next largest exergy destruction found to be in brine heater. Pumps have a share of 4% in total exergy destruction while 13% exergy is being destroyed during disposal of difference streams into the environment state. They also conducted an analysis for each flashing stage and concluded that the least exergy destruction occur in first flashing stage and increases gradually in later stages and more sharply in heat rejection stages.

There are three types of MSF desalination processes including once through, brine circulation and brine mixing. Brine circulation MSF is most efficient among all processes as it requires less heat transfer area and 70% less chemical consumption than the once through. Moreover the seasonal temperature variation of intake seawater does not affect the system performance [30,31].

In this work, the brine circulation MSF desalination plant is used for analyses. The detailed mathematical modeling of brine circulation MSF is developed, which also incorporate the pressure drop of brine flowing in condenser tubes. The model also include the exergy destruction equations for each component of the brine circulation MSF system. The developed model can be used to identify components that area responsible for greater losses in the system.

2.2 PROCESS DESCRIPTION

The brine circulation MSF desalination plant consists of four sections, a heat rejection section, a heat recovery section, a brine heater and a mixer. A schematic of the brine circulation MSF is illustrated in Figure 2.1. The heat input section consists of a brine heater that heats the seawater using steam from a back pressure turbine or extracted stream to heat the brine up to the top brine temperature. The heat recovery and heat rejection sections are of the same construction and divided into a number of stages. Each of them consists of a flashing chamber, a condenser, a demister and a distillate tray.

The intake seawater (M_f and M_{cw}) is pumped into condenser tubes of the heat rejection section at ambient temperature of the feed seawater ($T_{cw)}$ where its temperature increases by transferring the latent heat of condensing the vapor formed in each flashing chamber. The preheated intake feed is divided into two streams; one is the cooling water which is discharged back to the sea, while the other is the feed (M_f) which is introduced into the mixer to be mixed with the brine leaving the last stage of the heat rejection section. The purpose of the cooling water is to control the temperature of the circulated

brine (M_r) by controlling the salinity and removing extra heat energy added in the brine heater to the MSF system. The heat rejection section controls the temperature of the circulated brine (M_r) by recovering some energy of flashing vapor to brine feed and rejecting the remaining with the cooling water (M_{cw}). The circulated brine flows from the mixer and introduced in the tubes of the heat recovery section. As this recycled brine flows, across the stages, inside the condenser tubes it absorbs the latent heat of condensation in each stage. The recycled brine then enters into the tubes of brine heater where it is heated, due to the condensation of low pressure steam on the tube surface, to the maximum temperature, top brine temperature.

The chemicals, used to prevent fouling or scale formation, control the maximum top brine temperature that can be achieved in the MSF plant. The hot brine stream is directed into the first flashing chamber of the heat recovery section where it is evenly distributed along the stage width. A small amount of recycled brine flash off and forms distillate vapor which result in the decrease of temperature of circulated brine flow. The distillate vapor flows across the demister which retains brine droplets and then the distillate vapor condenses outside the condenser tubes releasing its latent heat to the feed stream flowing inside tubes. The vapor condensed outside the condenser tubes is collected in the distillate tray.

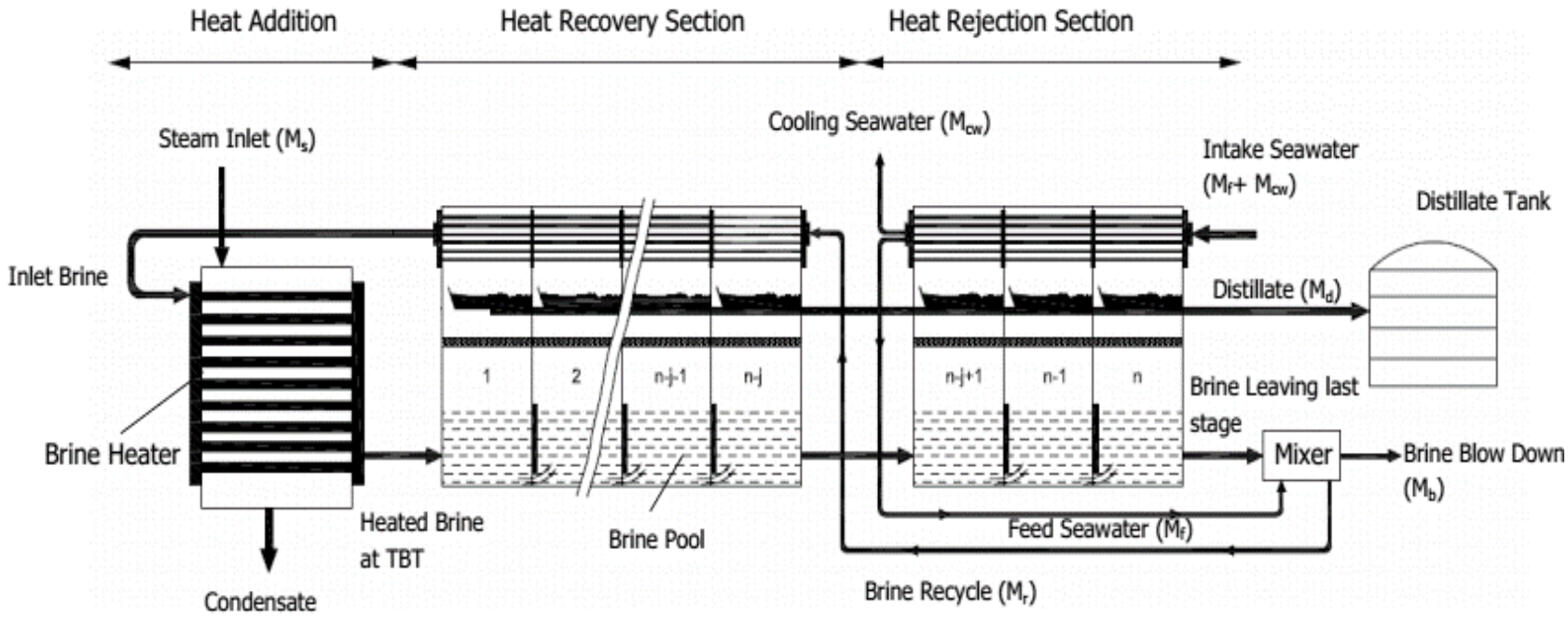

Figure 2.1: Schematic of brine recirculation Multistage Flash (MSF) Desalination

2.3 MATHEMATICAL MODEL OF MSF

Several studies related to the modeling of multistage flash (MSF) desalination are available in the literatures. The governing equations for the MSF are set of mass balances, energy balances, and heat transfer equations. The mathematical model of MSF-BR system is developed by considering the following assumptions.

- The MSF system is working under steady state condition.
- The distillate product is salt free.
- The condensed steam is not sub-cooled in the brine heater.
- Heat losses to the surrounding are negligible.

All thermophysical properties of seawater are taken from the correlations provided by Sharqawy *et al* [36] as a function of temperature and salinity. The effect of pressure on the enthalpy calculation was added assuming seawater is an incompressible fluid. The following are the important variables which have significant effect on the thermal performance of MSF brine circulation desalination plant.

1. Temperature of brine leaving the brine heater or Top Brine Temperature, TBT
2. The number of flashing stages, n
3. Intake feed brine temperature, T_{cw}
4. Temperature of rejected brine leaving the plant, T_b

2.3.1 Thermodynamic Analysis

The temperature drop for each flashing stage is considered equal and the temperature for each flashing stage is calculated by

$$T_{b,i} = T_{b,i-1} - \Delta T_b \tag{2.1}$$

where

$$\Delta T_b = \frac{TBT - T_b}{n} \tag{2.2}$$

where n is the total number of flashing stages and TBT is the top brine temperature.

2.3.1.1 Brine Heater

Figure 2.2 is a schematic of a brine heater, the energy balance equation for the brine heater can be written as following

$$m_r (h_{b,0} - h_{f,0}) = m_s h_{fg,s} \tag{2.3}$$

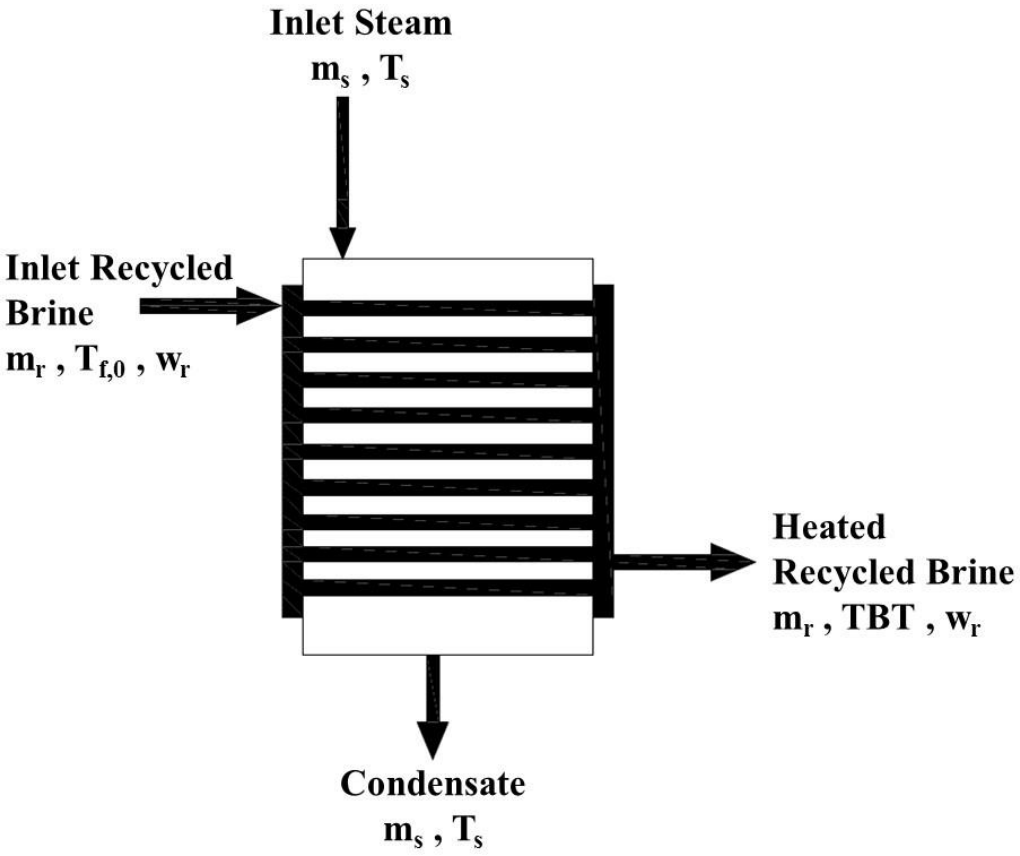

Figure 2.2: Schematic of a brine heater showing all model variables

2.3.1.2 Flashing Chamber

Figure 2.3 shows schematic of a flashing stage unit. The flashing chamber is divided into three regions; the brine pool (flashing chamber), the distillate tray, and the condenser tubes.

Applying seawater mass balance, salt mass balance, and first law of Thermodynamics respectively to the brine pool, the model equations are given as

$$m_{b,i-1} - m_{b,i} = m_{v,i} \tag{2.4}$$

$$m_{b,i-1} w_{b,i-1} = m_{b,i} w_{b,i} \tag{2.5}$$

$$m_{b,i-1} h_{b,i-1} - m_{b,i} h_{b,i} = m_{v,i} h_{v,g,i} \tag{2.6}$$

The above three equations are applicable for all flashing stages including heat recovery and the heat rejection sections.

Applying first law of Thermodynamics on the distillate tray and condenser tubes, the following energy balance equation is obtained for heat recovery section:

$$m_r \left(h_{f,i-1} - h_{f,i} \right) + \sum_{k=0}^{i} m_{v,k} h_{d,i} - \sum_{k=0}^{i-1} m_{v,k} h_{d,i-1} = m_{v,i} h_{v,g,i} \tag{2.7}$$

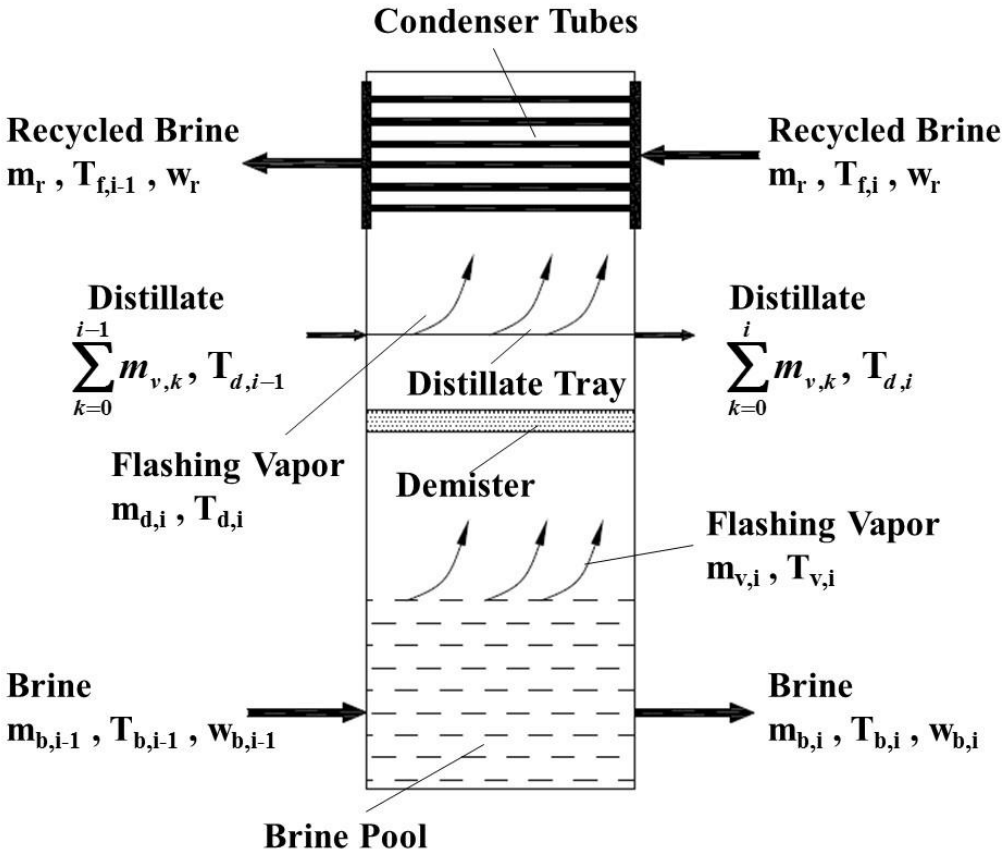

Figure 2.3: Schematic of a flashing stage of heat recovery section showing all model variables

The above equation is applicable for all condenser control volumes except stages of the heat rejection section (Figure 2.4). The energy balance equation for the first stage of heat rejection section is given by Eq.(2.8)

$$\left(m_f + m_{cw}\right)\left(h_{f,cw} - h_{f,n-j+1}\right) + \sum_{k=0}^{n-j+1} m_{v,k} h_{d,n-j+1} - \sum_{k=0}^{n-j} m_{v,k} h_{d,n-j} = m_{v,n-j+1} h_{v,g,n-j+1} \qquad (2.8)$$

The energy balance equation of the distillate tray and condenser tube for the flashing stages in the heat rejection section is given by Eq. (2.9)

$$\left(m_f + m_{cw}\right)\left(h_{f,i-1} - h_{f,i}\right) + \sum_{k=0}^{i} m_{v,k} h_{d,i} - \sum_{k=0}^{i-1} m_{v,k} h_{d,i-1} = m_{v,i} h_{v,g,i} \qquad (2.9)$$

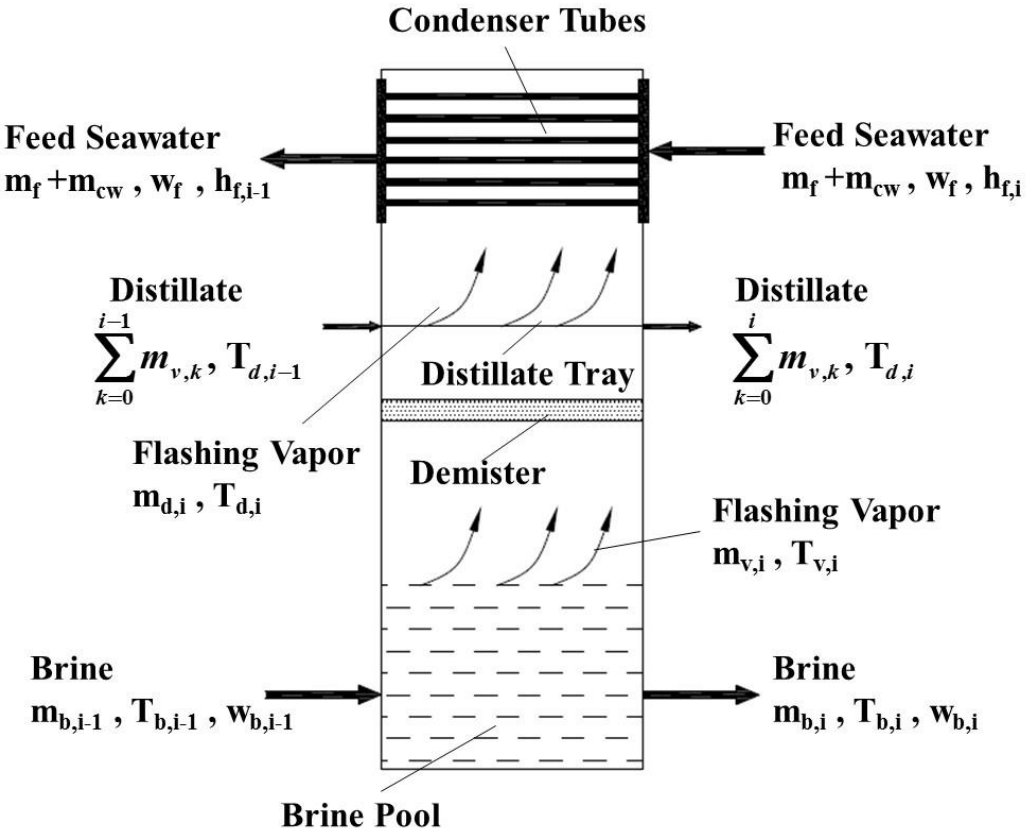

Figure 2.4: Schematic of a flashing stage of heat rejection section showing all model variables

2.3.1.3 Mixer

Figure 2.5 is the graphical representation of brine mixer, situated after last stage of heat rejection section, where the brine leaving from last stage and feed seawater are mixed and recycle brine stream is extracted while the remaining brine is rejected back to the sea.

Equations (2.10)-(2.12) are the seawater mass balance, salt mass balance, and energy balance for the brine mixer.

$$m_{b,n} - m_b + m_f - m_r = 0 \tag{2.10}$$

$$m_{b,n} w_{b,n} + m_f w_f = m_b w_b + m_r w_r \tag{2.11}$$

$$m_{b,n} h_{b,n} + m_f h_{f,cw} = m_b h_{b,n} + m_r h_r \tag{2.12}$$

By solving the above equations iteratively the mass flow rates and temperature profiles at each stage of MSF desalination process can be calculated.

The temperature of flashed vapor is less than the flashing brine temperature by the non-equilibrium allowance (NEA) and boiling point elevation (BPE).

$$T_{v,i} = T_{b,i} - BPE_i - NEA_i \tag{2.13}$$

While the vapor temperature above the demister is calculated by subtracting the temperature loss around demister due to pressure difference.

$$T_{d,i} = T_{v,i} - \Delta T_d \tag{2.14}$$

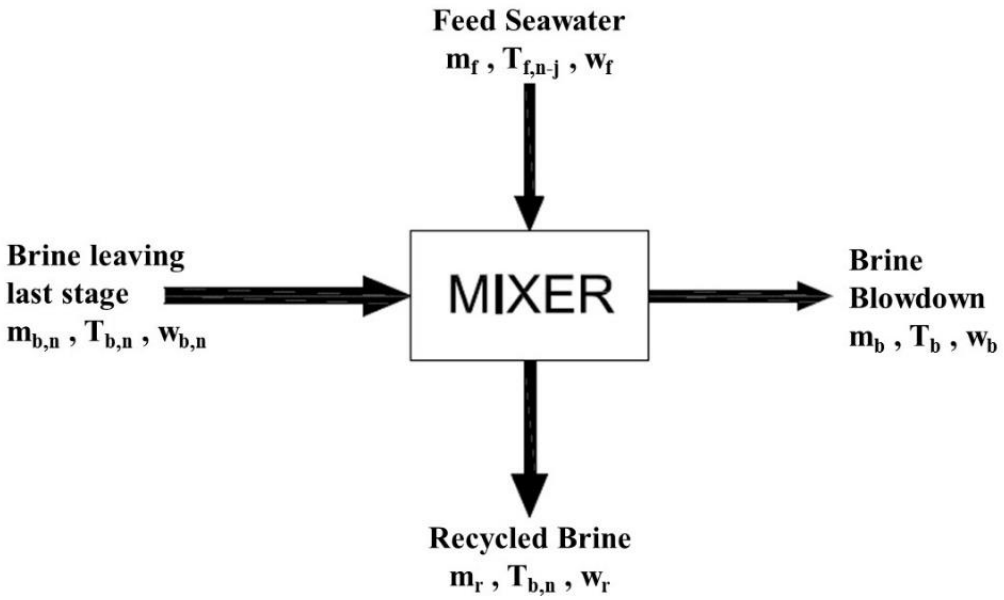

Figure 2.5: Schematic of brine mixer showing all model variables

2.3.1.4 Stage Dimensions

The design for the stage dimensions includes calculation of the stage length, stage width, gate height and the brine pool height. The length of each stage is set equal which is calculated for last stage and similarly width of each stage is considered equal and calculated for the first stage.

The gate height is calculated in the form of brine mass flow rate, stage pressure drop, brine density, stage width and weir friction coefficient. Equation (2.15) is used to calculate gate height for any stage [15]. In this equation the value of pressure drop should be in Pascal.

$$GH_i = \frac{m_{b,i-1}}{\left((C_d W)\left(2\rho_{b,i}\Delta P_{b,i}\right)^{0.5}\right)} \tag{2.15}$$

To prevent the leakage of vapors between stages, the brine pool height should be greater from gate height. Normally the brine pool height is taken greater than pool height by 0.2 m for blockage of bypass of vapors.

$$H_i = 0.2 + GH_i \tag{2.16}$$

The stage width is calculated from following formula

$$W = \frac{m_r}{V_b} \tag{2.17}$$

And similarly the length for the last stage is calculated by using mass flow rate formula

$$L = \frac{m_{v,n}}{\rho_{v,n} V_v W} \tag{2.18}$$

The boiling point elevation is calculated from the correlation provided by Sharqawy *et al*. [36] while the non-equilibrium allowance (NEA) is calculated from the following correlation [46]

$$NEA_i = (0.9784)^{T_{b,i-1}} (15.7378)^{H_i} (1.3777)^{V_b \cdot 10^{-6}} \tag{2.19}$$

2.3.1.5 Performance Parameters

The overall thermal performance of MSF Brine circulation desalination plant is expressed in terms of performance ratio, specific cooling water flow rate and specific heat transfer area.

The performance ratio (PR) is the measure of distillate flow rate produced by consuming unit steam flow rate.

$$PR = \frac{m_d}{m_s} \tag{2.20}$$

Specific cooling water flow rate (sM_{cw}) defined as the amount of cooling water required to produce unit distillate product.

$$sM_{cw} = \frac{m_{cw}}{m_d} \tag{2.21}$$

2.3.1.6 Pressure Drop

The pressure of stream at each stage of flashing chamber is the saturation pressure at corresponding temperature. While the pressure of stream flowing inside the tubes of condenser and brine heater is calculated by

$$P_{f,i-1} = P_{f,i} - \Delta P_{f,i} \tag{2.22}$$

$$P_{b,0} = P_{f,0} - \Delta P_{bh} \tag{2.23}$$

The pressure drop in the condenser tubes is calculated using the Darcy equation and the friction factor in the pipe is taken from Moody's diagram. Equation (2.24) is for the pressure drop in pipes while Eq. (2.25) is Colebrook relation for friction factor [47].

$$\Delta P_{f,i} = \frac{\rho_i \cdot f_i \cdot L_i \cdot v_i^2}{2 \cdot d_i} \tag{2.24}$$

$$\frac{1}{\sqrt{f}} = -2\log_{10}\left(\frac{\varepsilon/d}{3.7} + \frac{2.51}{Re\sqrt{(f)}}\right) \tag{2.25}$$

2.3.2 Exergy Analysis

Exergy is defined as the maximum amount of work obtainable when a system is brought to equilibrium from its initial state to environmental (dead) state. The system is considered to have zero exergy when it reached the environmental state (dead state). Selection of the environmental state varies with the research objective. In the current exergy analysis the intake seawater parameters are considered as dead state (P_0, T_0, w_0).

Flow exergy at each point is calculated using the correlations provided by Sharqawy *et al* [42] as functions of temperature, pressure and salinity, which is expressed as,

$$e = (h - h^*) - T_0(s - s^*) + \sum_{i=1}^{n} w_i(\mu_i - \mu_i^*) \tag{2.26}$$

where h, s, μ and w are specific enthalpy, specific entropy, chemical potential and mass fraction respectively. Properties with "*" in the above equation are determined at the dead state conditions (P_0, T_0, w_0). It should be noted that if the system and environmental are both pure substances (pure water), the chemical exergy (last term in Eq.(2.26)) will vanish. However for a multicomponent system (e.g. seawater) the chemical exergy must be considered.

Neglecting the kinetic and potential exergy, the exergy balance is similar to the energy balance performed using the first law of thermodynamics. However the exergy is not a conserved quantity due to irreversibilites (exergy destruction). Thus the exergy balance is expressed as

$$\sum Inlet\ Exergy - \sum Outlet\ Exergy\ =\ Exergy\ Destroyed \tag{2.27}$$

2.3.2.1 MSF components

To understand the exergy analysis of flashing stage unit, it is divided into three components, brine pool, distillate tray and condenser as shown in Figure 2.3 and Figure 2.4. By applying the exergy balances the following equations are obtained for brine pool, distillate tray respectively.

$$\dot{E}_{Bpool,i} = m_{b,i-1}e_{b,i-1} - m_{b,i}e_{b,i} - m_{d,i}e_{d,g,i} \tag{2.28}$$

$$\dot{E}_{DT,i} = \sum_{k=1}^{i-1} m_{d,k}e_{d,i-1} - \sum_{k=1}^{i} m_{d,k}e_{d,i} + m_{d,i}e_{d,i} \tag{2.29}$$

Similarly the exergy destruction for each condenser of heat recovery section is calculated by (Figure 2.3)

$$\dot{E}_{cond,i} = m_r\left(e_{f,i} - e_{f,i-1}\right) + m_{d,i}e_{d,g,i} - m_{d,i}e_{d,i} \tag{2.30}$$

And the exergy destruction for first condenser of heat rejection section and remaining rejection sections are calculated using Eq. (2.31) and Eq. (2.32) simultaneously (Figure 2.4).

$$\dot{E}_{cond,n-j+1} = \left(m_f + m_{cw}\right)\left(e_{f,n-j+1} - e_{f,cw}\right) + m_{d,n-j+1}e_{d,g,n-j+1} - m_{d,n-j+1}e_{d,n-j+1} \tag{2.31}$$

$$\dot{E}_{cond,i} = \left(m_f + m_{cw}\right)\left(e_{f,i} - e_{f,i-1}\right) + m_{d,i}e_{d,g,i} - m_{d,i}e_{d,i} \tag{2.32}$$

The total exergy destruction in each flashing stage is calculated by summing the exergy destruction in brine pool, distillate tray and condenser.

$$\dot{E}_{FS,i} = \dot{E}_{BPool,i} + \dot{E}_{DT,i} + \dot{E}_{Cond,i} \tag{2.33}$$

While the total exergy destruction in all the flashing stages is summation of exergy destruction of all stages.

$$\dot{E}_{FS} = \sum_{k=1}^{n} \dot{E}_{FS,k} \tag{2.34}$$

Similarly the exergy destruction in brine mixer and brine heater is calculates using Eq. (2.35) and Eq. (2.36) respectively.

$$\dot{E}_{Mixer} = m_{b,n} e_{b,n} - m_b e_{b,n} + m_f e_{f,m} - m_r e_r \tag{2.35}$$

$$\dot{E}_{BH} = m_r \left(e_{f,0} - e_{b,0} \right) + m_s \left(e_{s,in} - e_{s,out} \right) \tag{2.36}$$

The desalination plant involves four pumps, the exergy supplied to each of four pump is obtained using Eq. (2.37) to Eq. (2.40).

Seawater Pump

$$\dot{E}_{SP} = \left(m_f + m_{cw} \right) \left(e_{sp,out} - e_{sp,in} \right) \tag{2.37}$$

Distillate water pump

$$\dot{E}_{DP} = m_d \left(e_{dp,out} - e_{dp,in} \right) \tag{2.38}$$

Brine Pump

$$\dot{E}_{BP} = m_b \left(e_{bp,out} - e_{bp,in} \right) \tag{2.39}$$

Recirculating Pump

$$\dot{E}_{RP} = m_r \cdot \left(e_{rp,out} - e_{rp,in} \right) \tag{2.40}$$

The sum of exergy supplied to all pumps is

$$\dot{E}_{pumps,in} = \dot{E}_{SP} + \dot{E}_{DP} + \dot{E}_{BP} + \dot{E}_{RP} \tag{2.41}$$

But the pumps require electrical power to operate, there by considering a combined pump-motor efficiency, the exergy supplied in the form of electric power to the pump will be

$$\dot{E}_{pumps,act} = \frac{\dot{E}_{pumps,in}}{\eta_{pump}} \tag{2.42}$$

Similarly the exergy destruction in all pumps can be calculated by following equation

$$\dot{E}_{pumps} = \dot{E}_{pumps,act} - \dot{E}_{pumps,in} \tag{2.43}$$

The amount of exergy destruction in various components of MSF desalination plant (Figure 2.6) can be calculated by applying Eq.(2.27), which are

For the discharged seawater used for cooling

$$\dot{E}_{cooling} = m_{cw}\left(e_{f,cw} - e_{f,atm}\right) \tag{2.44}$$

For the brine disposed to the sea

$$\dot{E}_{brine} = m_{b}\left(e_{bp,out} - e_{b,atm}\right) \tag{2.45}$$

For the product water

$$\dot{E}_{product} = m_{d}\left(e_{dp,out} - e_{d,atm}\right) \tag{2.46}$$

For the feed water during throttling

$$\dot{E}_{TV} = m_{f}\left(e_{tv,in} - e_{tv,out}\right) \tag{2.47}$$

2.3.2.2 Second Law Efficiency

The second law efficiency is defined as the ratio of minimum work required for the desalination process to the total exergy supplied to the system.

$$\eta_{II} = \frac{\dot{W}_{min}}{\dot{E}_{in,total}} \tag{2.48}$$

or

$$\eta_{II} = 1 - \frac{\dot{E}_{desal}}{\dot{E}_{in,total}} \tag{2.49}$$

The minimum work required is equivalent to the minimum work of separation which is equal to the difference of the exergies of the outgoing streams (product and brine) and the exergies of the incoming stream (feed seawater).

$$\dot{W}_{min} = m_b e_{b,atm} + m_d e_{d,atm} - \left(m_f + m_{cw} \right) e_{f,atm} \tag{2.50}$$

The total exergy supplied to the desalination plant is the summation of flow exergy of heating steam and exergy input for driving pumps.

$$\dot{E}_{in,total} = \dot{E}_{in,steam} + \dot{E}_{pumps,act} \tag{2.51}$$

Where the exergy input to pump is calculated using Eq. (2.42) and exergy supplied by steam is calculated using Eq. (2.52)

$$\dot{E}_{in,steam} = m_s \left(e_{s,in} - e_{s,out} \right) \tag{2.52}$$

The total exergy destruction in the MSF desalination plant can be calculated using either from subtracting the minimum work of separation from total exergy supplied or by the summation of exergy destruction in all components of the system (Eq. (2.53) and Eq.(2.54)).

$$\dot{E}_{desal} = \dot{E}_{in,total} - \dot{W}_{min} \tag{2.53}$$

$$\dot{E}_{desal} = \dot{E}_{MSF} + \dot{E}_{Mixer} + \dot{E}_{BH} + \dot{E}_{cooling} + \dot{E}_{brine} + \dot{E}_{product} + \dot{E}_{pumps} + \dot{E}_{TV} \tag{2.54}$$

2.3.2.3 Exergy Destroyed in MSF Components

The percentage exergy destroyed in each component is determined by taking ratio of exergy destroyed in each component to the total exergy destruction in the desalination plant

$$Component = \frac{\dot{E}_{component}}{\dot{E}_{desal}} \tag{2.55}$$

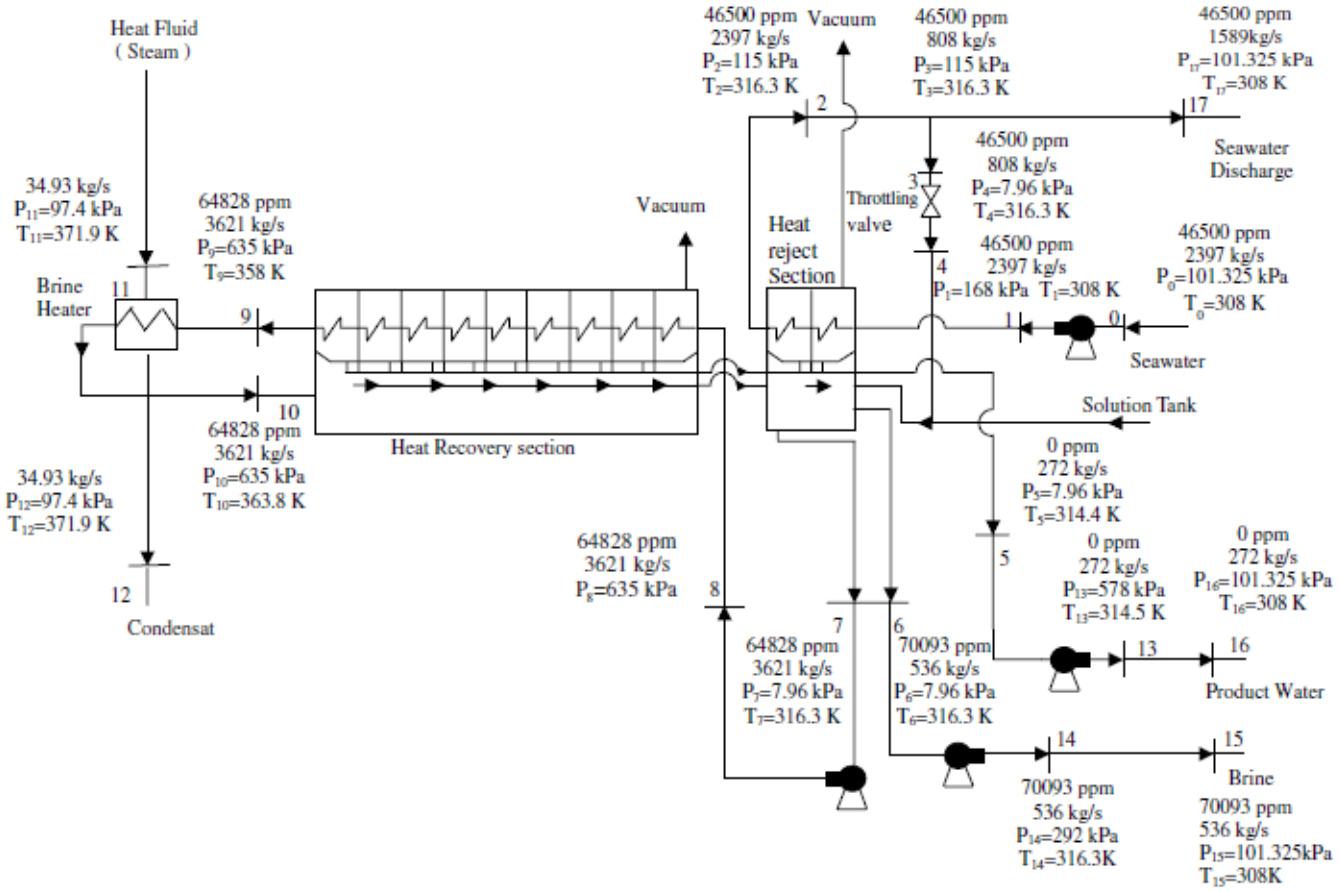

Figure 2.6: Schematic of MSF desalination plant in Jubail, Saudi Arabia [14]

2.4 RESULTS AND DISCUSSION

2.4.1 Model Validation

The mathematical model developed in the previous section is used to investigate the important design parameters and exergy analysis of brine circulation MSF desalination system. The input design parameters to the model are the number of stages (n), top brine temperature (TBT), distillate output (m_d), temperature and salinity of feed seawater (T_{cw}, w_f), brine blow down (T_b, w_b), and steam temperature (T_s). On the basis of these parameters, the mathematical model calculates the performance parameters, temperature profiles, flow rates, and concentration variations in all stages of the MSF system. The model can be used either to design a new plant or to study the effect of different operating variables on the performance of plants in operation.

The model equations are solved using the Engineering Equation solver (EES) software [48]. EES is a numerical solver that uses an iterative procedure to solve the equations. The convergence of the numerical solution is checked by using the following two variables: 1). Relative equation residuals , the difference between left hand and right hand sides of an equation divided by the magnitude of left hand side of the equation. 2). Change in variable, the change is the value of the variables within an iteration. The calculations converge if the relative equation residual is less than 10^{-6} or if change in variable is less than 10^{-9}. There are several publications which have previously used EES for thermodynamic analysis of the systems [14,21,49].

The results obtained from the model, are compared with the actual data of Jubail desalination plant in Saudi Arabia reported by Kahraman and Cengel [14] and presented in Table 2.1. Results are also compared with a case study presented by El-Dessouky and Ettouney [15] as given in Table 2.2.

Table 2.1: Comparison with the operating parameters of Jubail MSF plant [14].

Input Parameters			**Results Comparison**			
Parameter	**Unit**	**Value**	**Variable**	**Present Work**	**Jubail Plant**	**% Deviation**
n	-	22	**PR**	7.1	7.8	8.6
TBT	°C	90.8	**M_s (kg/s)**	38.2	34.9	9.5
M_d	kg/s	272	**M_f (kg/s)**	808.1	808	0
w_f	g/kg	46.5	**M_r (kg/s)**	3583	3621	1
w_b	g/kg	70.1	**w_r (g/kg)**	64.8	64.8	0
T_{cw}	°C	35	**$T_{f,0}$ (°C)**	84.6	85	0.5
T_b	°C	43.3				
T_s	°C	98.9				

Table 2.2: Comparison with a case study reported in El-Dessouky and Ettouney [15]

Input Parameters			**Results Comparison**			
Parameter	**Unit**	**Value**	**Variable**	**Present Work**	**Reference**	**% Deviation**
n	-	24	**PR**	7.6	7.2	4.7
TBT	°C	106	**M_s (kg/s)**	50.2	52.5	4.5
M_d	kg/s	378.8	**M_f (kg/s)**	947	947	0
w_f	g/kg	42	**M_r (kg/s)**	3625	3385	7.1
w_b	g/kg	70	**w_r (g/kg)**	62.7	62.5	0.3
T_{cw}	°C	25	**$T_{f,0}$ (°C)**	98.1	97.8	0.3
T_b	°C	40				
T_s	°C	116				

The detailed thermal analysis is performed for a large MSF desalination plant located in Jubail, Saudi Arabia which was presented by Kahraman and Cengel [14] and its detailed information is given in Table 2.1. Figure 2.7 shows the temperature distribution of the brine flowing inside the condenser tubes, the brine flowing in the flashing chamber, and distillate temperature. The temperature distribution for the brine flowing inside the condenser tubes deviates more from a straight line as it is calculated based on the energy balances while the flashing brine temperature is linear along the stages because it is assumed to have equal increase in all stages. The distillate temperature at each stage is less than the brine temperature due to the temperature drop at each stage arising from the non-equilibrium allowance (NEA) and boiling point elevation (BPE) in each stage. Figure 2.8 shows the BPE is slightly decreasing with the increase of salinity and decrease of vapor pressure along the flashing stages. While NEA is increasing with the decrease of brine temperature along the stages. This implies that the difference between the brine flashing temperature and the vapor temperature becomes larger as the brine temperature is decreased along the flashing stages. This is caused by increase in the surface tension of the brine at lower temperature as well as the brine viscosity.

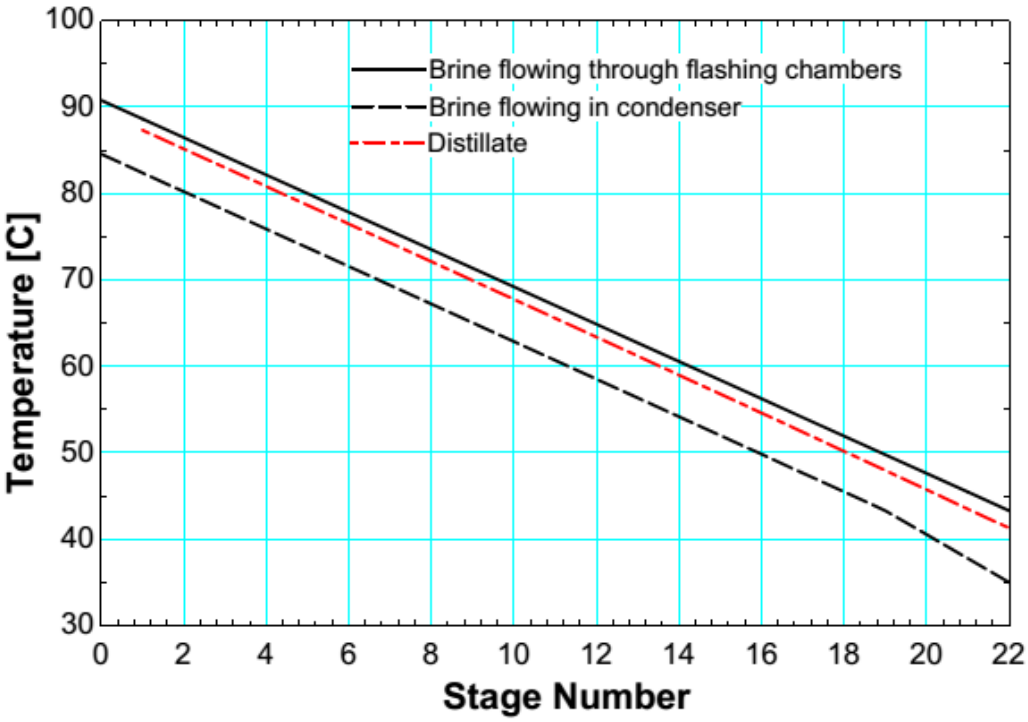

Figure 2.7: Temperature distribution of brine flowing in condenser tubes, brine flowing in flashing chambers, and distillate along the flashing stages

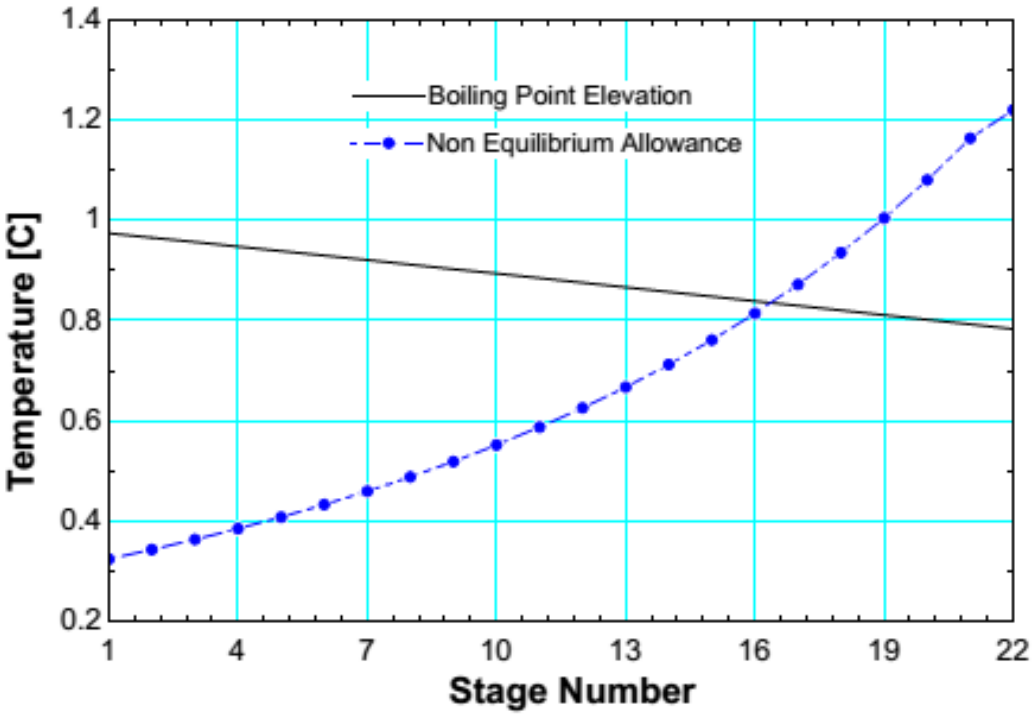

Figure 2.8: BPE and NEA variation along the flashing stages

Figure 2.9 shows the salinity variation of the brine flowing inside the flashing chambers and condenser tubes. In condenser tubes of heat rejection section the feed flows at constant salinity of 46.5 g/kg while in heat recovery section recycle brine flows at a constant salinity of 64.8 g/kg. Whereas the concentration of brine flowing inside the flashing chamber increases along the stages because of the vapor produced at each stage.

Figure 2.10 represents the distillate produced at each flashing stage. The amount of distillate produced decreases along the flashing stages due to the decrease in the vapor temperature because the flashing process (which produces the vapor) occurs at lower pressure at each flashing stage. The vapor produced in every stage explains the reduction in brine flow rate as it flows from a stage to another. The variation of the recycled brine flow rate along the flashing stages is shown in Figure 2.11.

Figure 2.12 shows the pressure of the both brines flowing in tubes of condenser and inside flashing chamber. In condenser tubes, the pressure dropped due to the frictional losses while inside flashing chamber the pressure of brine stream equals the saturation pressure corresponding to the stage temperature. In the first flashing chamber, there is a large pressure drop due to the sudden decrease from the pressure of the brine stream exiting the brine heater to the saturation pressure corresponding to the temperature in this stage.

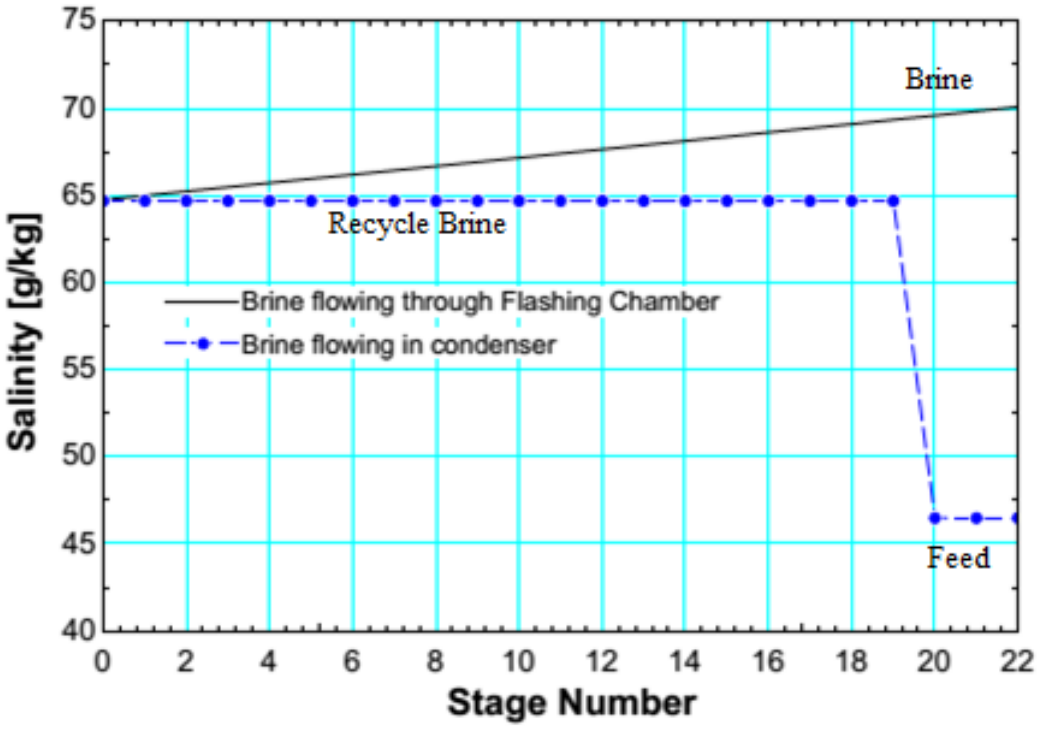

Figure 2.9: Variation of the salt concentrations of brine flowing inside the condenser tubes and through flashing chambers.

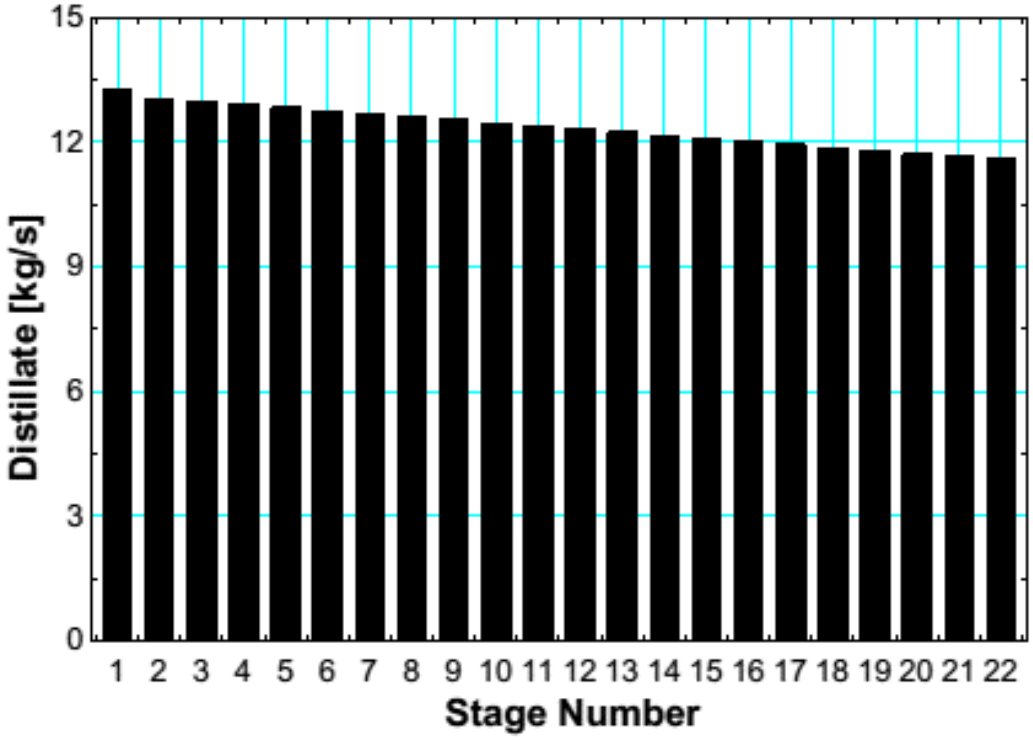

Figure 2.10: Distillate produced at each flashing stage

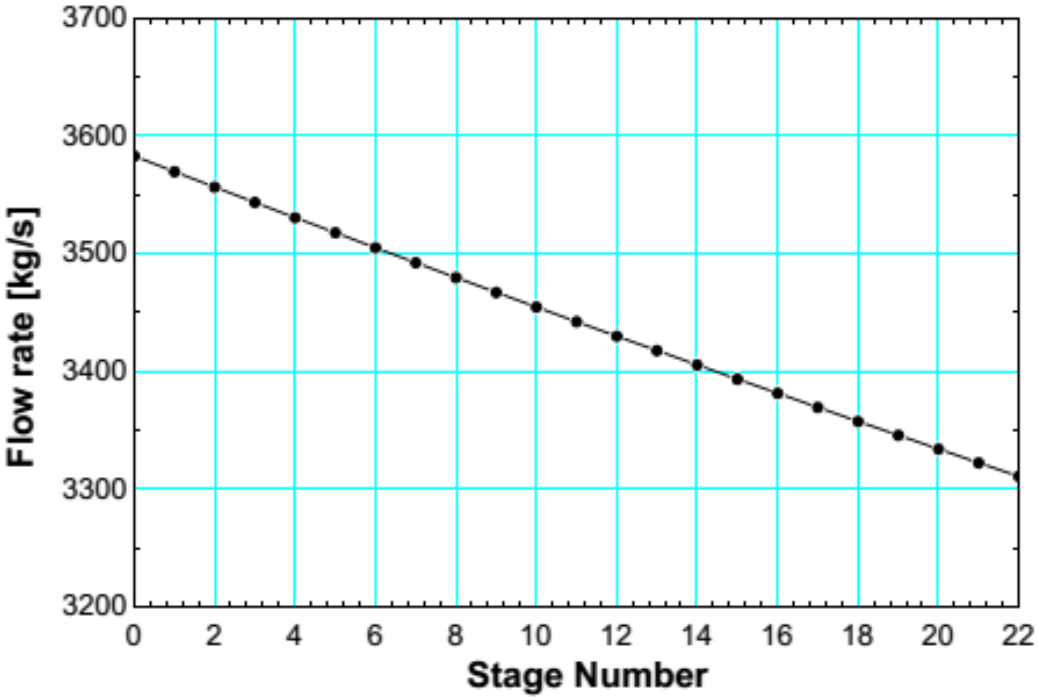

Figure 2.11: Variation of the flow rate of the recycled brine along the MSF stages (the difference between the first and the last stages is the total distillate)

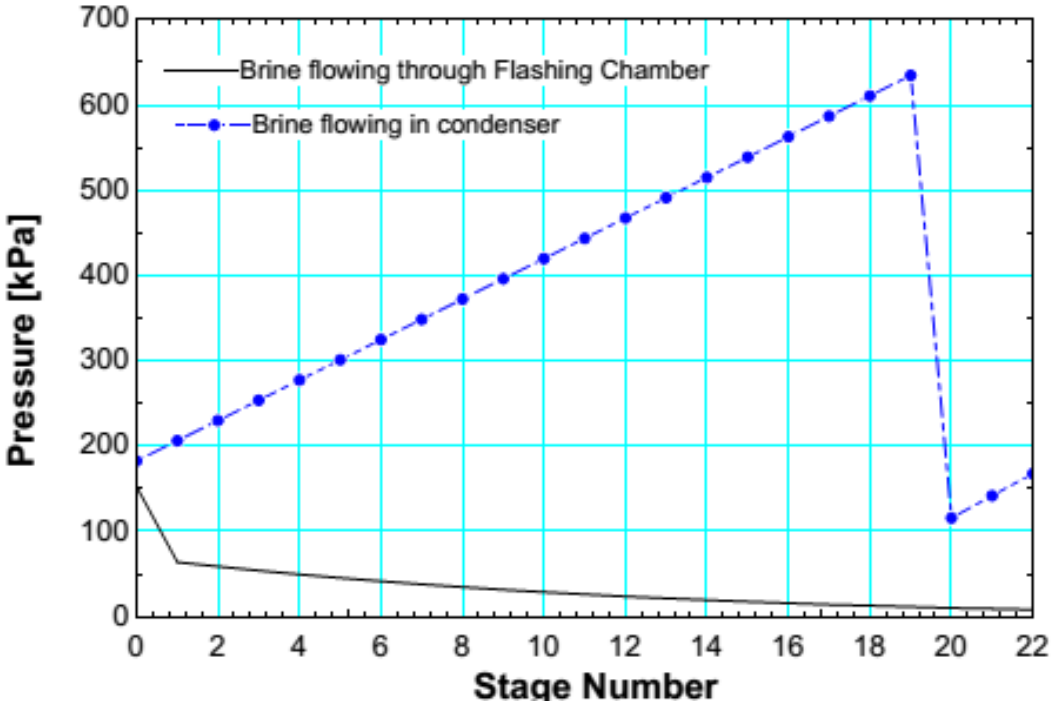

Figure 2.12: Pressure variation of the brine flowing inside the condenser tubes and through flashing chambers.

A detailed exergy analysis is performed for an MSF desalination plant which was studied by Kahraman and Cengel [14] but they used the thermophysical properties of Sodium Chloride solution to replace natural seawater properties. Later Sharqawy *et al*. [42] analyzed the same plant by using latest seawater properties and corrected the seawater flow exergy calculation method after precisely determining the chemical exergy of seawater.

The flashing stage is divided into three main components, brine pool, distillate tray and condenser tubes to investigate the exergy destruction at different locations of the flashing chamber. In this regard, the conditions of inlet feed seawater to the MSF is considered as the environmental (global) dead state which are T_0= 35 °C, P_0 = 101.325 kPa and w_0 = 46.5 g/kg.

The thermodynamic properties and the flow exergy rates of all streams are shown in Table A. 1 through Table A. 5 in the Appendix A. The flow exergy at each state is calculated by using the correlations provided by Sharqawy *et al*.[42].

Equation (2.28) is used to calculate the exergy destruction in brine pool of each flashing stage and Eq. (2.29) gives the exergy destruction in distillate tray, Similarly, Eq. (2.30) to Eq. (2.32) are applicable for the calculations of exergy destruction in the condenser.

Figure 2.13 shows the exergy destruction in the brine pool of flashing stages using Eq. (2.28) . It can be seen that at the first stage exergy destruction is higher due to high pressure drop at the first stage (see Figure 2.12.), from stage 2 to the last stage, the exergy

destruction increases due to the decrease in the amount of vapor produced. Figure 2.14 is illustration of exergy destruction in distillate tray using Eq. (2.29) while Figure 2.15 is representation of exergy destruction in condenser using Eq. (2.30) to Eq. (2.32).

The trend of exergy destructions in distillate tray and condenser can be better understood using Table A. 1 to Table A. 5 given in Appendix A. All the term are decreasing except accumulation of fresh water in the distillate tray but the multiplication of streams mass flow rate with flow exergy shows that exergy destruction in distillate tray increases from zero to a value maximum at middle stages and then start to decrease toward the last stage. On the contrary, the opposite effect for the condenser as exergy destruction decreases from the first stages to the middle stages and it increases toward the last stage.

From the all three components of flashing stage, the condenser has the highest exergy destruction because there is a large pressure drops in condenser tubes compared to the other components. In the condenser tubes of heat rejection stages, the increase of exergy destruction is even higher because it has even higher pressure drop in tubes compared to heat recovery stages.

The total exergy destruction is each stage is summation of exergy destruction in three components, calculated by Eq.(2.33), shown by Figure 2.16.

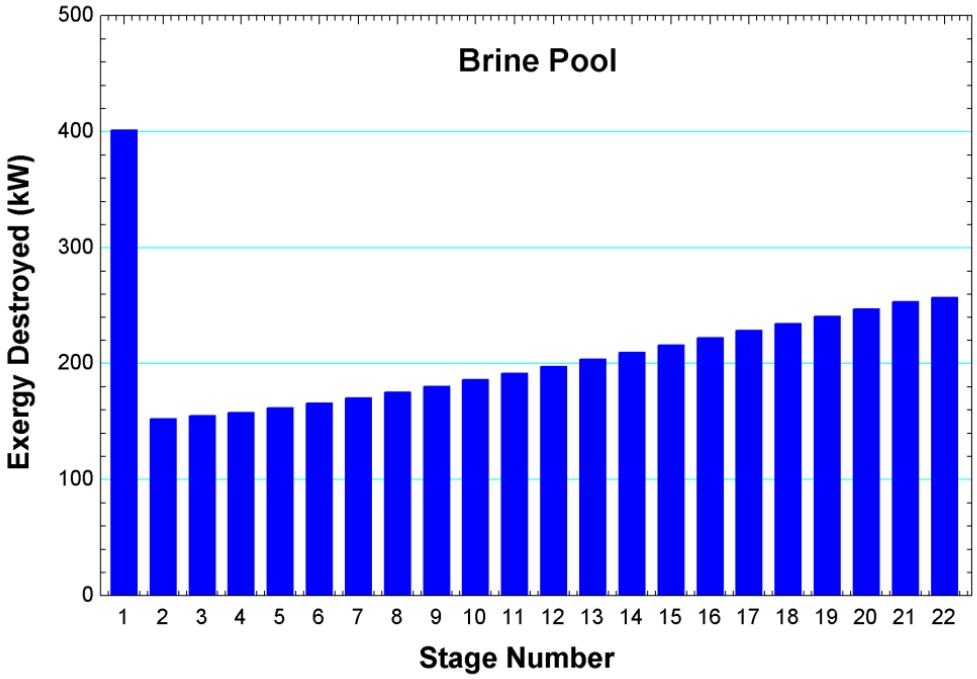

Figure 2.13: Exergy destruction in brine pool for each flashing stage

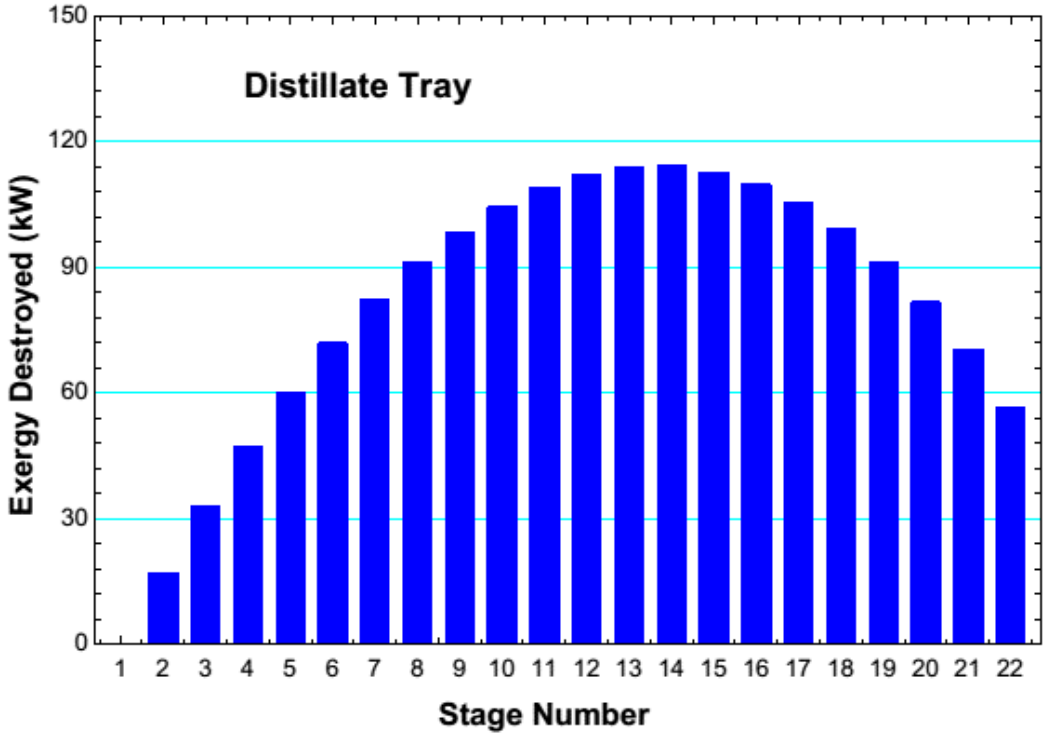

Figure 2.14: Exergy destruction in distillate tray for each flashing stage

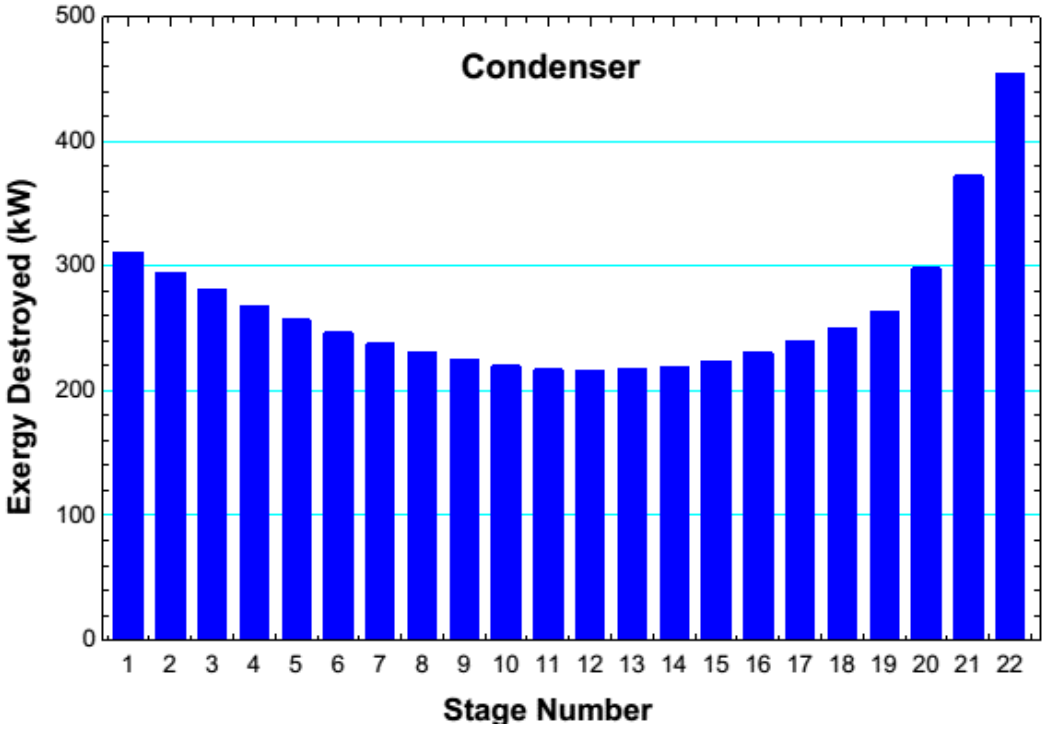

Figure 2.15: Exergy destruction in condenser for each flashing stage

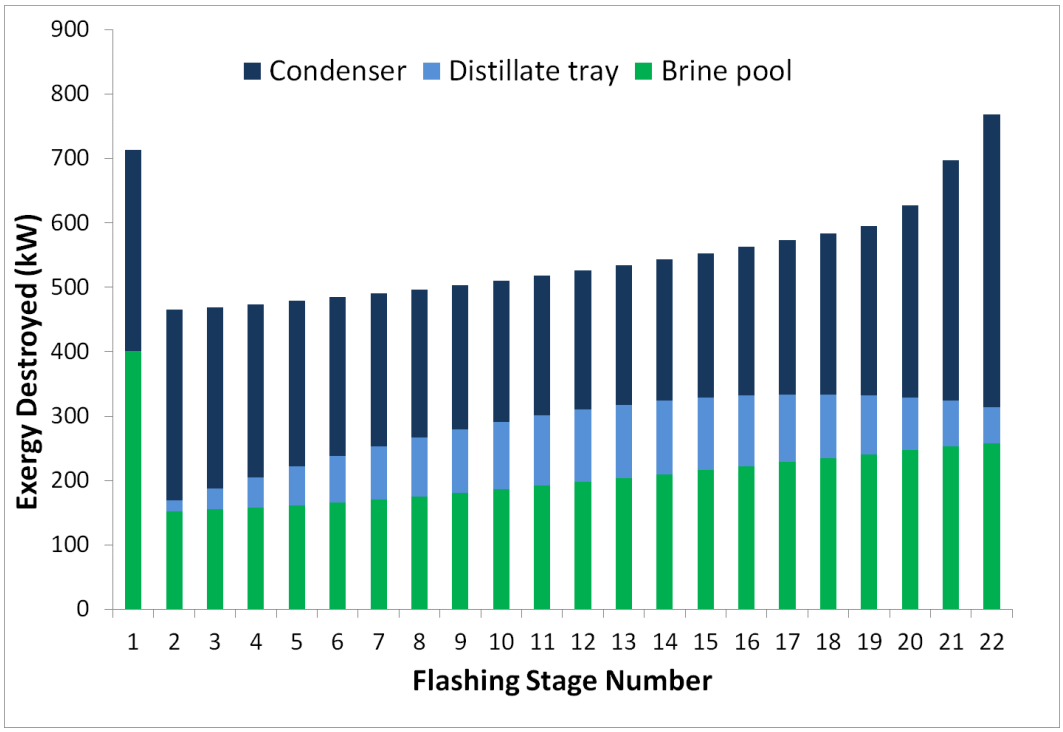

Figure 2.16: Exergy destruction in flashing stages of MSF

Table 2.3 summarizes the second law analysis of MSF. The total exergy supplied to the desalination plant is summation of flow exergy of heating steam and exergy supplied for driving pumps. The combined motor pump efficiency is taken as 75% [14] The plant involves four pumps (Figure 2.6), the exergy supplied to each pump is calculated using Eq. (2.37) to Eq. (2.40) and total exergy supplied to drive all pump is calculated using Eq. (2.42), while the flow exergy of heating steam is calculated using Eq. (2.52)

Table 2.3: Exergy analysis results for MSF plant.

Equipment	**Results**	**Percentage**
Seawater pump exergy input	179.5 kW	1.3 %
Distillate pump exergy input	156.2 kW	1.1 %
Brine pump exergy input	145.7 kW	1.1 %
Recirculating pump exergy input	2,161 kW	15.7 %
Total pump exergy input (including 75 % pump efficiency)	3,523 kW	19.2 %
Heating steam exergy	14,845 kW	80.8 %
Total exergy input	18,368 kW	
Minimum separation work	1,306 kW	
Total exergy destruction	17,062 kW	
Second Law Efficiency (%)	7.11 %	

Second law efficiency is the ratio of minimum work required for the desalination process to the total exergy input. Where the minimum work required equivalent to the minimum work of separation calculated by using Eq. (2.50).the plant has second law efficiency of 7.1 % (Eq. (2.48) or(2.49)).

Table 2.4 represents the exergy destruction in all the parts of MSF desalination plant. Where exergy destruction in heat recovery section (stage # 1-19) and heat rejection section (stage # 20-22) are calculated using Eq. (2.34). Similarly, exergy destruction in the mixer and the brine heater are calculated using Eq. (2.35) and (2.36) respectively. Equations (2.43) to (2.47) are used to calculate the exergy destruction in pumps, cooling process, brine disposal, product and throttling valve respectively.

The total exergy destruction of the desalination plant can be found by two method and both Eq. (2.53) and Eq. (2.54) give the same results. The fractions of exergy destroyed in the various components of desalination plant are determined using Eq.(2.55), shown in Figure 2.17. It can be seen that the largest exergy destruction occurs within flashing stages (71.3%). The next largest exergy destruction occur in brine heater (12.3 %), the pumps (5.2%) and discharge of cooling water back to sea (4.8%), while remaining 4.7% exergy destruction occur during throttling, discharge of brine blow down and product distillate.

Table 2.4: Exergy destruction in MSF components

Components	**Exergy Destroyed**	**Percentage**
Heat Recovery Section	10075 kW	59 %
Heat Rejection Section	2092 kW	12.3 %
Mixer	211 kW	1.2 %
Brine Heater	2393 kW	14 %
Pumps	881 kW	5.2 %
Cooling Process	821 kW	4.8 %
Brine Disposal	323 kW	1.9 %
Product	203 kW	1.2 %
Throttling	64 kW	0.4 %

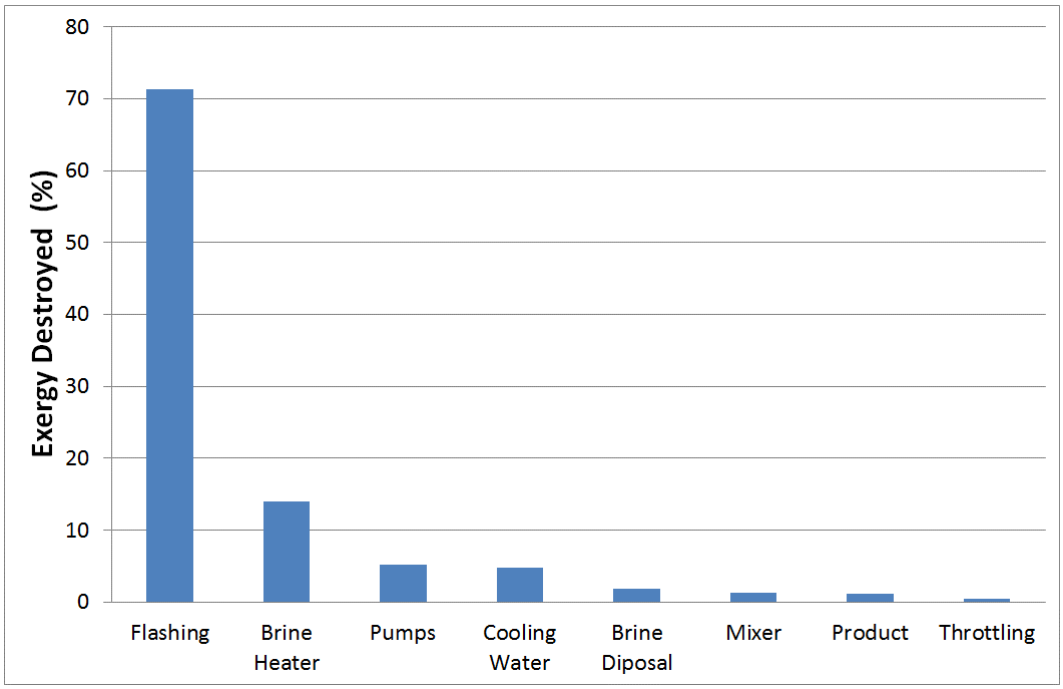

Figure 2.17: Percentage exergy destruction in MSF components

2.5 CONCLUSION OF MSF STUDY

A detailed steady state mathematical model for multistage flash (MSF) desalination, is developed, and is used with latest published seawater properties as a function of temperature, pressure and salinity. The model is solved using Engineering Equation Solver software (EES) and results in temperature profile, salinity variations, and amount of vapor produced at each flashing stage. The model also incorporates the effect of pressure drop in condenser tubes. The results of the energy analysis are used for performing exergy analysis of an existing MSF desalination plant sited in Jubail, Saudi Arabia. The analysis shows that the plant has a second law efficiency of 7.11%. It is found out that the largest exergy destruction occurs during flashing (71%), while brine heater accounts for 12% of total exergy destruction. The pumps constitute 5% while during discharge of cooling water to sea 4.8% exergy destruction occurs. As the largest exergy destruction occurs in flashing stage, to locate the location of maximum exergy destruction, the detailed analysis of flashing stages is also performed. Each flashing stage is divided into three components brine pool, distillate tray, and condenser. The results indicate that the total exergy destruction in first stage is higher as the pressure drop of recycle brine is very higher and from the second stage of heat recovery section, the exergy destruction increases gradually and sharply in heat rejection stages is the highest. Moreover, from the three components of flashing stage, the share of exergy destruction is higher in condenser tubes.

CHAPTER 3

PRESSURE RETARDED OSMOSIS

3.1 LITERATURE REVIEW

In pressure retarded osmosis (PRO), water permeates through a semi-permeable membrane from a low hydrostatic pressure – high osmotic pressure stream (feed stream) to a high hydrostatic pressure – low osmotic pressure stream (draw stream). The transfer of water increases the volume flow rate of the pressurized draw stream and energy is obtained by depressurizing the draw stream through a hydro turbine. The concept of PRO was first proposed by Sidney Loeb [13]. Since then, several models have been developed and experiments were conducted to determine the performance of many proposed PRO systems. Mehta and Loeb [50] discussed the adverse effect of internal concentration polarization which acts as a resistance to permeate transfer inside the membrane layer under PRO operating conditions through analytical and experimental results.

Ahmad and William [51] presented various concepts of salinity gradient energy (SGE) from disposed brine and the possible power generation when implementing osmotic power plants with disposed brine. They investigated different salinity gradient

processes including reversed electrodialysis (RED), pressure retarded osmosis (PRO), vapor compression (VC) and hydrocratic generation (HG) and concluded that PRO has superior potential for energy harvesting because of the substantial amount of energy that can be generated and lack of CO_2 emissions that will harm the natural climate. Moreover they also performed mathematical calculations of energy harvesting for mixing of high saline brine (100,000 and 250,000 ppm), with river water (500 ppm), normal seawater (35,000 ppm), Arabian Gulf seawater (46,000 ppm) and waste water (10,000 ppm) using the model developed by Forgacs [52].

Loeb [53] investigated the energy cost and power production at Dead Sea using pressure retarded osmosis for two types of plants prior to the PRO. Moreover, he also analyzed the influence of various operating parameters on the produced energy cost and power production. Loeb [54] conducted a detailed study focusing on economics of energy production using pressure retarded osmosis. This study was limited to spiral wound membrane by using river water as feed and seawater as draw solution. He concluded that although the development of appropriate spiral wound membrane for PRO is not easy, this harmless and renewable source of energy justifies the investigation on a large scale.

Panyor [55] investigated the pressure retarded osmosis as a renewable energy source from dilution of seawater with the fresh water on the coast of Italy. He emphasized on the importance of osmotic power plant using PRO process. Sharqawy *et al*. [56] proposed an energy recovery system for reverse osmosis desalination plant using the pressure retarded osmosis (PRO). The results indicate that the PRO has a second law efficiency of 20% and

found out that the input power is reduced by 38% relative to original reverse osmosis system with the usage of PRO as an energy recovery device (ERD).

Skilhagen *et al*. [57] discussed the concept of osmotic power and also identified the energy potential, the financial aspects, and the environmental implications through the work of Statkraft. They mentioned the latest developments in the membrane science that have led to the installation of first prototype osmotic power plant in Norway. Enomoto *et al*. [58] studied the feasibility of PRO power generation by using commercial reverse osmosis membranes. They used the tap water as a feed solution and seawater as draw solution in spiral wound membrane and measured the permeation volume for the estimation of power generation. The power output per unit volume determined using the commercial membrane was 0.62 W/m^2 which can be increased up to 2.43 W/m^2 by incorporating their suggested improvements in membrane modules.

Lee *et al*. [59] performed the analysis for feasibility study of PRO as a method for energy generation from salinity gradient resources. They performed the experiments using various RO membranes to project the PRO performance with several feed and draw resources. In addition, they developed a PRO model which incorporates the effect of concentration polarization. It was found that the concentration polarization inside the membrane lowers the water flux under PRO operation. They concluded that the power generation from PRO is technically feasible but not viable using current reverse osmosis membranes.

Achilli *et al*. [16] developed a predictive PRO model which includes the influence of draw and feed solutions, concentration polarization, and hydraulic pressure. This model incorporates both internal and external concentration polarization and predicts the water flux and power density under specific conditions. The parameters necessary to calculate the water flux in PRO were obtained from experiments, water permeability and salt permeability were determined under RO conditions, while the solute resistivity was obtained under FO conditions. They performed bench scale PRO experiments using flat sheet CTA FO membrane and NaCl draw and feed solutions. The maximum hydraulic pressure achieved during the experiment was 970 kPa and at that pressure maximum power densities of 2.7 and 5.1 W/m^2 were achieved. The experimental results were compared with predictive PRO model for water flux and power density. They found out that the internal concentration polarization has greater effect in reducing the power density while the external concentration polarization has relatively smaller effect in reducing osmotic driving force.

Thorsen and Holt [60] analyzed the PRO process for energy production from seawater and fresh water using commercially available RO membrane with the realistic conditions for plant operation. The power density of 2.7 W/m^2 was measured from a small sample of developed membrane. In addition, they investigated the PRO process and developed guidelines for the development of membrane suitable for PRO process. They concluded that the current RO membrane has semi permeable properties suitable for higher performance but the structure parameter of the membrane must be in order of 0.5mm or less in order to obtain a power density of 5 W/m^2.

Zwan *et al*. [61] developed a two dimensional hydrodynamic mass transfer model applicable for flat sheet membranes for the performance analysis of osmotic power module at a large plant scale. The model results were compared with available lab-scale results in the literature. They found that using counter flow configuration gives 15 % more power output than PRO of a parallel flow configuration. The maximum power generated using the commercially available membrane was about 4.5 W/m^2. The maximum power output per cubic meter of fresh water by mixing of seawater (at 35,000 ppm) and fresh water was 0.5 MJ/m^3 which increased to 1.6 MJ/m^3 if a higher salinity brine of 200,000 ppm is used with seawater.

Xu *et al*. [62] investigated experimentally the effect of draw solution concentration and operating conditions on PRO permeate flux and using classical ICP models. The analysis indicates that the permeate flow increased at the higher draw solution concentration, but its behavior is not linear due to internal concentration polarization. ICP becomes even more dominant when high salinity draw solutions are used. The numerical model results agreed well with the experimental results however, it overestimated the permeate flux if the external concentration polarization on the feed solution side is significant.

Sharqawy *et al*. [63] discussed the analogous between heat exchangers and PRO mass exchangers. They developed closed form analytical solutions of the effectiveness and Mass Exchange Units (MTU). They combined the local transport equation for permeate flow with the conservation of mass and linearized equation for osmotic pressure and determined dimensionless expressions for parallel and counter flow PRO exchangers.

Recovery ratio was obtained as a function of dimensionless parameters such as mixing ratio, mass transfer unit, and osmotic pressure ratio. The resulting effectiveness-MTU model for osmotic mass exchanger can be used as an initial design tool for PRO systems. A numerical model, which uses the nonlinear osmotic pressure function, was also used for power production and energy recovery from desalination plants. The error associated with linearized osmotic pressure function was found to be less than 5.5%.

Chou *et al*. [64] developed a specially designed PRO hollow fiber membrane, characterized the basic structure and properties of newly developed PRO membrane and evaluated its performance to demonstrate the potential of power generation. PRO-hollow fiber membranes have a water permeability of 9.22×10^{-9} (m/s.kPa), salt permeability of 3.86×10^{-8} (m/s), and structural parameter of 4.6×10^{-4} (m). This membrane can withstand hydrostatic pressure of 9 bars. They performed PRO experiments, with active layer facing the draw solution, for several scenarios of draw and feed solution, including seawater (0.5M NaCl) and brine water (1.0M NaCl) as draw solution while the river water (10mM NaCl), waste water (40mM NaCl) and concentrated waste water (80mM NaCl) were used as feed solutions. A power density of 10.6 W/m^2 was achieved with the seawater brine (1.0M NaCl) and wastewater brine (40mM NaCl) using the developed PRO hollow fiber membranes.

Han *et al*. [65] developed a high performance PRO membrane with excellent mechanical strength and power density. This membrane can withstand pressure of 15 bars. They used a lab-scale PRO setup with various synthetic water sources. A power density ranging from 7 to 12 W/m^2 were achieved using seawater (0.59M NaCl) and

brine (1.0M NaCl) as draw solution and river water (10mM NaCl), waste water (40mM NaCl) and concentrated waste water (80mM NaCl) as feed solution.

Chou *et al*. [66] developed a novel high performance hollow fiber membrane for the application of power production from salinity gradients using pressure retarded osmosis. They characterized the basic structure and properties of newly developed PRO hollow fiber membrane and evaluated the membrane performance in PRO. Water and salt permeability coefficients were obtained under RO conditions while structural parameter of membrane was determined under FO conditions. The draw solution was on the active layer side of the membrane and the membrane could withstand a hydrostatic pressure up to 15 bars. The NaCl solutions were used to estimate the osmotic power generation for both draw (1.0 M) and feed solutions (1mM and 10mM). The experiments were performed by varying the pressure from 5 to 15 bars and it was found that the water flux first decreased in the pressure range of 5 to 7.5 bars, then increased at higher pressure and remained almost constant. The concentration of the salt was 0.03 mole per liter that was much lower compared to the flat sheet membranes. This PRO hollow fiber membrane achieved a power density of 20.9 W/m^2 for a draw solution of 1.0M NaCl and feed solution of 1mM NaCl solution.

Sivertsen *et al*. [67] examined the power production and pressure drop in hollow fiber membrane using different flow configurations. They investigated the effect of different variables including membrane characteristics and module dimensions on the PRO performance and pressure drop for all configurations used. They found out that the overall PRO performance is similar for all configurations. The radial flow configuration

has the larger pressure drop in shell side compared to the longitudinal flow configuration, which required larger membrane area of a given element size.

Gerstandt *et al*. [68] optimized the power output from a PRO plant for two different type of membranes i.e., TFT and CA membrane. The initial power density achieved from the TFT membrane was 0.1 W/m^2 which was optimized and reached to a value of 3.5 W/m^2 whereas the starting value for CA membrane was 0.5 W/m^2 and after optimization of membrane performance was 1.3 W/m^2, and to make PRO profitable, the power density of the membrane is determined to be 5 W/m^2.

Achilli and Childress [12] reviewed the literature published from the midst of twentieth century to the time when first prototype osmotic power plant was built. They concluded that despite the large number of published material on pressure retarded osmosis, there is very minimal available experimental data on power density. The recent power density values reported in literature are three times more than the earlier results due to the improved membrane characteristics and modules. In addition, they concluded that, the RO membranes are not suitable for PRO operations. Moreover, the hollow fiber membrane used in earlier experiments gave poor results. In recent studies the spiral wound and flat sheet membranes specially designed for PRO process resulted in high power density.

Helfer *et al*. [69] analyzed the technical, economical, environmental, and other aspects of osmotic process. They combined the outcomes of modern research and the advancement achieved in the last few years and the hurdles that need to be overcome for

the implementation of osmotic power production on commercial scale. They concluded that the most important benefit of PRO technology is its ability to generate a continuous and reliable source of power compared to other renewable sources and its low environmental impacts. The study identified that the PRO technology has been improving rapidly, particularly in recent years. At the current stage of progress the low osmotic power outputs are technical barriers to an economical power production. Osmotic power will become financially viable when membrane with output power density of 5 W/m^2 or more are commercially available as then it will be more cost effective than the currently available renewable energy sources, and the desalination plants will more likely be primary market for osmotic power as these systems employ similar technology and require a large amount of energy to produce fresh water.

3.2 PROCESS DESCRIPTION

Osmosis is a process of transportation of water through a semi-permeable membrane from a solution of high water chemical potential (low species concentration) to a solution of lower water chemical potential (high species concentration). This process is normally called forward osmosis (FO), driven by a difference of the osmotic pressure ($\Delta\pi$) of two streams across a membrane, which allows transfer of permeate and rejects most of the salt contents. In FO process, the two streams are either not pressurized or pressurized to same magnitude, resulting $\Delta P = 0$. The FO process results in concentrating the low salinity stream and diluting of the high salinity stream.

In reverse osmosis (RO), pressure is applied to the high salinity solution, this pressure is greater than the osmotic pressure difference ($\Delta P > \Delta\pi$). As a result of this applied pressure, water permeates from the high salinity side to the low salinity side, opposite to the natural osmotic process, through the membrane. Most of the small-scale modern seawater desalination plants are working on the RO principle. Pressure retarded osmosis (PRO) can be regarded as an intermediary process between FO and RO. In this process, a pressure is applied to the high salinity solution, similar to RO but this pressure is lower than the osmotic pressure difference ($\Delta P < \Delta\pi$), but the permeate moves toward the high salinity solution, similar to FO. The representation of these three processes is shown in Figure 3.1.

In PRO process, the feed solution, a low salinity stream, and the draw solution, a high salinity stream, are pumped at opposite sides of a semi-permeable membrane. Water permeates through the membrane from the low pressure stream (feed solution) to the higher pressure stream (draw solution) due to the osmotic pressure difference. This increases the volume flow rate of the pressurized draw stream and energy is obtained by depressurizing the draw stream through a hydro turbine. For this system, the osmotic pressure difference between the draw stream and the feed stream must be higher than the hydraulic pressure difference to achieve transfer of permeate through the membrane and to have a net power output. The schematic diagrams of pressure retarded osmosis (PRO) process for two configurations, parallel and counter-flow, are shown in Figure 3.2 and Figure 3.3 respectively.

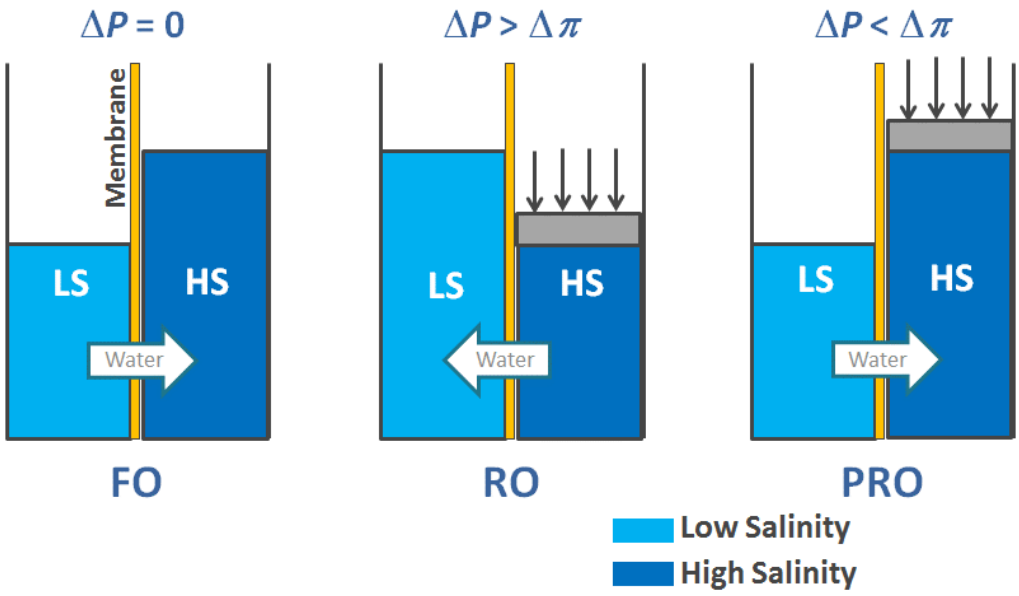

Figure 3.1: Schematic of FO, RO and PRO processes

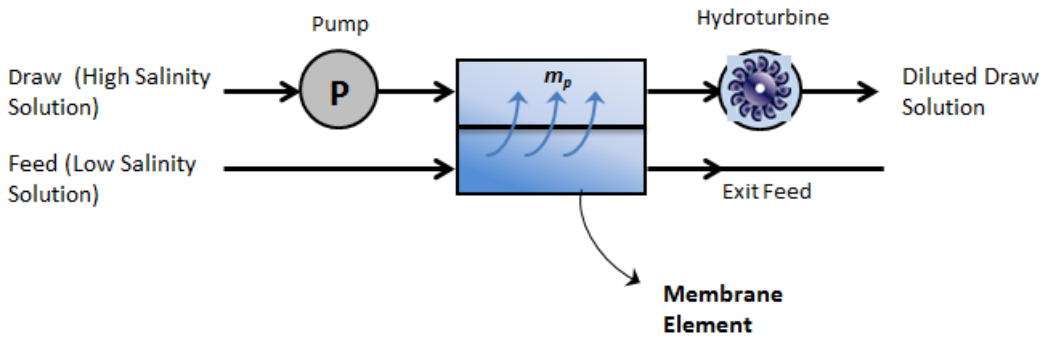

Figure 3.2: Schematic of parallel-flow pressure retarded osmosis process

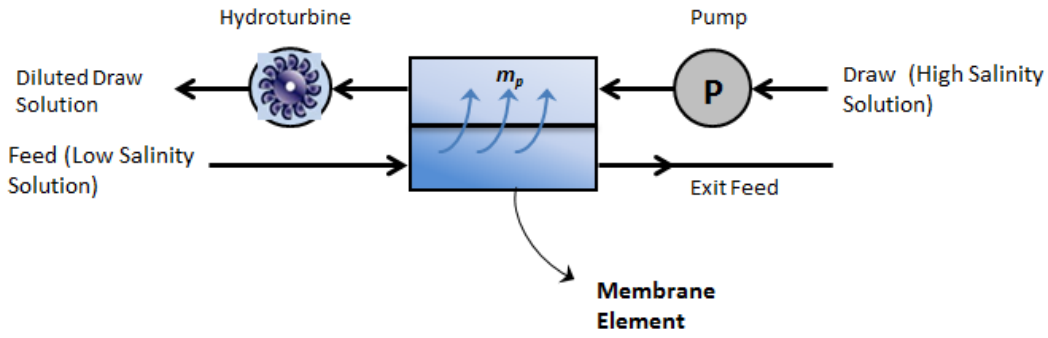

Figure 3.3: Schematic of counter-flow pressure retarded osmosis process

3.3 MATHEMATICAL MODEL OF PRO

A one-dimensional model is developed for a PRO system that takes into consideration the salinity variation of both the feed and brine streams along the membrane area.

The PRO model consists of four mass balance equations and two transport equations. The mass balance equations are written for water molecules and salt molecules on the draw side and feed side for both the cases of parallel flow and counter flow configurations. The PRO membrane is divided into finite number of meshes, the subscripts "i" represents that the equations are applied on each of the mesh.

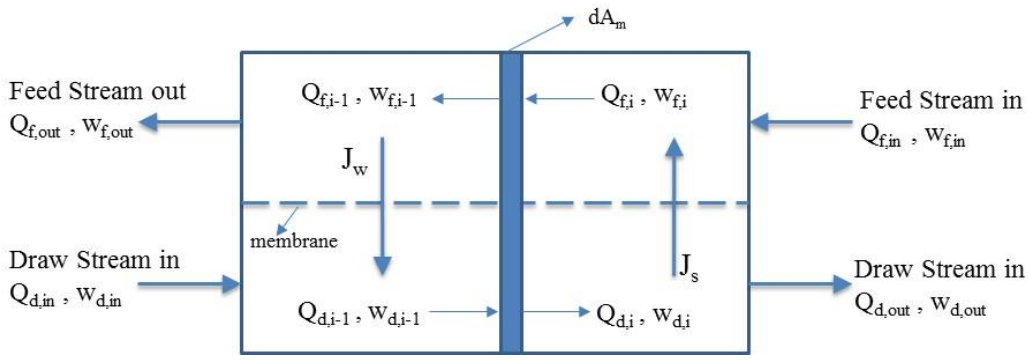

Figure 3.4: Schematic of a counter flow PRO process

A- Water mass balance:

1- Parallel-flow configuration

$$\left(1-w_{f.i}\right)Q_{f,i}=\left(1-w_{f.i-1}\right)Q_{f,i-1}-J_{w,i}dA_m \tag{3.1}$$

$$\left(1-w_{d,i}\right)Q_{d,i}=\left(1-w_{d,i-1}\right)Q_{\mathrm{d},i-1}+J_{w,i}dA_m \tag{3.2}$$

2- Counter -flow configuration

$$\left(1-w_{f.i}\right)Q_{f,i}=\left(1-w_{f.i-1}\right)Q_{f,i-1}-J_{w,i}dA_m \tag{3.3}$$

$$\left(1-w_{d,i}\right)Q_{d,i}=\left(1-w_{d,i-1}\right)Q_{\mathrm{d},i-1}-J_{w,i}dA_m \tag{3.4}$$

B- Salt mass balance:

1- Parallel flow configuration

$$w_{f,i}Q_{f,i}=w_{f,i-1}Q_{f,i-1}+J_{s,i}dA_m \tag{3.5}$$

$$w_{\mathrm{d},i}Q_{\mathrm{d},i}=w_{\mathrm{d},i-1}Q_{\mathrm{d},i-1}-J_{s,i}dA_m \tag{3.6}$$

2- Counter flow configuration

$$w_{f,i}Q_{f,i}=w_{f,i-1}Q_{f,i-1}+J_{s,i}dA_m \tag{3.7}$$

$$w_{\mathrm{d},i}Q_{\mathrm{d},i}=w_{\mathrm{d},i-1}Q_{\mathrm{d},i-1}+J_{s,i}dA_m \tag{3.8}$$

where Q_{f} and Q_{d} are the volume flow rate of feed stream and draw stream, respectively, in (m^3/s), while J_{w} is the water flux permeated from the feed stream to draw stream and dA_{m} represents the membrane surface area of a mesh. w_{f} and w_{d} are the salinity of feed stream and draw stream respectively in (kg/kg), and J_{s} (m/s) is the salt

flux. The mixing ratio is defined as the ratio of volume flow rate of draw solution stream to the volumetric flow rate of feed input.

$$MR = \frac{Q_{d,in}}{Q_{\mathrm{f},in}} \tag{3.9}$$

The equations for water transport and salt transport across the membrane in PRO are

$$J_{\mathrm{w},i} = A\left(\Delta\pi_i - \Delta P_i\right) \tag{3.10}$$

$$J_{s,i} = B\left(w_{d,i} - w_{f.i}\right) \tag{3.11}$$

where A (m/s-kPa) and B (m/s) are the water permeability coefficient and salt permeability coefficient respectively, $\Delta\pi$ (kPa) is the osmotic pressure difference across the membrane (difference between osmotic pressure at the draw solution and feed solution), and ΔP (kPa) is the hydraulic pressure difference. It is assumed that there is a negligible hydraulic pressure drop along the feed stream and draw stream paths.

Concentration polarization is the main hurdle in membrane permeation as it diminishes the effective osmotic pressure difference across the membrane. Concentration polarization is the accumulation of salt contents near the membrane interface. As a result of water permeation across the membrane, the salt is concentrated on the feed side of the membrane surface, and diluted on the draw side of the membrane surface.

External concentration polarization (ECP) occurs on the active layer side and internal concentration polarization (ICP) occurs in the support layer side as results of the salt

being concentrated inside the support layer of the feed side. Lee at al. [59] developed an expression for water flux which incorporates the effect of internal concentration polarization in PRO applications. The water flux is determined by

$$J_w = A\left(\pi_{d,m}\frac{\left(1-\left(\frac{w_f}{w_{d,m}}\right)\exp\left(J_w k_s\right)\right)}{1+\left(\frac{B}{J_w}\right)\left(exp\left(J_w k_s\right)-1\right)}-\Delta P\right) \tag{3.12}$$

where $w_{d,m}$ is the salt concentration of the draw solution at the membrane surface, k_s is the solute resistivity for diffusion within the support layer which represent the influence of internal concentration polarization on water flux.

Dilutive external concentration polarization (ECP) results in the salt content being diluted on the draw solution side of the membrane. The external concentration polarization modulus ($\pi_{d,m}/\pi_{d,b}$) is calculated using

$$\left(\frac{\pi_{d,m}}{\pi_d}\right)=\left(-\frac{J_w}{K_m}\right) \tag{3.13}$$

where K_m is the mass transfer coefficient in the draw side. In order to consider the effect of both internal and external concentration polarization on water flux in PRO, Achilli *et al*. [16] modified Eq. (3.12) using Van't Hoff equation which gave ($w_{f,}/w_{d,m} = \pi_f/\pi_{d,m}$) and substituting the external concentration polarization modulus from Eq. (3.13). The resulting equation for water flux including both ICP and ECP is

$$J_w = A\left(\left(\pi_d\right)exp\left(-\frac{J_w}{K_m}\right)\frac{\left(1-\left(\frac{\pi_f}{\pi_d}\right)exp\left(J_w k_s\right)exp\left(\frac{J_w}{K_m}\right)\right)}{1+\left(\frac{B}{J_w}\right)\left(exp\left(J_w k_s\right)-1\right)}-\Delta P\right) \tag{3.14}$$

where the water flux (J_w) is a function of membrane characteristic (A and B), mass transfer coefficient (k_m), solute resistivity (k_s), osmotic pressures of draw stream and feed stream (π_d and π_f) and applied hydraulic pressure (ΔP). Osmotic pressures are calculated using correlations provided by Sharqawy *et al*. [36] as a function of temperature, pressure, and salinity. Due to large concentration difference across the semi-permeable membrane, a small amount of salt permeates from the draw stream to the feed stream which results in the reduction of effective osmotic pressure difference across membrane. Therefore, salt flux (J_s) should be taken into consideration in the PRO model. The expression for salt flux (J_s) [61] as a function of water flux (J_w), salt permeability (B), solute resistivity (k_s) and salinities of two stream is given,

$$J_{s,i} = \left(\frac{B}{k_s B+1}\right)\left(w_{d,i} - w_{f,i} - k_s J_{w,i} w_{f,i}\right) \tag{3.15}$$

The total permeate flow rate Q_p (m^3/s) transferred through the membrane is the summation over all meshes of the product of water flux and membrane area as given by Eq. (3.16).

$$Q_p = \sum_{i=1}^{n} J_{w,i} dA_m \tag{3.16}$$

The power produced from the PRO system is equal to the product of the total permeate flow rate and the hydraulic pressure difference across the membrane as given by Eq. (3.17). The power density is calculated by dividing the produced power by the total membrane area as given by Eq... (3.18).

$$Power = Q_p \left(P_{d,in} - P_{f,in} \right) \tag{3.17}$$

$$\text{Power Density} = Q_p \left(\frac{P_{d,in} - P_{f,in}}{A_m} \right) \tag{3.18}$$

The governing equations for a PRO configuration (3.1 – 3.18) are solved numerically to calculate the permeate flow rate, generated power, and power density. Under idealized conditions at which the concentration polarization and pressure drop are negligible and there is no salt diffusion, the water flux decreases as hydraulic pressure increases, and finally reaching zero at $\Delta\pi=\Delta P$ (flux reversal point). Concurrently, power increases with increasing of hydraulic pressure and reaches a maximum at $\Delta P=\Delta\pi/2$ then decreasing with further increase of hydraulic pressure until it reaches zero at the flux reversal point. Under actual conditions, reverse salt diffusion and concentration polarization reduce the effective osmotic pressure difference which lowers the permeate flow rate and power as compared to the idealized case; stream wise variations in osmotic pressure difference further affect the maximum power point.

3.4 RESULTS AND DISCUSSION OF PRO

3.4.1 Model Validation

The model equations for PRO are solved numerically using EES software to calculate the variation of the flow rates and salinities along the membrane, permeate flow rate, power, and power density. The results of the computational model are compared with the experimental data provided by Achilli *et al*. [16].

Table 3.1 gives the membrane characteristics which are used in the model to match with the experimental conditions applied by Achilli *et al*. [16]. The membrane area was 18.75 cm^2, volume flow rate (draw and feed stream) was 0.5 liter/min, and the inlet temperature of both streams is 25°C. The comparison between simulated results of current study and experimental values of Achilli *et al*. [16] are given in Table 3.2 which indicates an excellent agreement with the experimental data. Apart from these reported values, Achilli *et al*. [16] performed experiments for two draw streams with concentration of 35 and 60 g/kg, three different feed streams including, fresh water values for, 2.5 g/kg NaCl solution and 5 g/kg NaCl solution. The comparison of the numerical model with these six different experimental results, for power density and water flux, are shown in Figure 3.5 and Figure 3.6.

Table 3.1: Membrane characteristics and operating parameters for PRO

Parameter	Value
Water permeability coefficient (*A*)	1.87×10^{-9} (m/s-kPa)
Salt permeability coefficient (*B*)	1.11×10^{-7} (m/s)
Mass transfer coefficient (K_m)	8.48×10^{-5} (m/s)
Solute resistivity (K_s)	$4.5\times10^{+5}$ (s/m)
Intake draw stream	8.33×10^{-6} (kg/s)
Mixing ratio	1

Table 3.2: Comparison between present work and Achilli *et al*. [16] results

	Achilli [16]	**Present work**	**Achilli** [16]	**Present work**
Draw Solution Salinity (g/kg)	35	35	60	60
Feed Solution Salinity (g/kg)	0	0	0	0
Hydraulic Pressure (kPa)	972	972	972	972
Water Flux (10^{-6} m/s)	2.81	2.51	5.21	5.08
Power Density (W/m^2)	2.73	2.44	5.06	4.94
Normalized Power Density (Power Density / $\Delta\pi$ - ΔP)	1.52×10^{-3}	1.50×10^{-3}	1.30×10^{-3}	1.34×10^{-3}

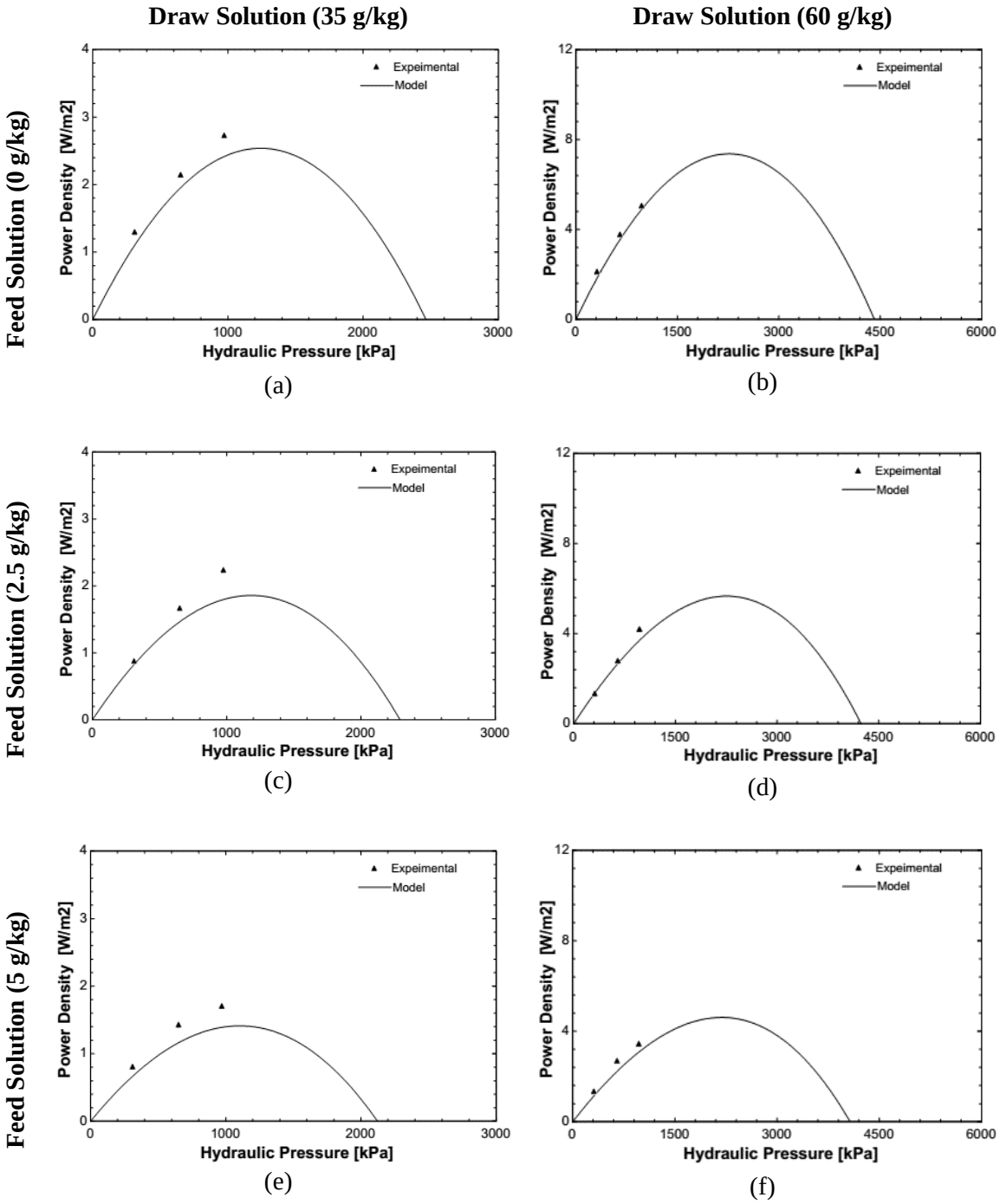

Figure 3.5: Model validation for power density as a function of hydraulic pressure with experimental results [16]

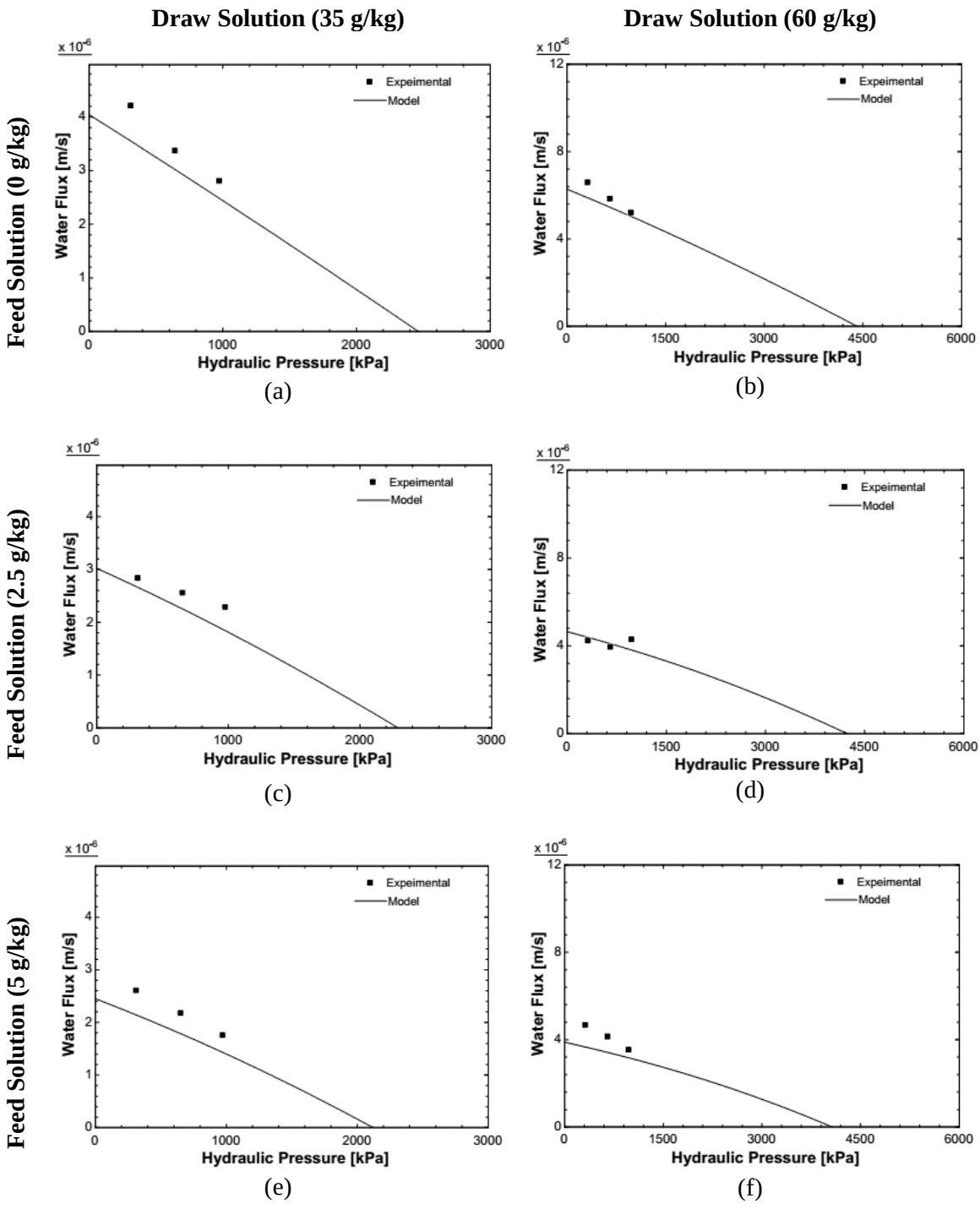

Figure 3.6: Model validation for water flux as a function of hydraulic pressure with experimental results [16]

3.4.2 Comparison between Parallel and Counter Flow Configurations

The PRO process is analogous to heat exchanger and can be used with different flow configurations i.e., parallel and counter flow configuration. In this work, the comparative analysis of parallel and counter flow configurations has been performed. The membrane characteristics used are same as used earlier for model validation while the membrane area and flow rates are taken from a commercially available RO membrane SWC5 1640 (Hydranautics corporation) [70], given in Table 3.1. The salinity of the draw stream is 70g/kg and for the feed stream is 35g/kg with a feed inlet flow rates of 6.5 kg/s and the total membrane area used for comparison study is 3792 m^2.

3.4.2.1 Parallel Flow Configuration

The variation of draw and feed salinity along the membrane for the parallel flow with and without considering the effect of concentration polarization are shown in Figure 3.7. A normalized area is used which is the accumulated area at a given location divided by the total membrane area. Draw and feed streams are in the same direction, the draw stream enters at 70 g/kg which decreases along the membrane with the addition of water flux and leaves at about 60g/kg, while the feed stream enters at 35 g/kg and leaves at 42 g/kg. Figure 3.8 represents the water flux variation along the membrane with and without considering the effect of concentration polarization. It can be noted that the transportation of water flux is maximum at the entrance as the salinity difference between the two streams is higher which decreases along the membrane. In the case with considering the effect of concentration polarization, the water flux reaches zero at about half of the

membrane, because at that point the osmotic pressure difference becomes equal to the hydraulic pressure difference and the flux reversal point occurs.

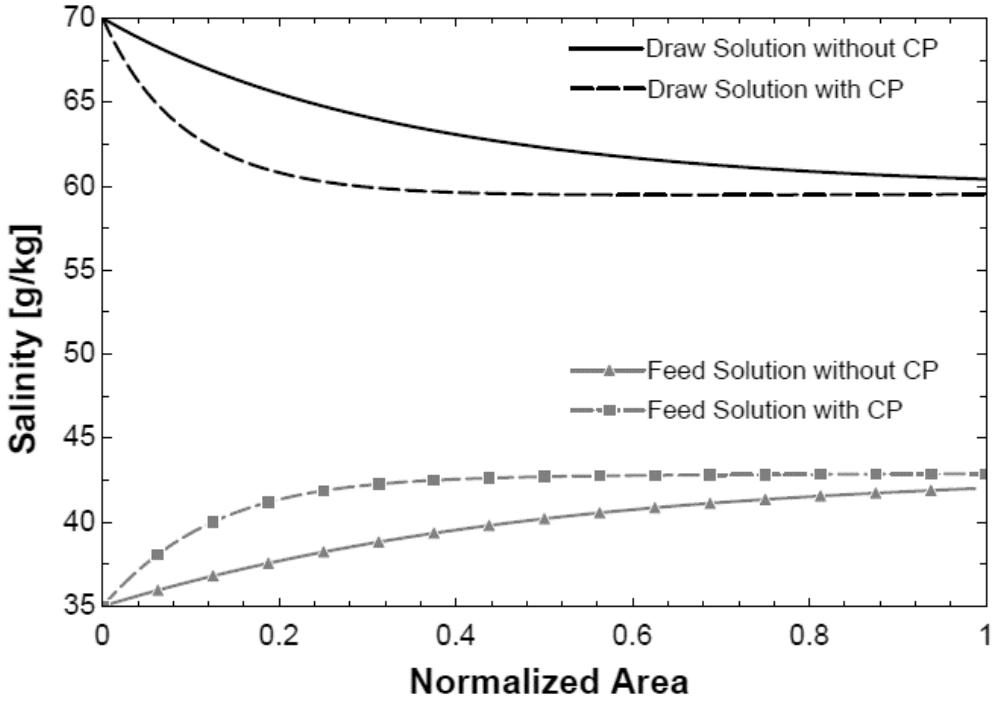

Figure 3.7: Variation of draw and feed streams concentrations along the membrane (parallel flow configuration)

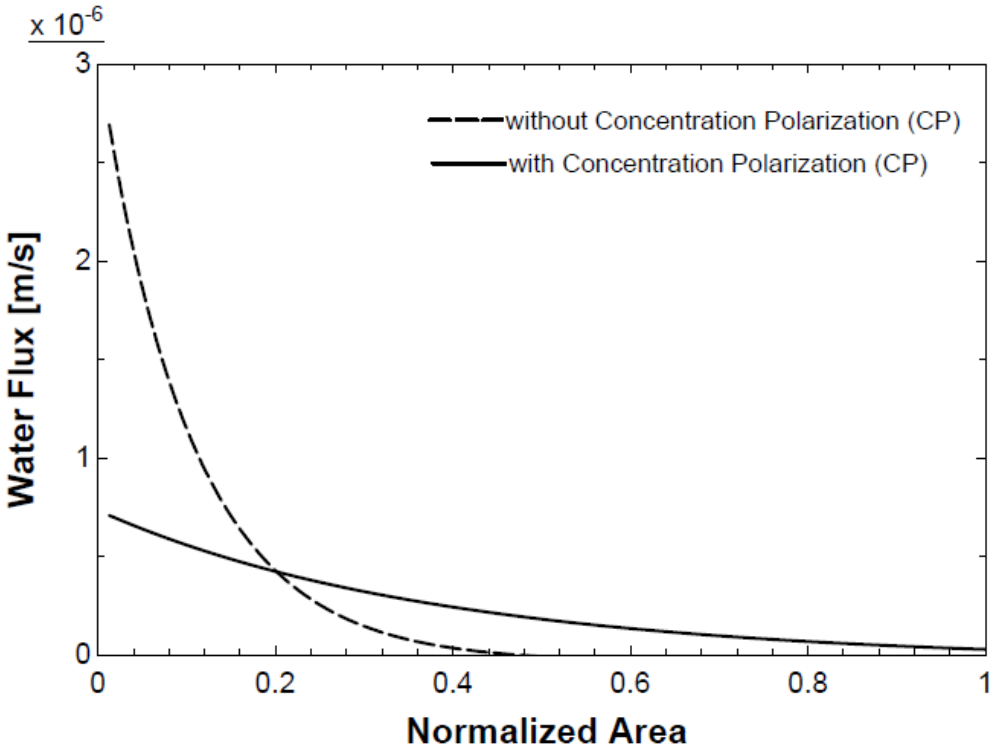

Figure 3.8: Variation of water flux along the membrane (parallel flow configuration)

3.4.2.2 Counter Flow Configuration

The variation of draw and feed salinity along the membrane for counter flow with and without considering the effect of concentration polarization are shown in Figure 3.9. The draw and feed streams are flowing in the opposite direction, the draw stream enters at 70 g/kg and decreases along the membrane area as a result of dilution, with the addition of permeate, leaves the process at 58.7g/kg (54.2g/kg without CP), while the feed stream enters at 35 g/kg and leaves at 43.7g/kg (49.5g/kg without CP). Figure 3.10 represents the water flux variation along the membrane with and without considering the effect of concentration polarization.

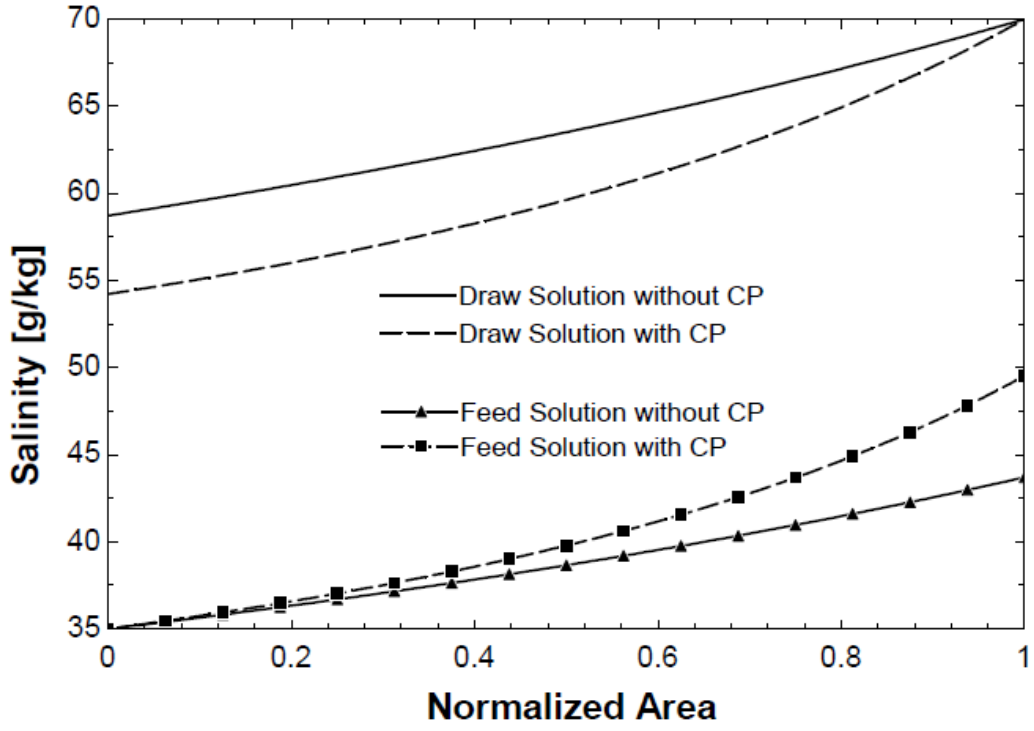

Figure 3.9: Variation of draw and feed streams along the membrane (counter flow configuration)

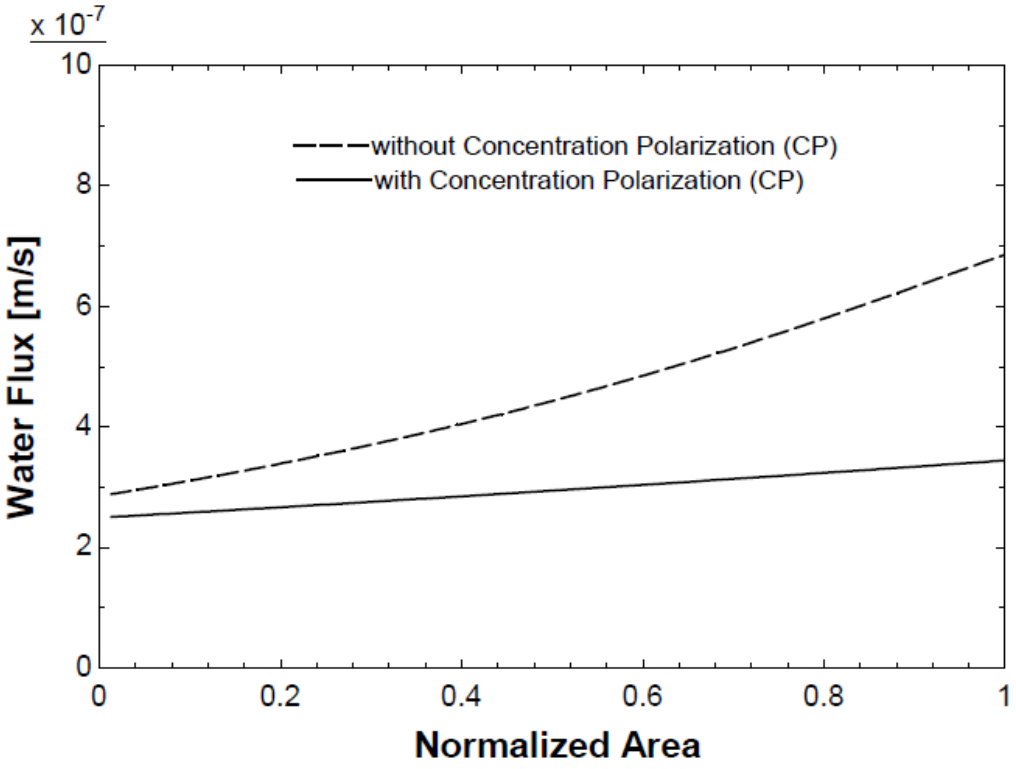

Figure 3.10: Variation of water flux along the membrane (counter flow configuration)

3.4.2.3 Comparison between parallel and counter-flow configurations

The water flux, with and without considering the effect of concentration polarization, along the membrane for parallel and counter flow configuration are shown in Figure 3.11. For parallel flow configuration, it can be noted that after certain value of membrane area the water flux decreases to zero and flux reversal point occurs, which limit the total power output from the system. From the comparison of parallel and counter flow configuration, it can be concluded that the counter flow configuration is the better option. Therefore, for all the further analysis of PRO process the counter flow configuration will be used.

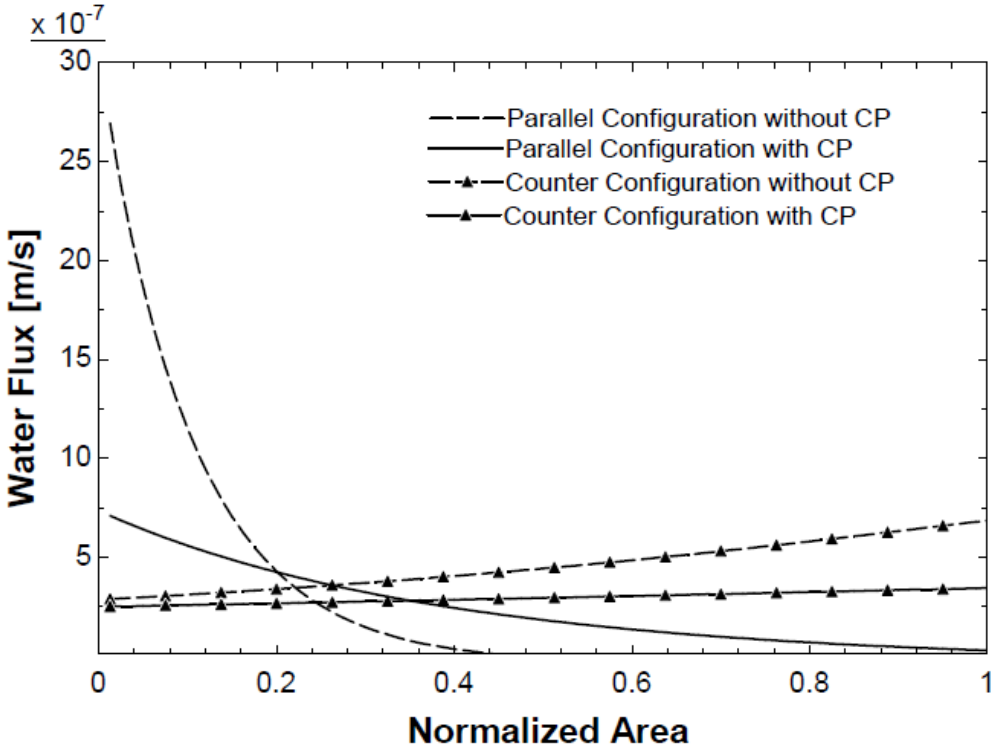

Figure 3.11: Water flux variation along the membrane area for parallel and counter flow configurations

3.4.3 Performance Analysis of PRO System

This section covers the effect of different operating parameters and membrane characteristics on the performance of PRO system for optimized operating conditions. The input to the PRO system is same as used earlier for comparison of parallel and counter flow configuration, given in Table 3.1. The salinity of draw stream is 70g/kg and feed stream is 35g/kg with the intake flow rates of 6.5 kg/s. The total membrane area used for this analysis is 1264 m^2. The counter flow configuration is used for performance analysis of PRO system.

3.4.3.1 Effect of Concentration Polarization (CP)

There is a significant difference in the power density calculations with and without the effect of concentration polarization (CP). The reverse salt diffusion and concentration polarization lowers the effective osmotic pressure difference across the membrane. Consequently, it reduces the amount of permeate transfer from the feed solution to the draw solution, which results in decreasing the power and power density. The effect of concentration polarization becomes even more significant at higher concentration of feed and draw solutions. The effect of concentration polarization can be seen from Figure 3.11 to Figure 3.15

3.4.3.2 Effect of Hydraulic Pressure (ΔP)

As the hydraulic pressure increases, the power density also increases and reaches a maximum value at almost half of the osmotic pressure difference. After that point the power density decreases with the increase of hydraulic pressure until it reaches zero.

3.4.3.3 Effect of Membrane Area (A_m)

Figure 3.12 shows the effect of membrane area on the power density and the power produced by the PRO process. The power density decreases with the increase of membrane area while the power produced increases with the increase of membrane area.

3.4.3.4 Effect of Mixing Ratio (MR)

Figure 3.13 represents the effect of the mixing ratio on the power density with and without considering effect of concentration polarization. The mixing ratio is the ratio of the volumetric flow rate of draw solution to the feed solution. As the mixing ratio increases, the feed stream decreases, consequently the amount of permeate transfer decreases which results in a decrease of the power density.

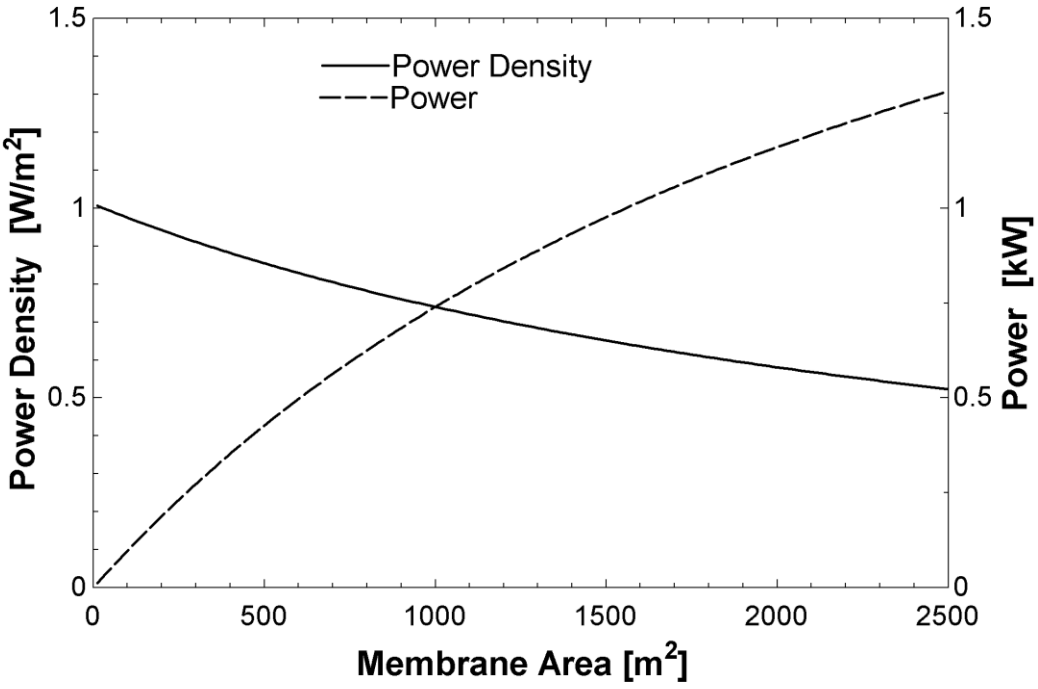

Figure 3.12: Effect of membrane area on power density and power, with considering the effect of CP, by varying membrane area whereas fixing all other parameters.

(w_d = 70 g/kg, w_f = 35 g/kg, MR=1 Q = 6.5 kg/s, T = 25 °C, ΔP = 1400 kPa, A= 1.87×10^{-9} m/s-kPa, B = 1.11×10^{-7} m/s, $K_m = 8.48\times10^{-5}$ m/s, $K_s = 4.5\times10^{5}$ s/m)

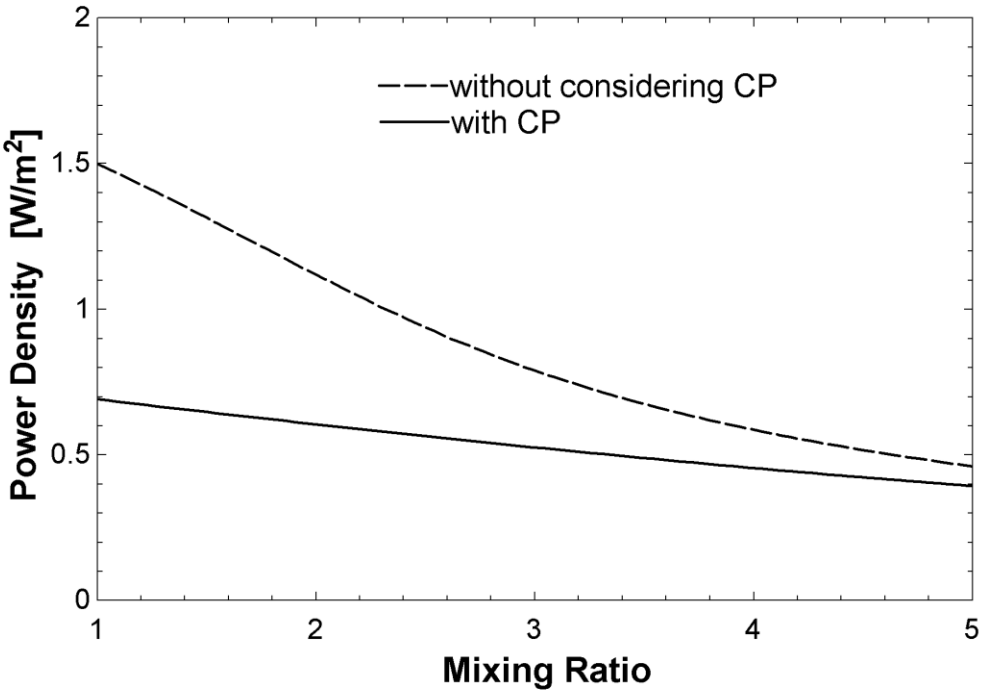

Figure 3.13: Effect of mixing ratio on power density, with and without considering CP, by varying the mixing ratio whereas fixing remaining parameters. (w_d = 70 g/kg, w_f = 35 g/kg, Q = 6.5 kg/s, A_m = 1264 m^2 , T = 25 °C, ΔP = 1400 kPa, A= 1.87×10^{-9} m/s-kPa, B = 1.11×10^{-7} m/s, K_m = 8.48×10^{-5} m/s, K_s = 4.5×10^{5} s/m)

3.4.3.5 Effect of Water Permeability (A)

The performance of PRO system is much dependent on the membrane characteristics particularly the water permeability coefficient. A large increase in the power density will be achieved if the membrane has a high water permeability coefficient. Figure 3.14 indicates that there is a significant increase in the power density with the increase of water permeability coefficient.

3.4.3.6 Effect of Salt Permeability (B)

Salt permeability coefficient is the salt flux transfer through the membrane at unit salt concentration difference. The lower the salt permeability coefficient, the higher the power density can be achieved as shown in Figure 3.15.

3.4.3.7 Effect of Mass Transfer Coefficient (K_m)

Figure 3.16 shows the effect of the mass transfer coefficient on the power density. Power density increases with the increase of mass transfer coefficient.

3.4.3.8 Effect of Solute Resistivity (k_s)

Figure 3.17 represents the effect of solute resistivity on the power density. With the increase of solute resistivity the power density decreases.

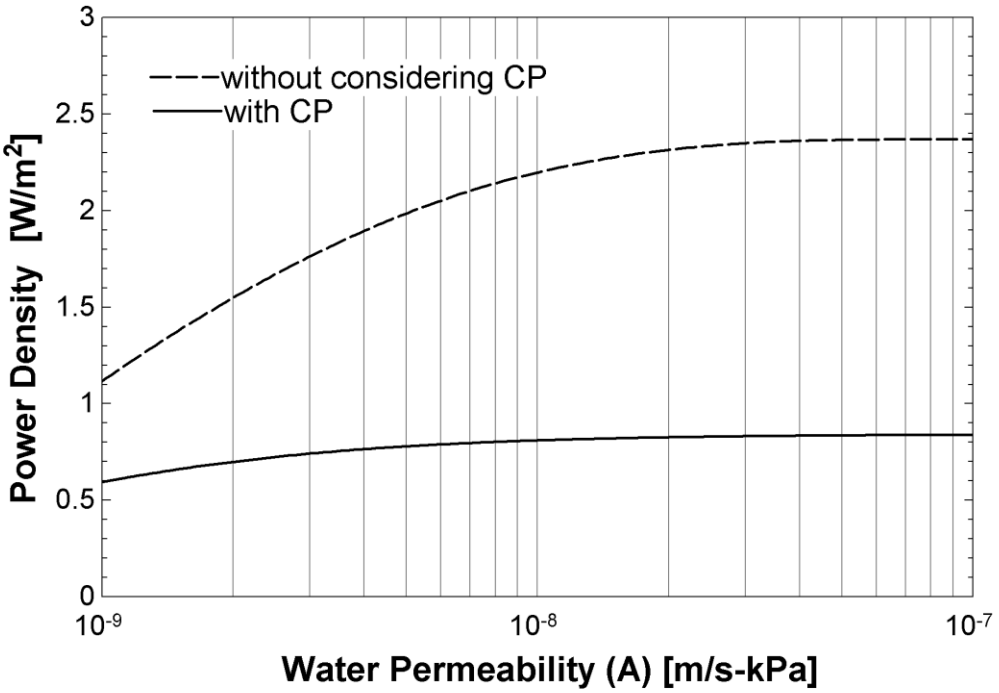

Figure 3.14: Effect of water permeability on power density, with and without considering CP, by varying the values of water permeability whereas all other parameters are fixed. (w_d = 70 g/kg, w_f = 35 g/kg, MR=1, Q = 6.5 kg/s, A_m = 1264 m^2 , T = 25 °C, ΔP = 1400 kPa, B = 1.11×10^{-7} m/s, K_m = 8.48×10^{-5} m/s, K_s = 4.5×10^{5} s/m)

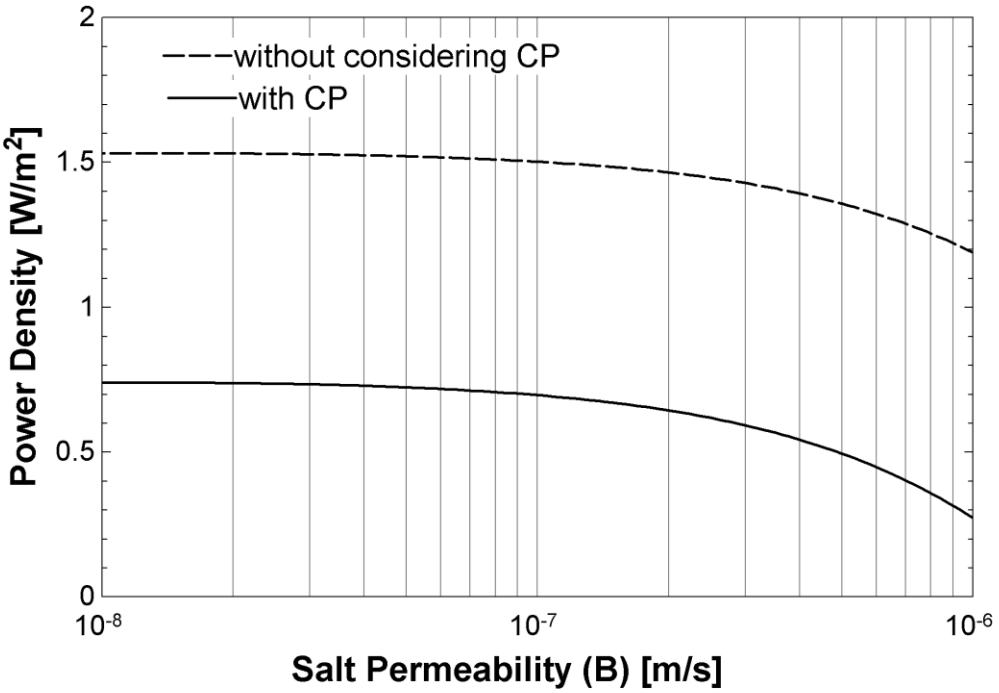

Figure 3.15: Effect of salt permeability on power density, with and without considering CP, by varying the values of salt permeability and fixing all other parameters.

(w_d = 70 g/kg, w_f = 35 g/kg, MR=1, Q = 6.5 kg/s, A_m = 1264 m^2 , T = 25 °C, ΔP = 1400 kPa, A= 1.87×10^{-9} m/s-kPa, K_m = 8.48×10^{-5} m/s, K_s = 4.5×10^{5} s/m)

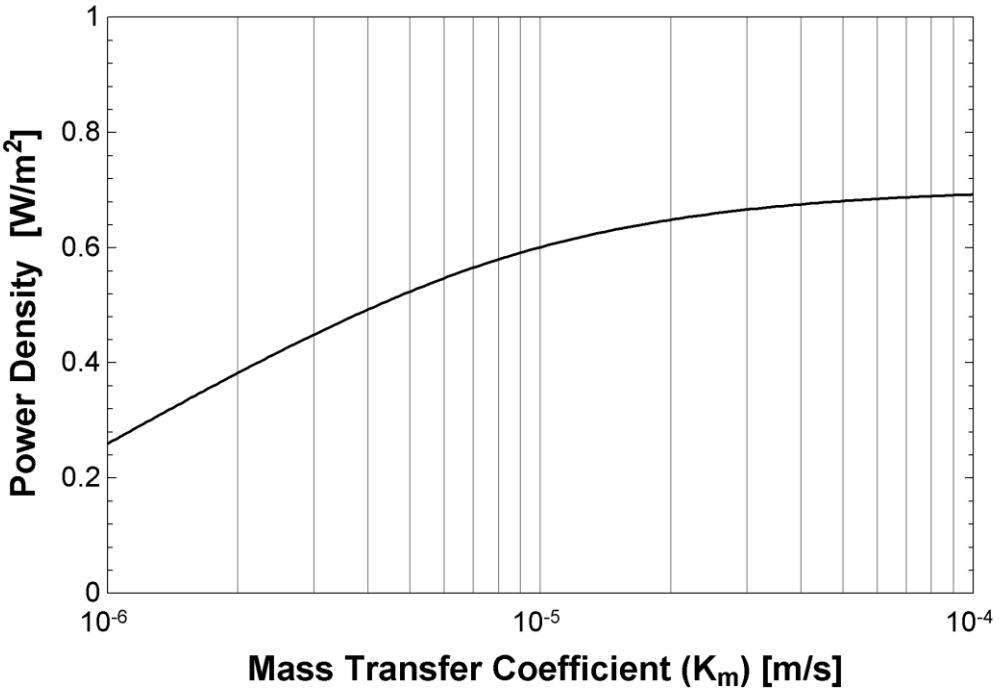

Figure 3.16: Effect of mass transfer coefficient on power density, including the effect of CP, by varying the mass transfer coefficient and fixing all other parameters.

(w_d = 70 g/kg, w_f = 35 g/kg, MR = 1, Q = 6.5 kg/s, A_m = 1264 m^2 , T = 25 °C, ΔP = 1400 kPa, A= 1.87×10^{-9} m/s-kPa, B = 1.11×10^{-7} m/s, K_s = 4.5×10^{5} s/m)

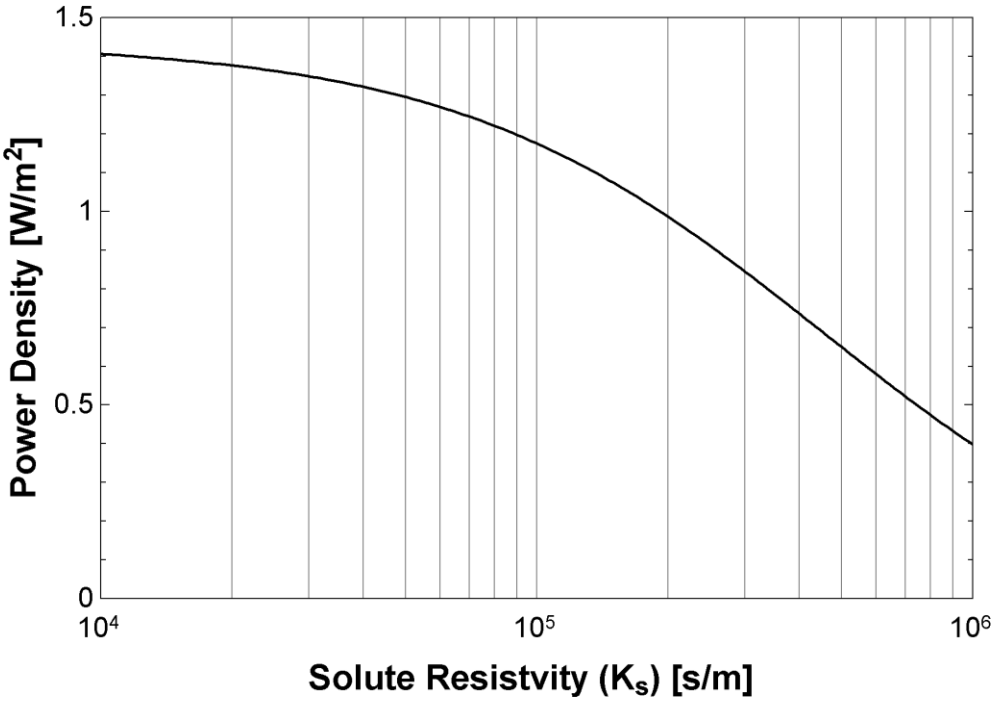

Figure 3.17: Effect of solute resistivity on power density, with the effect of CP, by varying the solute resistiving whereas all other parameters are fixed.

(w_d = 70 g/kg, w_f = 35 g/kg, MR=1, Q = 6.5 kg/s, A_m = 1264 m^2 , T = 25 °C, ΔP = 1400 kPa, A= 1.87×10^{-9} m/s-kPa, B = 1.11×10^{-7} m/s, K_m = 8.48×10^{-5} m/s)

3.4.3.9 Effect of Temperature

The effect of temperature on power density and water flux is shown in Figure 3.18. The water flux and power density increase with the increase of temperature of the flow streams, because with the increase of temperature the water permeability coefficient increases and the salt permeability coefficient decreases. The inlet temperature of feed seawater is in the range from 15 to 35 °C, while the temperature of the disposed brine of desalination plants is normally higher than the feed seawater.

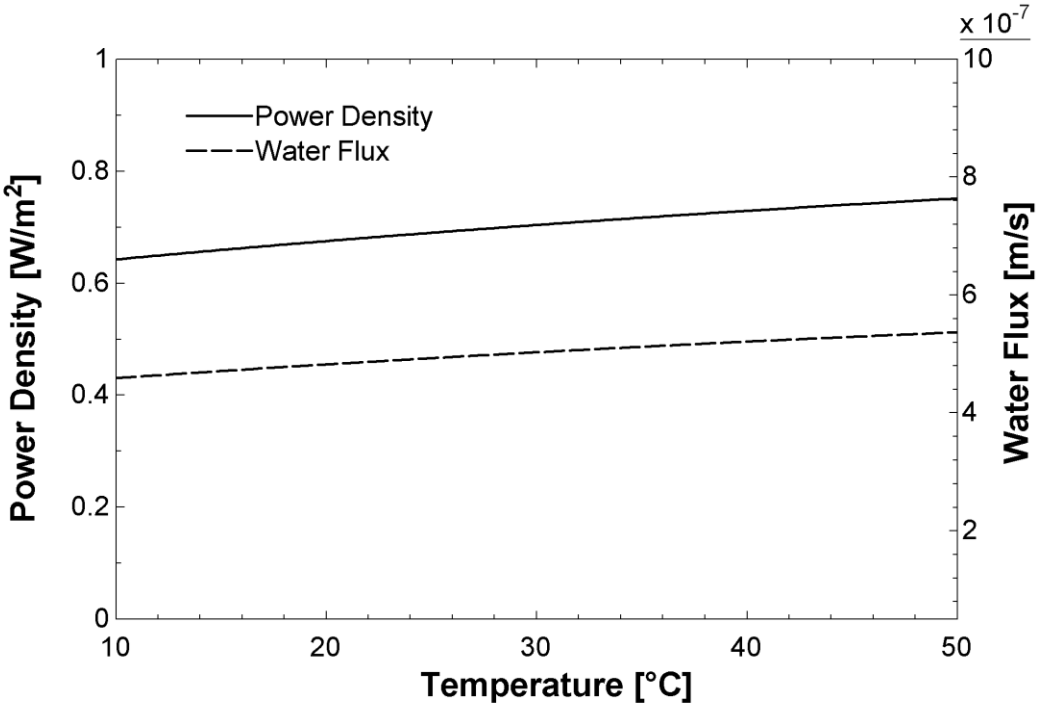

Figure 3.18: Effect on temperature on power density and water flux, with the effect of CP, by varying the temperature of feed and draw stream while fixing the remaining parameters. (w_d = 70 g/kg, w_f = 35 g/kg, MR=1, Q = 6.5 kg/s, A_m = 1264 m^2 , ΔP = 1400 kPa, A= 1.87×10^{-9} m/s-kPa, B = 1.11×10^{-7} m/s, K_m = 8.48×10^{-5} m/s, K_s = 4.5×10^{5} s/m)

CHAPTER 4

ENERGY UTLIZATION OF BRINE FROM DESALINATION PLANTS

All desalination plants reject brine which is at a higher salinity than the supplied feed seawater. This brine is usually discharged back to the feed seawater source. The discharge of the concentrated brine can damage aquatic ecosystems in particular if it contains pretreatment chemicals. Diluting this brine will reduce the environmental hazards associated with the discharged high salt concentration brine. Energy can be generated when the high salinity brine stream is mixed with the low salinity feed stream before discharging it. It is important to mention here that PRO technology has not been introduced as an energy recovery device (ERD) in desalination plants.

4.1 MSF-PRO

In this work, the PRO system is used to estimate the potential of energy generation from the disposed brine of a Multistage Flash (MSF) desalination plant. The blow down brine from the Jubail MSF desalination plant in Figure 2.6 is used as a draw solution in the PRO system. The total brine disposal from the plant is 536 kg/s with a salinity of 70g/kg. Figure 4.1illustrates the proposed MSF-PRO system.

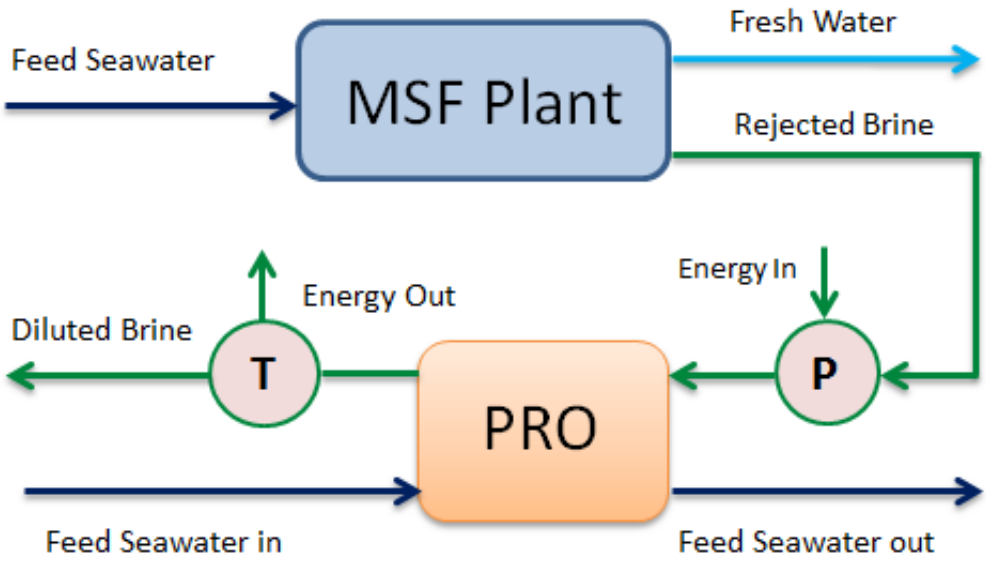

Figure 4.1: Proposed MSF-PRO plant

4.1.1 Operating Parameters

The proposed PRO system for energy recovery from brine disposal is illustrated in Figure 4.2. The one dimensional mathematical model developed in Section 3.3 is used to estimate the power generation. The counter flow configuration is used and the membrane characteristics are taken from a commercially available RO membrane SWC5 1640 (Hydranautics corporation) [70]. The membrane characteristics and operating parameters for the PRO system are listed in Table 4.1. The total blow down from the desalination plant is 536kg/s with a salinity of 70 g/kg. The feed seawater for the MSF plant has a salinity of 46.5 g/kg, which is used as a feed solution for the PRO system. The area of one pressure vessel is 1264m^2, with an intake draw stream of 6.5 kg/s.

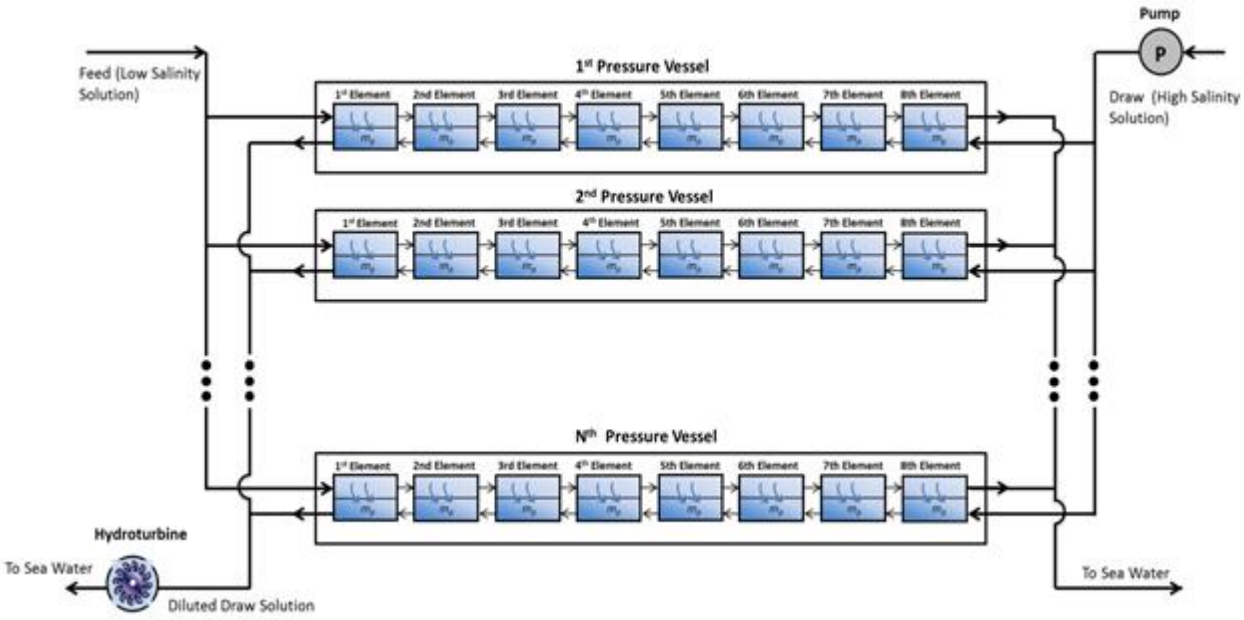

Figure 4.2: Pressure retarded osmosis (PRO) system in parallel vessels

Table 4.1: Input Parameters of PRO System

Parameter	**Value**
Water permeability coefficient (A)	1.87×10^{-9} (m/s-kPa)
Salt permeability coefficient (B)	1.11×10^{-7} (m/s)
Mass transfer coefficient (K_m)	8.48×10^{-5} (m/s)
Solute resistivity (K_s)	$4.5\times10^{+5}$ (s/m)
Feed solution salinity (w_f)	46.5 (g/kg)
Draw solution salinity (w_d)	70 (g/kg)
Intake draw stream to one pressure vessel	6.5 (kg/s)
Mixing ratio	1.0
Total blow down from MSF plant (draw solution)	536 (kg/s)

4.1.2 Results and Discussion

The variation of the draw and feed salinity along the normalized membrane area is shown in Figure 4.3. The draw stream enters at a salinity of 70 g/kg and decreases along the membrane due to addition of permeate flow and exits at a salinity of 59.4 g/kg. On the other hand, the feed stream enters the system at salinity of 46.5 g/kg and leaves at 56.5 g/kg. The normalized area is the accumulated area at a given location divided by the total membrane area and it ranges from zero to one.

Water flux transfer from the feed stream to the draw stream and it varies with the pressure difference across the membrane. However, the salts transfers in the opposite direction of water flux, from the draw stream (high salinity) to the feed stream (low salinity), due to the salt concentration difference. The variation of water flow rate, salt flow rate with and without considering concentration polarization (CP) are illustrated in Figure 4.4. As the pressure difference increases, the water flow rate also increases. Similarly salt flow rate also increases, as the difference between salinities is higher at the later stages of the system.

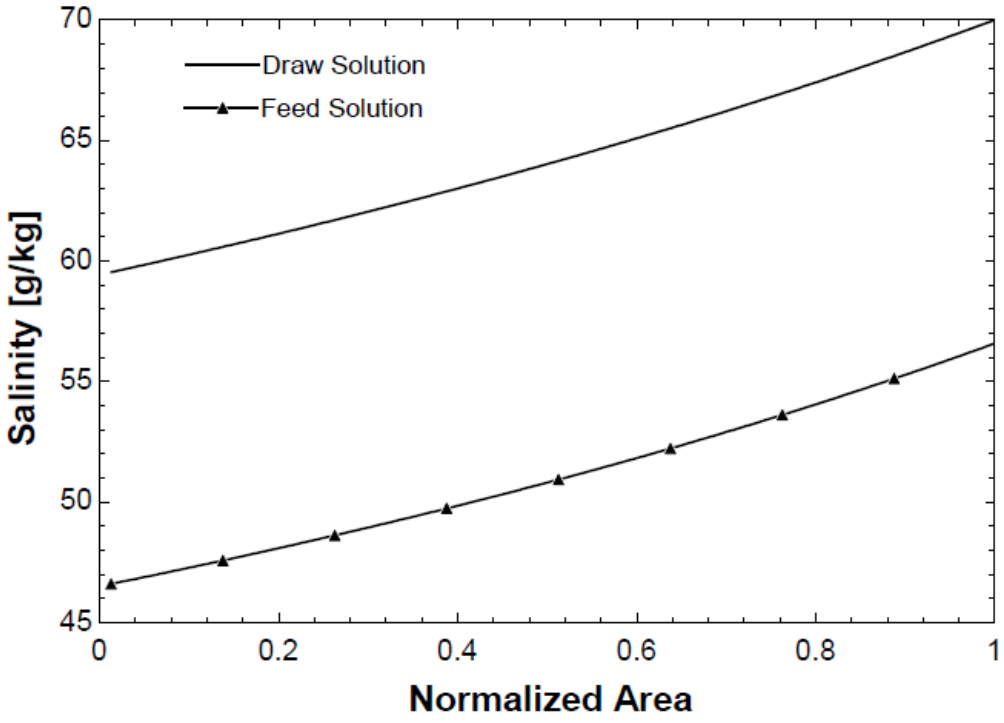

Figure 4.3: Variation of draw and feed solution salinity along the membrane, with CP

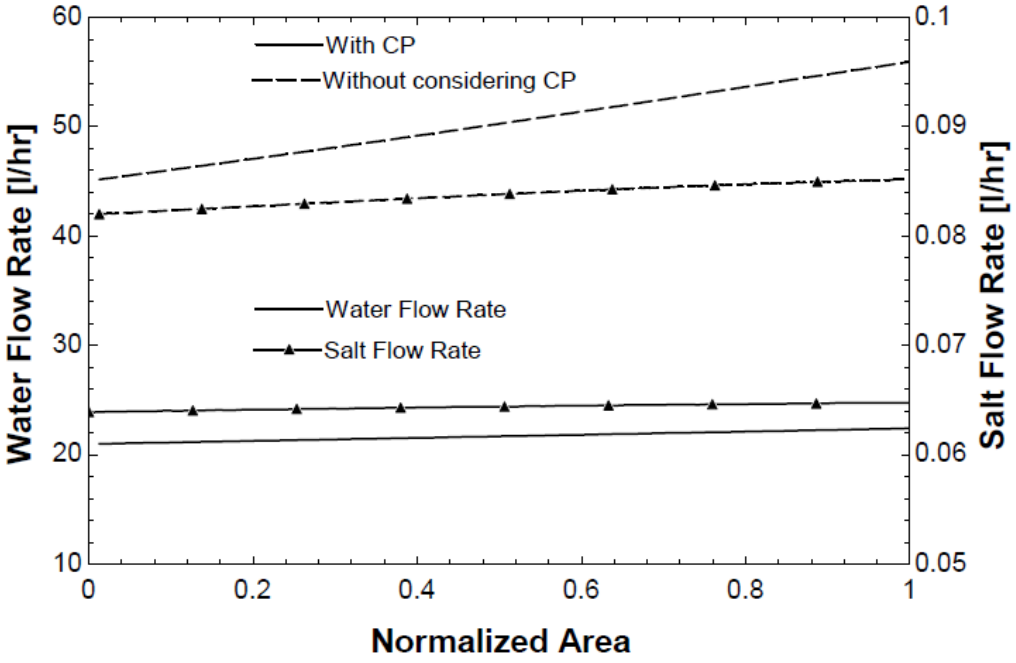

Figure 4.4: Variation of water flow rate, salt flow rate with and without considering CP

The total power produced by the PRO system with and without considering concentration polarization (CP), as a function of hydraulic pressure difference, is shown in Figure 4.5. It is noted that the maximum power obtained from the PRO plant without considering CP is 72.1 kW. Considering the effect of CP, the power produced is 30.8 kW at a hydraulic pressure of 1010 kPa. This power is very small compared to the pumping power required for the Jubail MSF Desalination plant (i.e., 3649 kW) [14]. However, this process can be improved by optimizing the operating conditions and the system configuration. The maximum reversible mixing work that can be achieved from this PRO system with streams of 70 and 46.5 g/kg is 0.4 kJ/kg (or 214.4 kW for the draw solution of 536 kg/s). Therefore, the proposed system shown in Figure 4.1 has a second law efficiency of about 33% (14% with considering CP). The results are much dependent upon membrane characteristics like the water permeability coefficient and flow/module conditions such as the mass transfer coefficient. An improvement in the membrane properties could significantly increase the power produced by PRO plant. About 46% (16% with considering CP) increase in power could be achieved if a membrane with water permeability coefficient of 2×10^{-8} instead of 1.87×10^{-9} (m/s-kPa) is used (Figure 4.6).

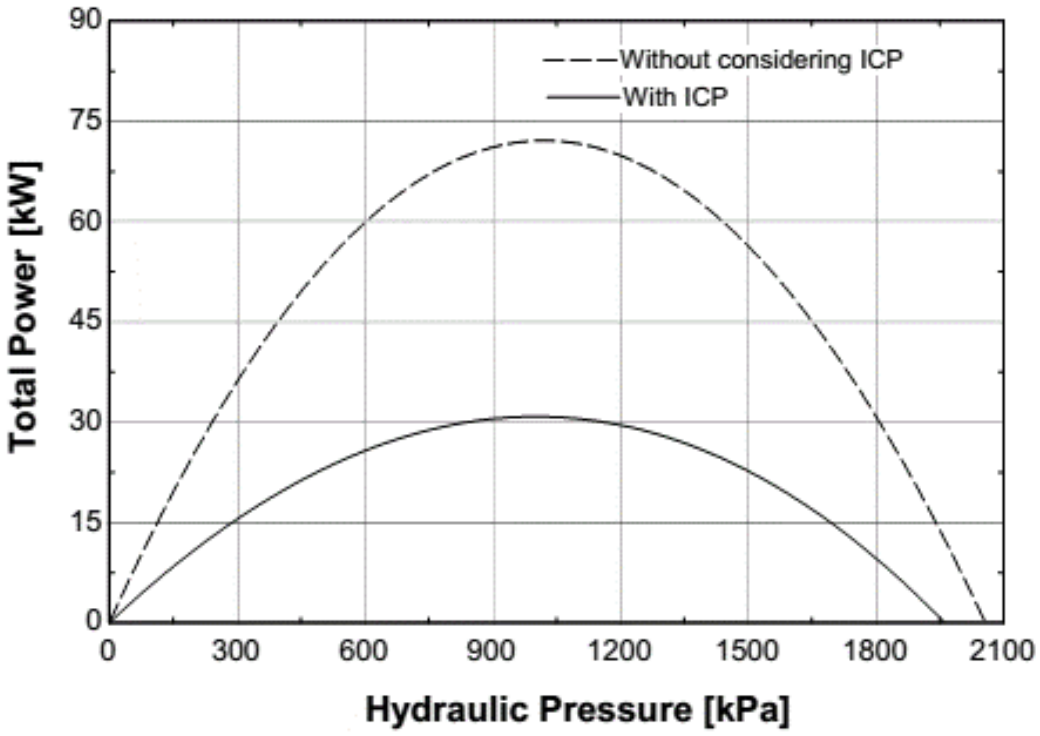

Figure 4.5: Total power produced by PRO system as a function of hydraulic pressure with and without considering CP

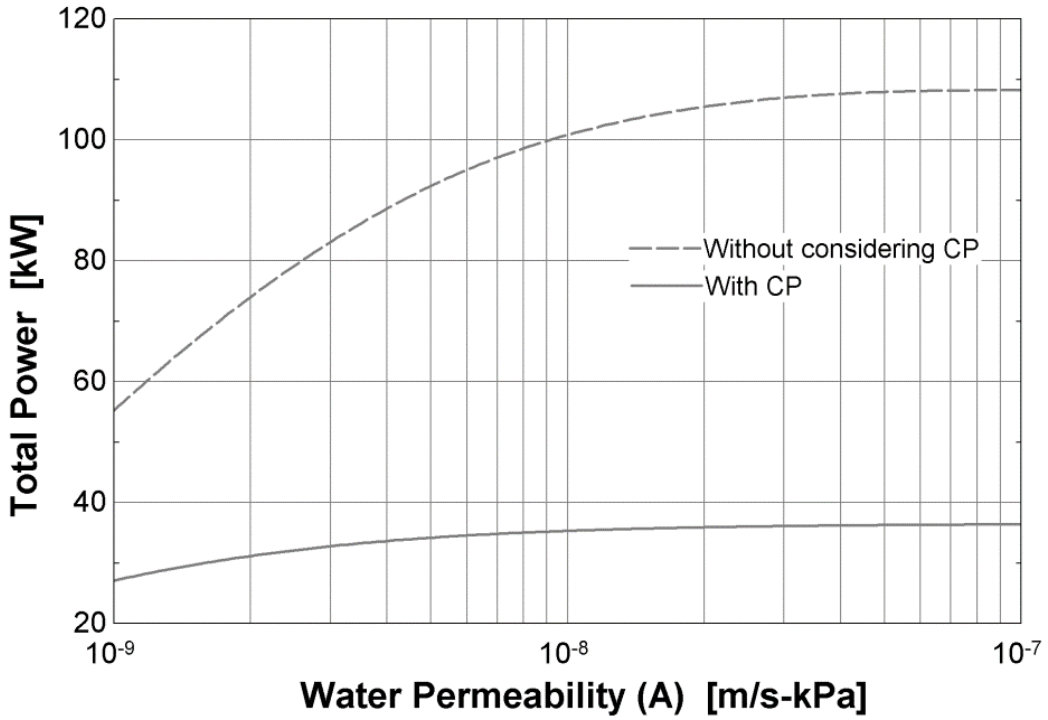

Figure 4.6: Effect of water permeability on power produced by PRO system

4.2 RO-PRO

In this section, the pressure retarded osmosis (PRO) system is used to estimate the energy generation using the rejected brine of reverse osmosis (RO) desalination plant. The PRO system is coupled with RO plant, the proposed RO-PRO system is illustrated in Figure 4.7. The rejected brine from RO plant, at high pressure, is first depressurized up to the optimum hydraulic pressure required for the PRO system and then used as a draw solution in PRO. Feed seawater is at the same salinity as used for the RO feed. During the osmosis process the water permeates from the feed solution to the draw solution. The exit increased draw solution is now depressurized using hydro turbine (assuming turbine of 100% efficiency).

The power obtained using the RO turbine can be calculated as follow

$$\text{Turbine Power (RO)} = Q_{\text{d,in}} (\text{P}_{RO} - \text{P}_{d,in}) \tag{4.1}$$

Similarly the increased power produced using the PRO process is

$$\text{Turbine Power (PRO)} = (Q_{\text{d},in} + Q_p)(\text{P}_{d,in} - \text{P}_{\text{f},in}) \tag{4.2}$$

Finally the total power obtained from the RO-PRO system is

$$\text{Total Power} = \text{Turbine Power (RO)} + \text{Turbine Power (PRO)} \tag{4.3}$$

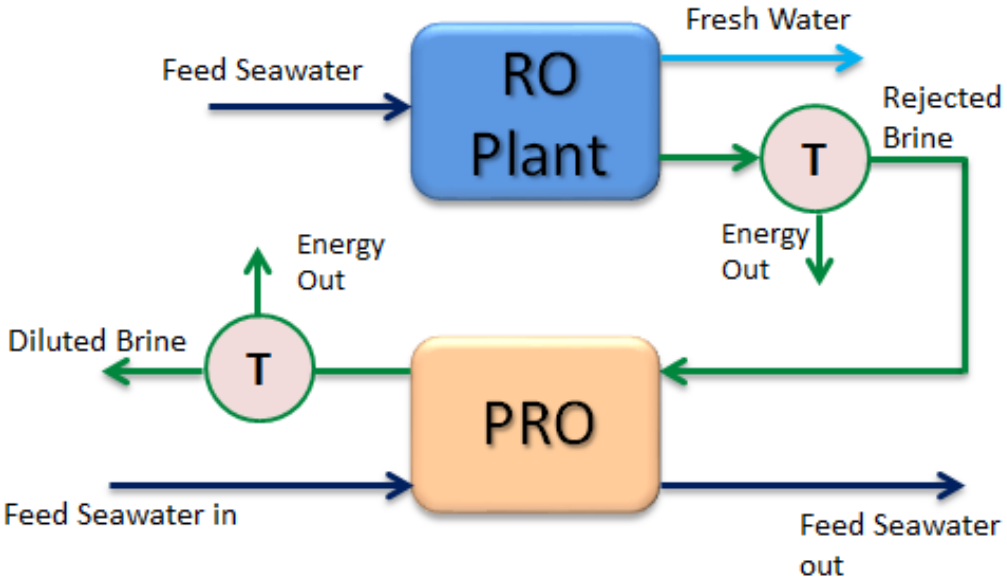

Figure 4.7: RO-PRO plant

4.2.1 Results and Discussion

The analysis of the RO-PRO system is performed using the data from "Sharm El-Sheikh RO Desalination Plant" reported by Mabrouk *et al*. [71], the reported data is listed in Table 4.2. The total rejected brine from the reverse osmosis (RO) desalination plant is 94.5 kg/s with a salinity of 64g/kg at a pressure of 6700 kPa. The feed solution for the system has a salinity of 45 g/kg. The membrane characteristics are same as used earlier, shown in Table 4.1. The area of one pressure vessel is 1264m^2, with intake draw stream is 6.5kg/s.

Table 4.2: Sharm El Sheikh RO Desalination Plant Data [71]

Parameter	Value
Daily Product capacity	0.0405 m^3/s
Feed Quantity	0.1354 m^3/s
Reject quantity	0.0945 m^3/s
Feed TDS	45,000 ppm
Reject TDS	64,000 ppm
Feed temp	27 ℃
Rejected Brine Pressure	6700 kPa

The detailed mathematical model for PRO, described in Section 3.3 for counter flow configuration, is used to estimate the power generation from the rejected brine of seawater reverse osmosis desalination plant.

The power obtained using RO and PRO turbines and the total power produced by the RO-PRO system, considering the effect of concentration polarization, as a function of hydraulic pressure is shown in Figure 4.8. With the increase of hydraulic pressure the power produced by the RO turbine decreases while the power produced using PRO turbine increases. Whereas, the total power produced from the RO-RPO system is first increased up to about the half of the osmotic pressure difference while it decreases after that. The maximum power obtained from RO-PRO system is 631.4 kW (641.5 kW without CP) at a hydraulic pressure of 800 kPa (Figure 4.9).

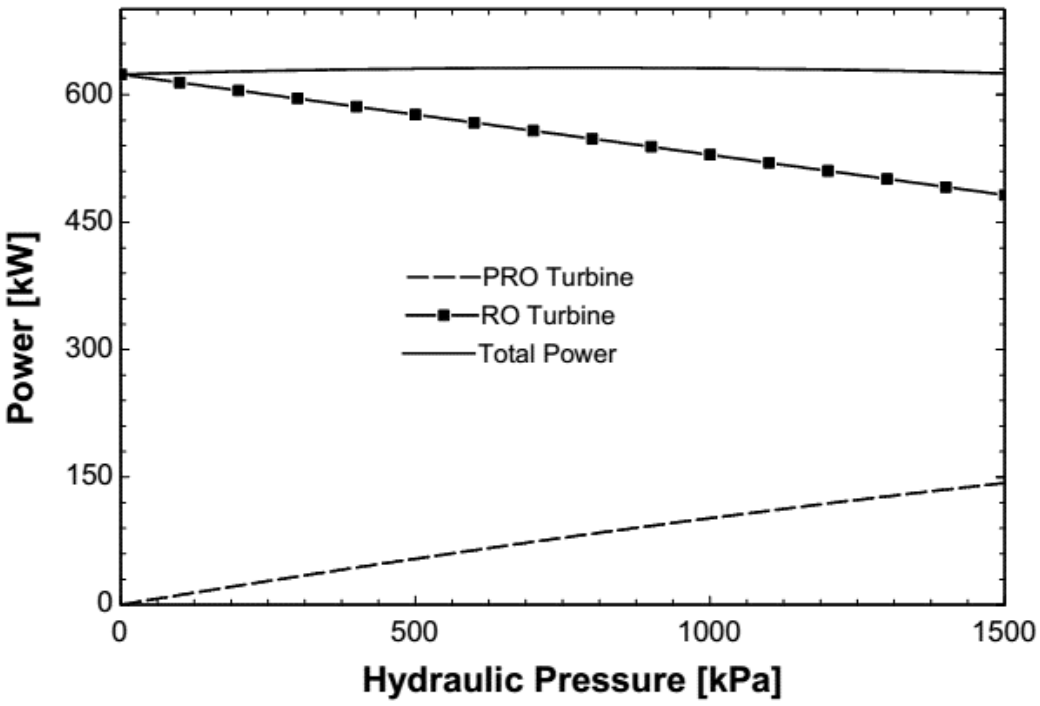

Figure 4.8: Power produced from PRO system using the brine rejected from RO desalination plant as it varies with the hydraulic pressure

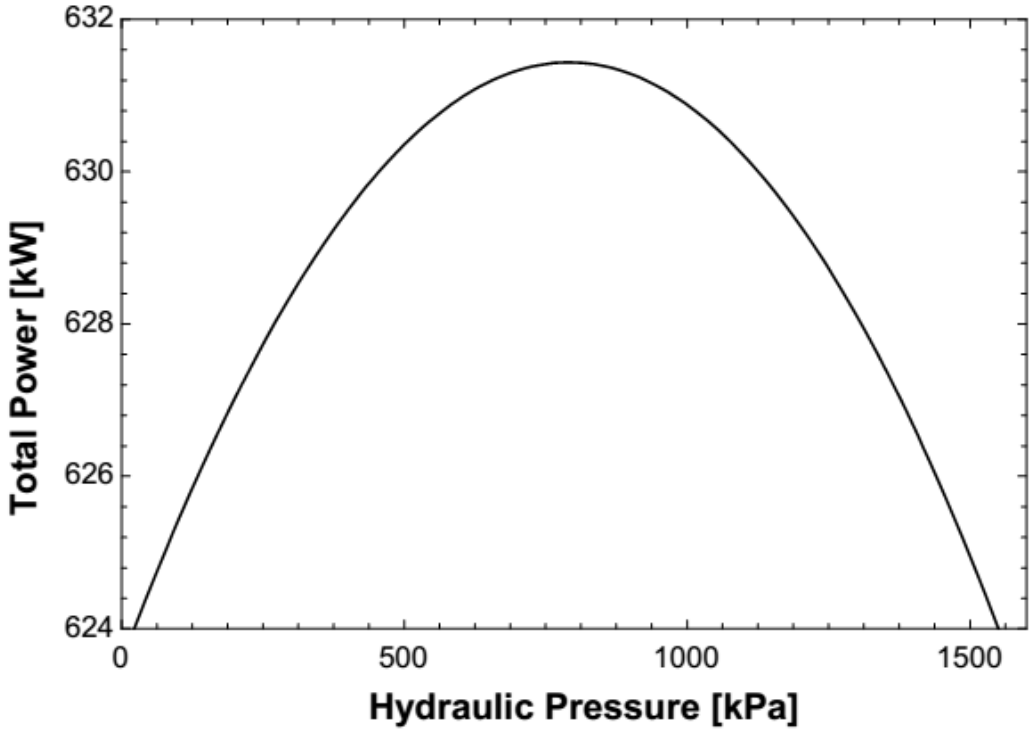

Figure 4.9: Power produced by PRO system with the variation of hydraulic pressure

4.3 POSSIBLE COMBINATION OF STREAMS

Different feed and draw concentrations are used to estimate the potential of power production from pressure retarded osmosis process. There are four different types of streams with different concentrations available, which are normally categorized as following

1. Fresh water (0 ppm)
2. Wastewater (5,000-10,000 ppm)
3. Seawater (35,000-47,000 ppm)
4. Discharged Brine (70,000 ppm)

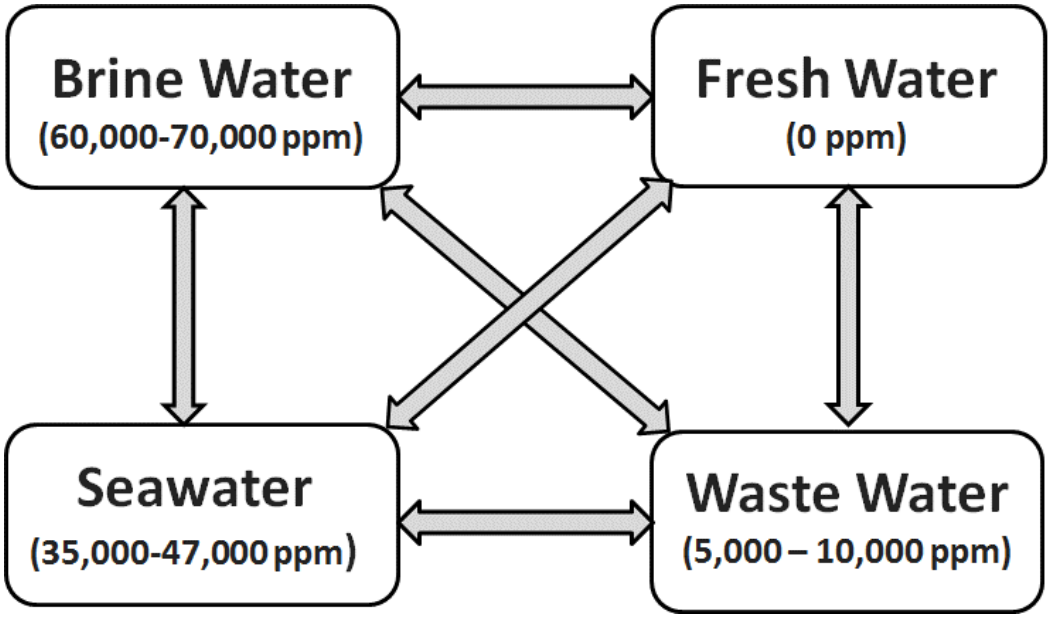

Figure 4.10: Possible combinations of feed and draw solutions streams for PRO

The membrane properties are taken from Osays Water Incs. reported by Hancock *et al*. [72] and operating parameters are taken from [73] which are mentioned in Table 4.3. In this study, the analysis of PRO is performed using different combinations of available feed and draw solution to achieve maximum power production per each cubic meter of the draw stream.

Table 4.3: Input Parameters of PRO System

Parameter	**Value**
Membrane Area	1700 (m^2)
Water permeability coefficient (A)	1.13×10^{-8} (m/s-kPa)
Salt permeability coefficient (B)	1.73×10^{-7} (m/s)
Mass transfer coefficient (K_m)	8.48×10^{-5} (m/s)
Solute resistivity (K_s)	$1.76\times10^{+5}$ (s/m)
Intake draw stream	12.7 (kg/s)
Mixing ratio	1.0

4.3.1 Results and Discussion

Several possible combinations of salinities are used to estimate the energy generation using pressure retarded osmosis. Results are reported in Table 4.4 using the mathematical model provided in Section 3.3 for the power with and without considering the effect of concentration of polarization. In addition, the maximum reversible work is calculated using Gibbs energy equation.

The maximum power obtained if disposed brine, from desalination plant, is used as a draw solution and fresh water is used as a feed solution in the pressure retarded osmosis process. This scenario is not a feasible option as there is already shortage of fresh drinking water in Middle East and specifically in Saudi Arabia.

The best option in Saudi Arabia is to use brine and wastewater as a draw and feed streams respectively. By using these two stream the potential of power production is highest and this can also be a practical option as both of these stream are normally dumped. To fully use these resources, future installment of desalination and wastewater plants should be built near to each other to exploit the useful energy from these two wasted streams.

The combination of brine and seawater does not provide sufficient power. The amount of work produces is low compared to the work consumed in the desalination plants. This case has been analyzed comprehensively in Section 4.1.

The use of seawater as a draw solution with the fresh water as a feed is also a good solution. This can be possible where the river water is pouring into the Sea and pressure osmosis process (PRO) can be used to obtained energy from endless resources. For this case special geographic location is required and this site is not available in Saudi Arabia.

The wastewater can be used as a feed solution with the draw solution of seawater. This combination does provide some power but need detailed economic studies to use these two streams in the PRO systems.

The wastewater and fresh water is also used to estimate the useful power but as the water chemical potential between these two are very low. Hence, these are not feasible to use for power generation using PRO.

Table 4.4: Summary of Results for Different Combinations of Draw and Feed Streams

Draw Stream	**Feed Stream**	**Max. Reversible work**	**Ideal Work (without CP)**	**Actual Work (with CP)**	**Notes**
(ppm)	**(ppm)**	**(kWh/m3)**	**(kWh/m3)**	**(kWh/m3)**	
Brine (70,000)	Fresh water	3.19	0.626	0.534	Not practical
	Waste water (5,000)	2.467	0.525	**0.35**	**High potential**
	Sea water (35,000)	0.339	0.115	0.0583	Low work produced compared with work consumed
Seawater (35,000)	Fresh water	1.05	0.257	0.209	Geographic location
	Waste water (5,000)	0.701	0.164	**0.105**	**Need detailed economic studies**
Wastewater (5,000)	Fresh water	0.027	0.011	0.009	Not practical

CHAPTER 5

PROPOSED DESIGNS FOR PRO SYSTEMS

The following two designs are proposed to obtain maximized energy from PRO system using fixed amount of intake draw stream.

1. Multi-Stage PRO
2. Multi-Pass PRO

5.1 MULTI-STAGE PRO

This system consists of multi-stage pressure retarded osmosis (PRO) units. In a single stage, water from low salinity feed solution permeates through membranes to the pressurized high salinity draw solution, which is then depressurized by hydro turbine to obtain power output. As a result of water transfer from low salinity feed solution, the exit feed solution from the PRO unit will be having high salinity depending on the flow configuration (Parallel or Counter flow). This exit feed solution from first PRO unit is pressurized and used as a draw solution in the next PRO stage and is used with the low salinity feed solution. Similarly, the water from the low feed solution penetrates though

the semi permeable membrane to the high salinity draw solution which, with higher volume flow rate, is depressurized to get power output by a hydro turbine. Similar to the exit feed solution of the first stage the exit feed solution of second stage also has higher salinity which is used for the next stage as a high salinity draw solution, and this can be extended to N-stages. Consequently, by using the fixed amount of discharged brine of seawater desalination plants the total power output is significantly improved. Figure 5.1 and Figure 5.2 illustrate schematic diagrams of parallel flow and counter flow multi-stage PRO systems.

The input flow rate and concentration of draw stream for each stage can be calculated by using the following formulas

$$Q_{d,in_i} = Q_{\mathrm{f},out_{i-1}} = Q_{\mathrm{f},in_{i-1}} - Q_{\mathrm{p}_{i-1}} \tag{5.1}$$

$$w_{d,in_i} = w_{\mathrm{f},out_{i-1}} \tag{5.2}$$

where the “i” ranges from 1 to n number of stages. Similarly the total power produced by the multi-stage PRO system is the summation of power produced by each PRO unit and can be calculated using Eq. (5.3)

$$\text{Total Power} = \sum_{k=1}^{n} Q_{\mathrm{p}_k} \Delta P_k \tag{5.3}$$

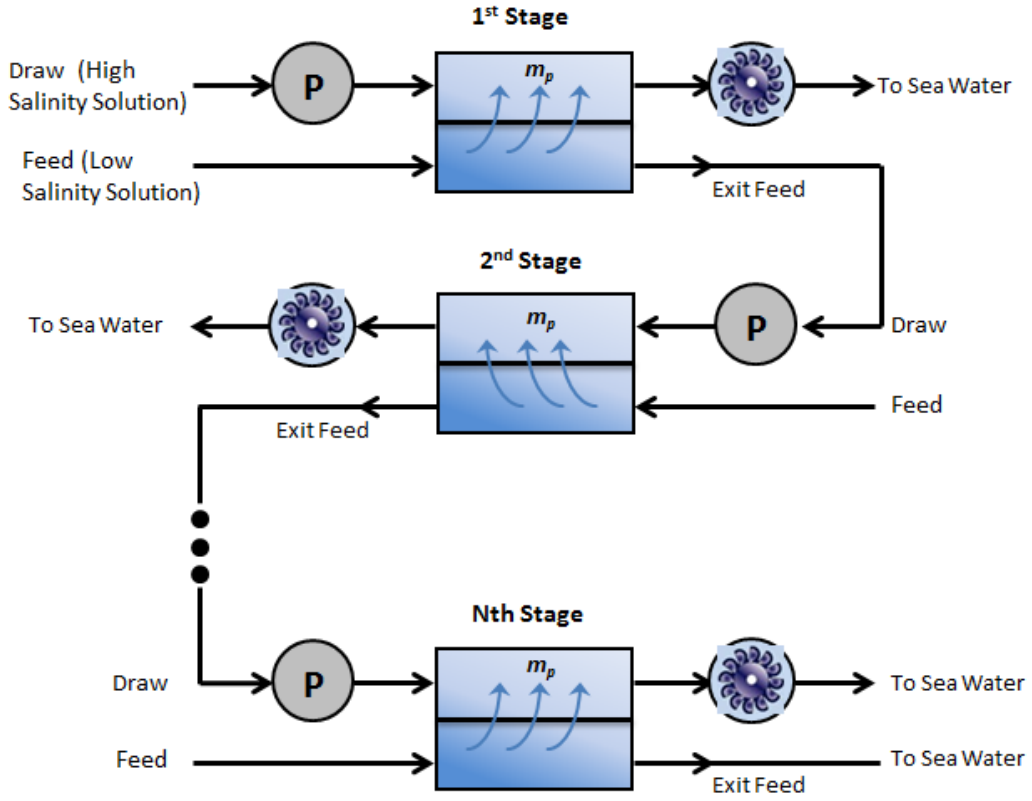

Figure 5.1: Multi-stage parallel-flow PRO system

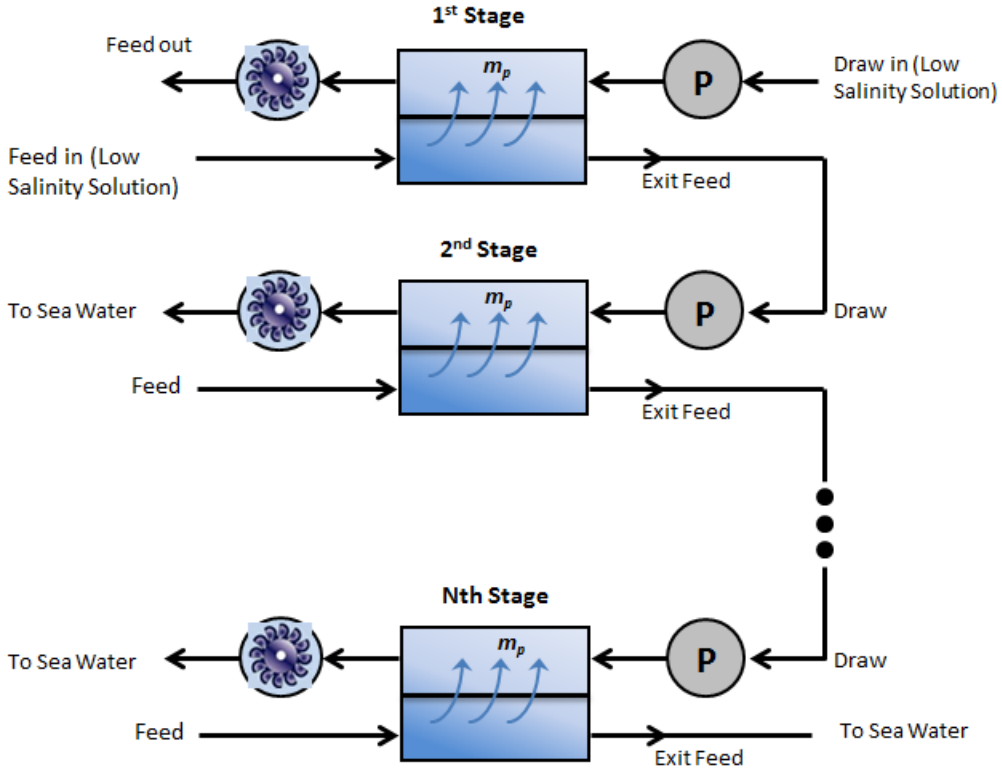

Figure 5.2: Multi-stage counter-flow PRO system

5.2 MULTI-PASS PRO

This system consists of multiple passes of draw streams. In this process, the exit draw stream of first PRO unit will be depressurized through a hydro turbine to the optimum hydraulic pressure of the second pass. Now the diluted brine enters as an input draw stream, with a new feed stream, to the second PRO pass. The exit draw stream of second unit will be depressurized to the optimum hydraulic pressure of the third PRO unit and this can be extended to n-passes. It can be summarized for the multi-pass PRO system that the exit stream of each stream will be depressurized to the optimum hydraulic pressure of the next unit and will also enter as an input draw stream for next unit. This will drastically increase the total power produced for the fixed amount of input draw stream. The schematic diagrams of parallel flow and counter flow multi-pass PRO systems are shown in Figure 5.3 and Figure 5.4.

The intake flow rate and salinity of draw stream to each unit (from second onward) will be as follow

$$Q_{d,in_i} = Q_{\mathrm{d},out_{i-1}} = Q_{\mathrm{d},in_{i-1}} + Q_{\mathrm{p}_{i-1}} \tag{5.4}$$

$$w_{d,in_i} = w_{\mathrm{d},out_{i-1}} \tag{5.5}$$

The total power produced by the multi-pass PRO system can be calculated using the following equation

$$\text{Total Power} = Q_{\text{p},1}(\text{P}_{d,1} - \text{P}_{d,2}) + \sum_{k=2}^{n} Q_{d,out_k}(\text{P}_{d,\text{k}} - \text{P}_{d,\text{k}+1}) \quad \text{where } \text{P}_{d,n} = 101.3 \text{ kPa} \tag{5.6}$$

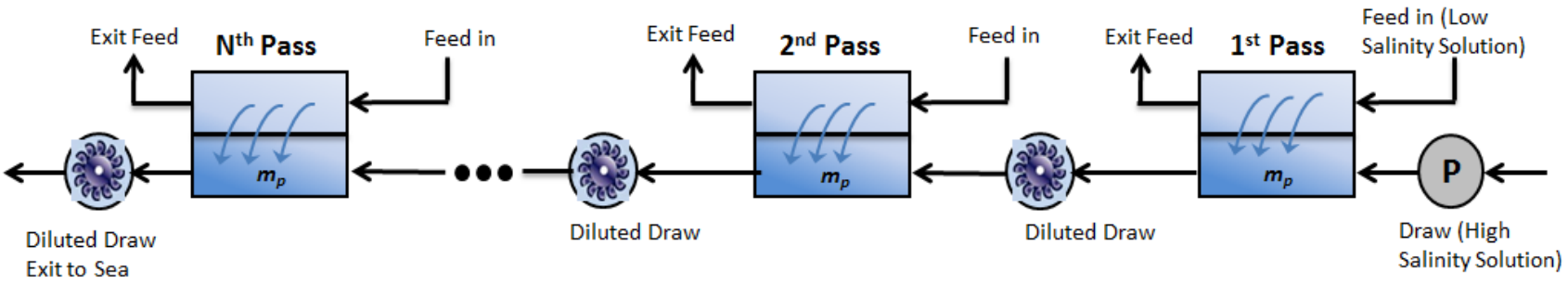

Figure 5.3: Multi pass parallel-flow PRO system

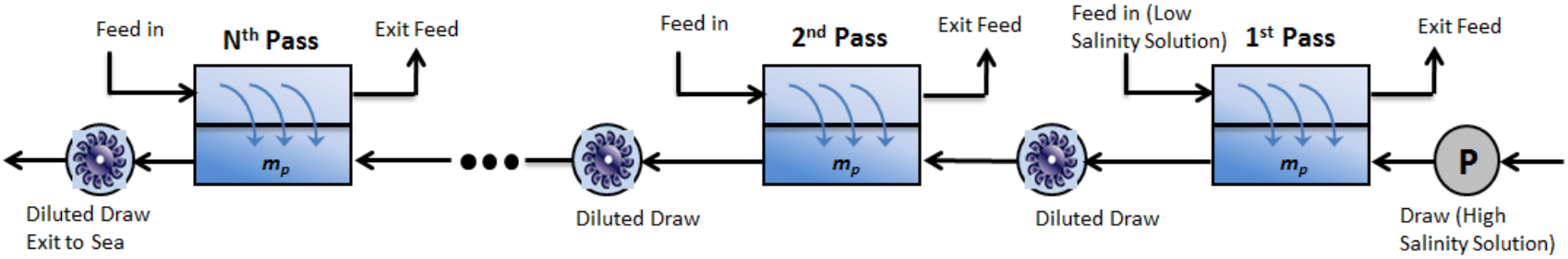

Figure 5.4: Multi pass counter-flow PRO system

5.3 RESULTS AND DISCUSSION

The mathematical model for PRO, explained in Section 3.3, is used to analyze the performance of multi-stage and multi-pass PRO systems. The operating parameters and membrane characteristics are shown in Table 4.3. The draw stream intake for PRO system has a salinity of 70 g/kg while the feed solution of salinity 35g/kg is used for each pass/stage of PRO. The membrane area used is 1700 m^2 with an input draw solution of 12.7 kg/s. The counter flow configuration is used for the analysis of PRO systems.

5.3.1: Single Stage/Unit PRO

The results for Single PRO stage/unit are shown in Figure 5.5 and Figure 5.6, with and without considering the effect of concentration polarization. Figure 5.5 represents the hydraulic and osmotic pressure variation along the membrane for single stage/unit PRO system. The optimum hydraulic pressure for the system is 1400 kPa at which the maximum power is achieved.

5.3.1.1 Without Concentration Polarization (CP)

The feed stream enters the system at a salinity of 35g/kg and leaves at a salinity of 50.3 g/kg while the pressurized draw streams gets diluted during the process due to the addition of water permeate from the feed solution and its salinity decreases from 70 to the 53.7g/kg, shown in Figure 5.6. The total power produced for single stage/unit PRO

system, without considering the effect of concentration polarization, is 5.26kW or 0.414 kJ/kg of draw stream (see Table B. 1).

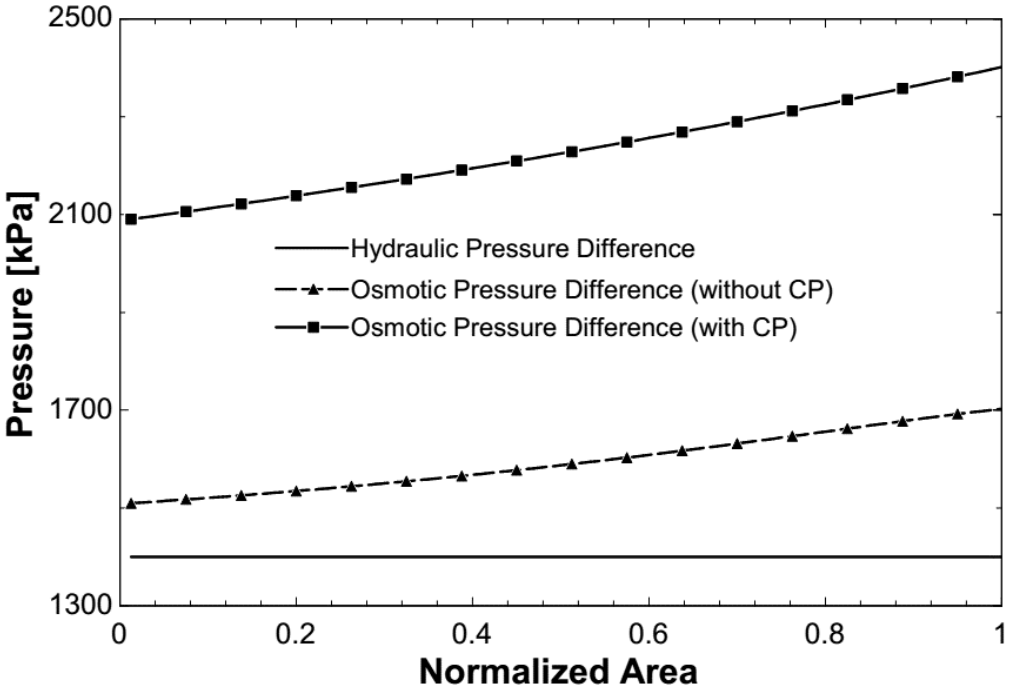

Figure 5.5: Hydraulic and osmotic pressure variation along the membrane for single stage/unit PRO

5.3.1.2 With Concentration Polarization (CP)

In case of considering the effect of concentration polarization, the draw solution salinity decreases to 60.5 g/kg while the feed salinity increases from 35 to 41.7 g/kg because of the transportation of permeate from low salinity solution to high salinity solution, shown in Figure 5.6. The total power produced, including the effect of concentration polarization, for PRO system is 2.67 kW or 0.210 kJ/kg of draw stream (see Table B. 1).

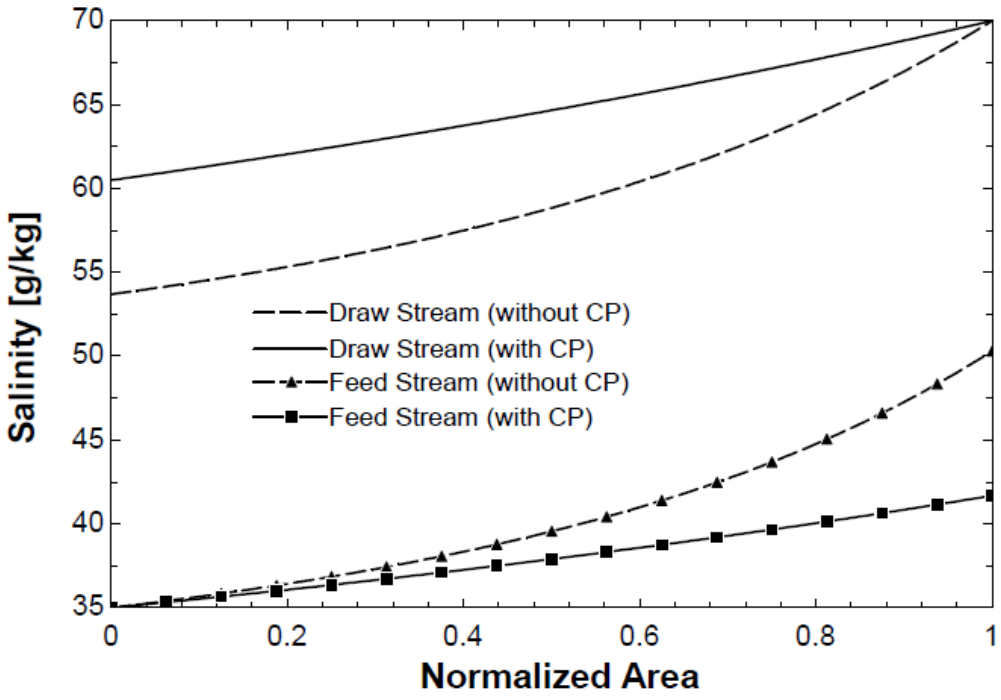

Figure 5.6: Salinity variation along the membrane for single stage/unit PRO

5.3.2: Multi-Stage PRO

5.3.2.1 Without Concentration Polarization (CP)

Figure 5.7 to Figure 5.9 show the results for multistage PRO system without considering the effect of concentration polarization. The hydraulic and osmotic pressure difference variation, of each stage, along the membrane for three stages PRO system is shown in the Figure 5.7. Figure 5.8 represents the salinity variation, of each stage, along the membrane for three stages PRO system.

The pressurized draw solution with a salt concentration of 70 g/kg enters the first stage and due to the addition of water permeate leave it with higher volume flow rate and lower salinity of 53.7 g/kg which is then depressurized using a hydro turbine to obtain power. On the contrary, the salinity of feed solution due to loss of water increases from 35 g/kg to the 50.3 g/kg. The exit feed stream is pressurized and used as a draw stream to the second stage.

Similarly like the first stage, in the second stage, the volume flow rate of the draw stream increases with the addition of permeate which is then depressurized to obtain power. The exit feed solution of second stage, with a salinity of 41.4 g/kg, is pressurized and used a draw solution to the third stage. In third stage the water permeate transfers from the feed solution to the draw solution which increases the volume of draw solution. This draw solution is then depressurized using hydro turbine.

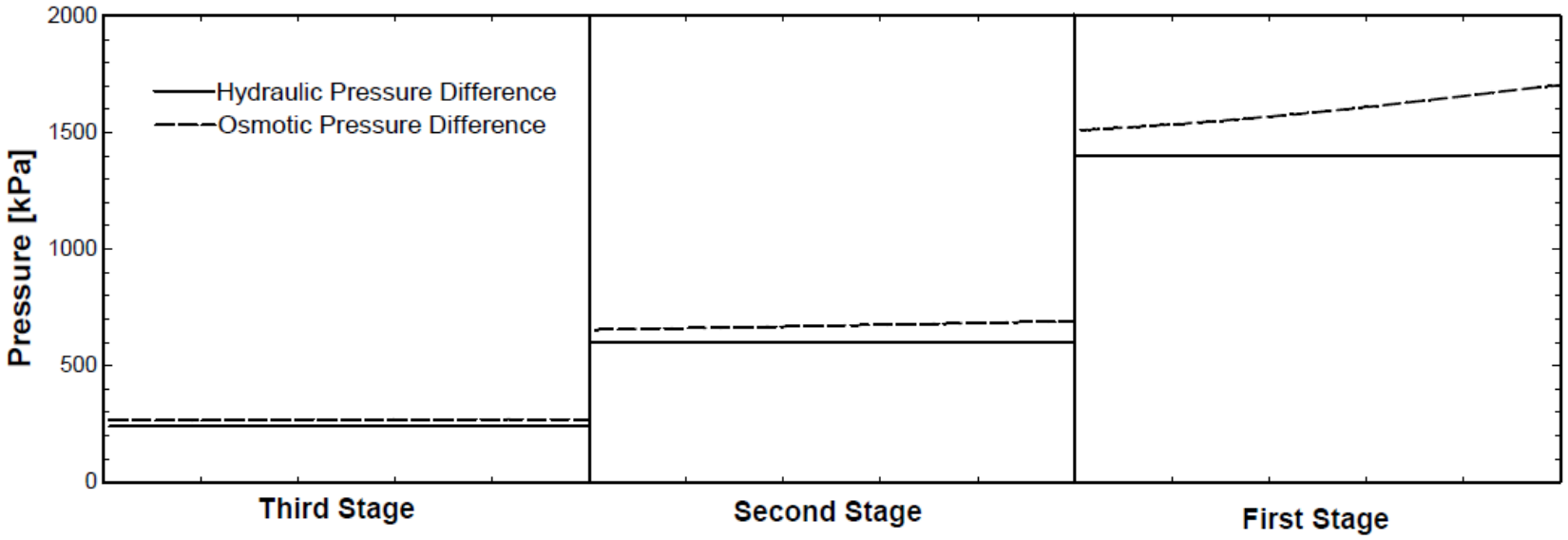

Figure 5.7: Hydraulic and osmotic pressure difference variation along the membrane for three stages PRO system, without CP

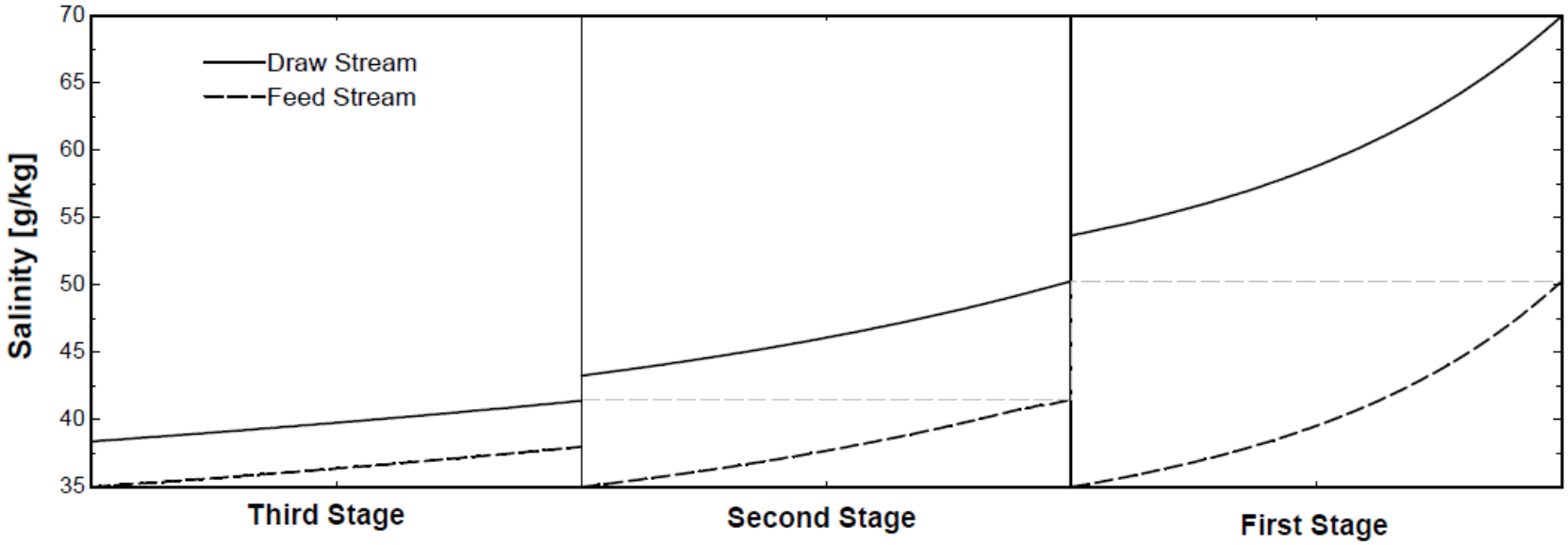

Figure 5.8: Salinity variation along the membrane for three stages PRO system, without CP

The accumulated power produced for three stages PRO system without considering the effect of concentration polarization is shown in Figure 5.9. The total power produced from three stages PRO system is 6.22 kW or 0.49 kJ/kg of draw stream. The total power produced is 18 % more than the power produces using single stage PRO system.

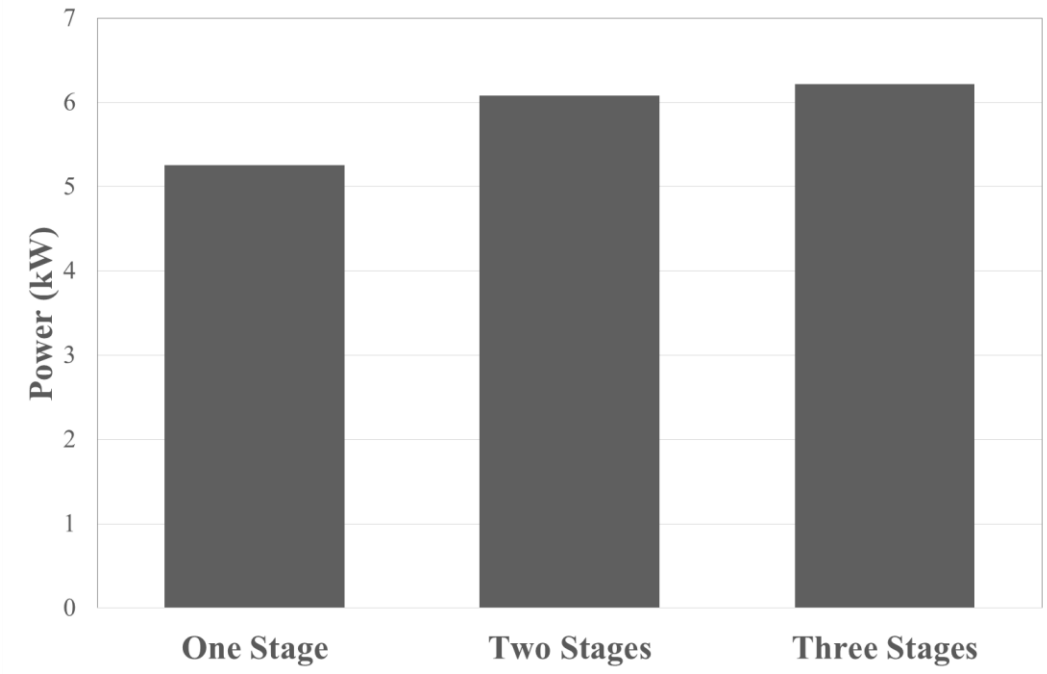

Figure 5.9: Accumulated power produced from three stages PRO system, without CP

5.3.2.2 With Concentration Polarization (CP)

The results for multistage PRO system including the effect of concentration polarization are shown from Figure 5.10 to Figure 5.12. Figure 5.10 represents the hydraulic and osmotic pressure variation along the membrane of two stages PRO system. The salinity variation along membrane for two stages PRO system is shown in Figure 5.11.

The pressurized draw solution with salt concentration of 70 g/kg enters the first stage and with addition of water permeate leave the first stage with salt concentration of 60.5 g/kg which is then depressurized through hydro turbine. Whereas the feed solution enters at first stage with salt concentration of 35 g /kg and leave it with increased salinity of 41.7 g/kg. This exit feed solution is pressurized and sent to the second stage where it is used a draw solution with the new feed solution. Similarly like the first stage, in second the permeate transfers from the feed solution to draw solution which is then depressurized through hydro turbine.

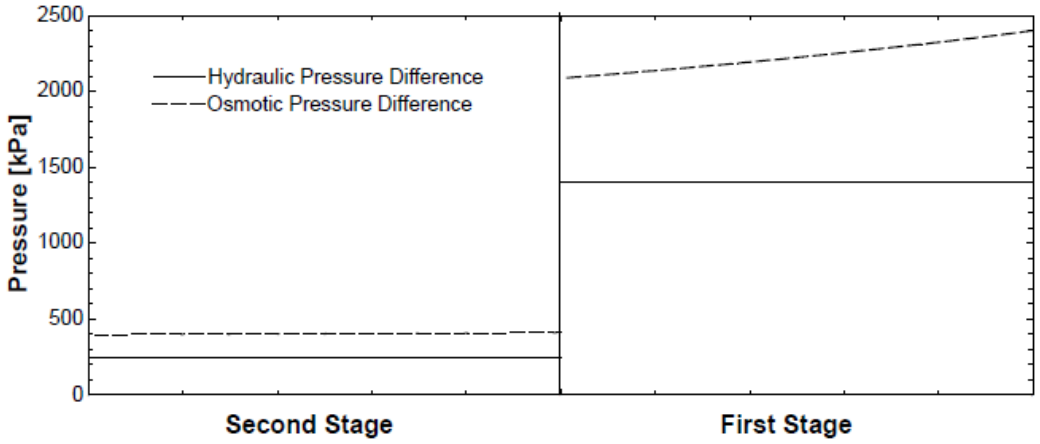

Figure 5.10: Hydraulic and osmotic pressure difference variation along the membrane for two stages PRO system, with CP

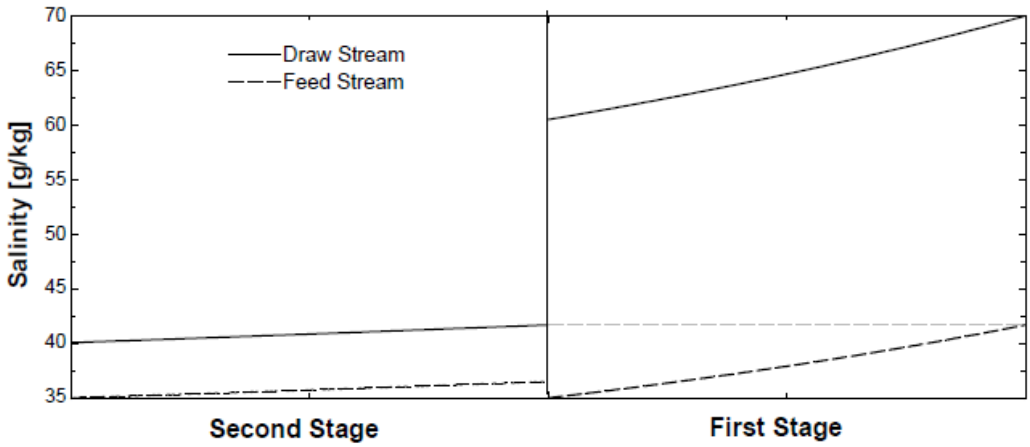

Figure 5.11: Salinity variation along the membrane for two stages PRO system, with CP

The accumulated power produced for two stage PRO system without considering the effect of concentration polarization is shown in Figure 5.12. The total power produces using two stages PRO system is 2.78 kW or 0.219 kJ/kg which is four percent more than the power produced using single stage PRO system for the fixed amount of intake draw stream.

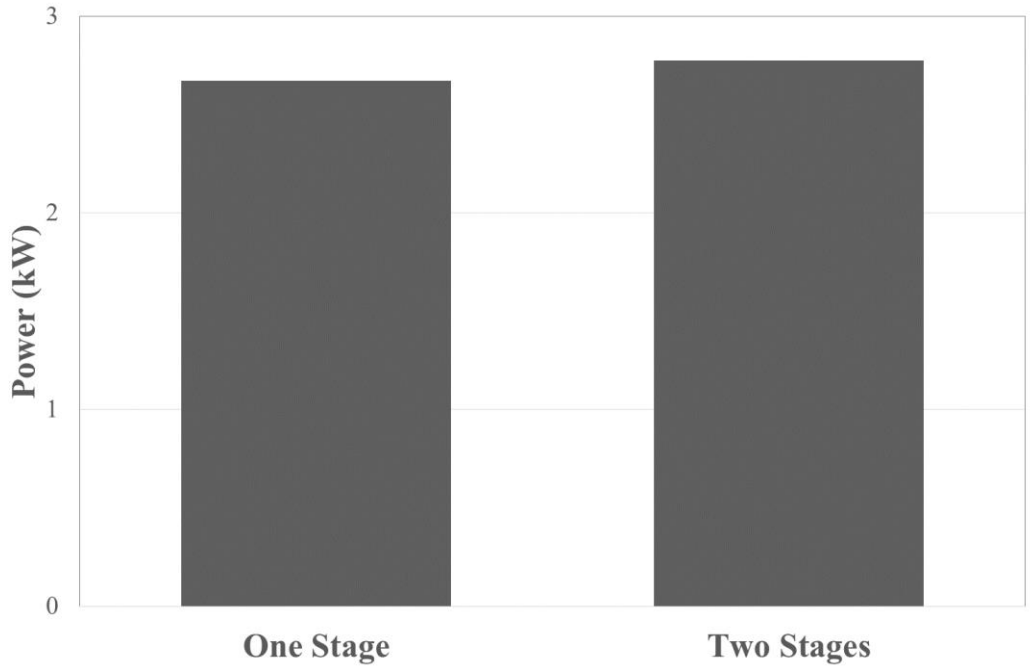

Figure 5.12: Accumulated power produced from two stages PRO system, with CP

5.3.3: Multi-Pass PRO

5.3.3.1 Without Concentration Polarization (CP)

Figure 5.13 to Figure 5.15 show the results for multi-pass PRO system without considering the effect of concentration polarization. The hydraulic and osmotic pressure difference variation, of each unit, along the membrane for four passes PRO system is shown in Figure 5.13, it also represents the depressurizing of draw stream after each pass. Figure 5.14 represents the salinity variation, of each stage, along the membrane for four passes PRO system.

The pressurized draw stream (1501 kPa) enters the first unit with salt concentration of 70 g/kg which decreased along the membrane with the addition of permeate and leaves with salt concentration of 53.7 g/kg. This exit draw stream is then depressurized until it reaches the optimum hydraulic pressure (801 kPa) required for second unit and then it enters to second unit as input draw stream.

In second unit the water permeate from feed solution transferred to the draw solution, which increases its volumetric flow rate and diluted draw stream reached to salinity of 45.7 kPa when it leaves the second unit and enters as draw stream to the third unit. Between the second and third unit the draw stream is depressurized to the required hydraulic pressure (476 kPa) of third unit.

Similarly, in third unit the volume of draw stream increases and salinity decreases to 40.9 g/kg which is depressurized from 476 to 331 kPa, which is optimum hydraulic pressure of fourth unit. This draw stream now enters to the fourth unit.

The draw stream leaves the fourth unit with lower salinity of 36.5 g/kg due to the addition of water permeate. This draw stream is completely depressurized through a hydro turbine to the atmospheric pressure.

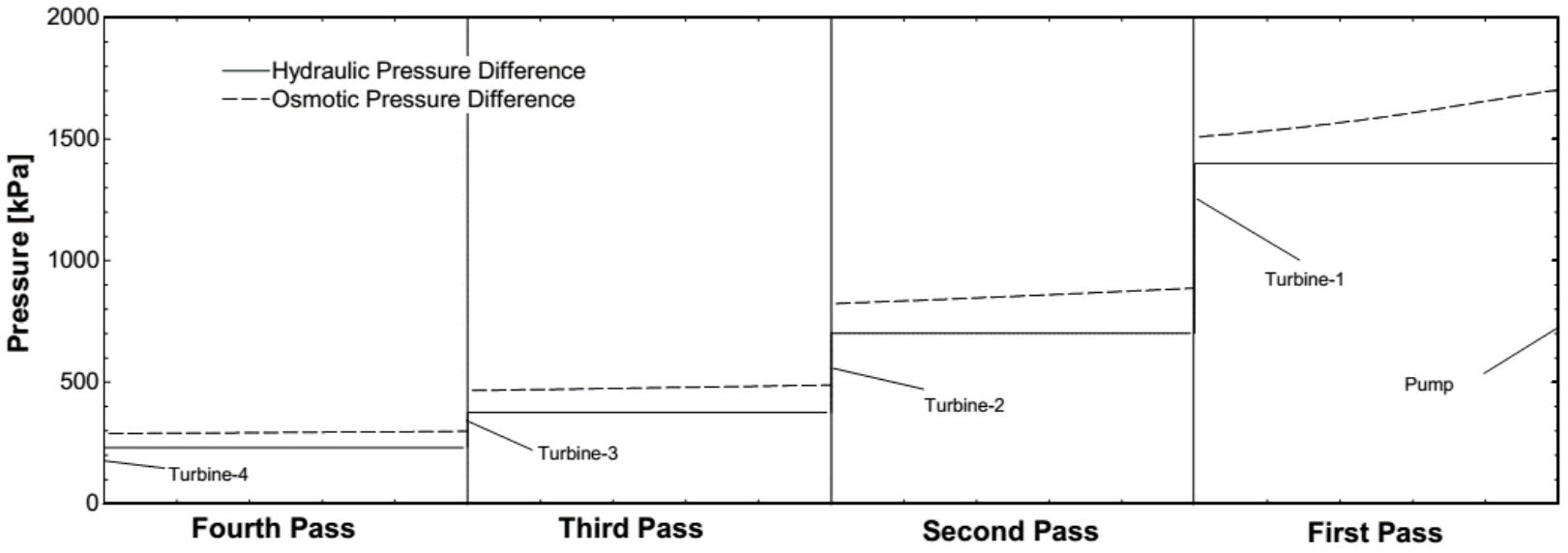

Figure 5.13: Hydraulic and osmotic pressure difference variation along the membrane for four passes PRO system, without CP

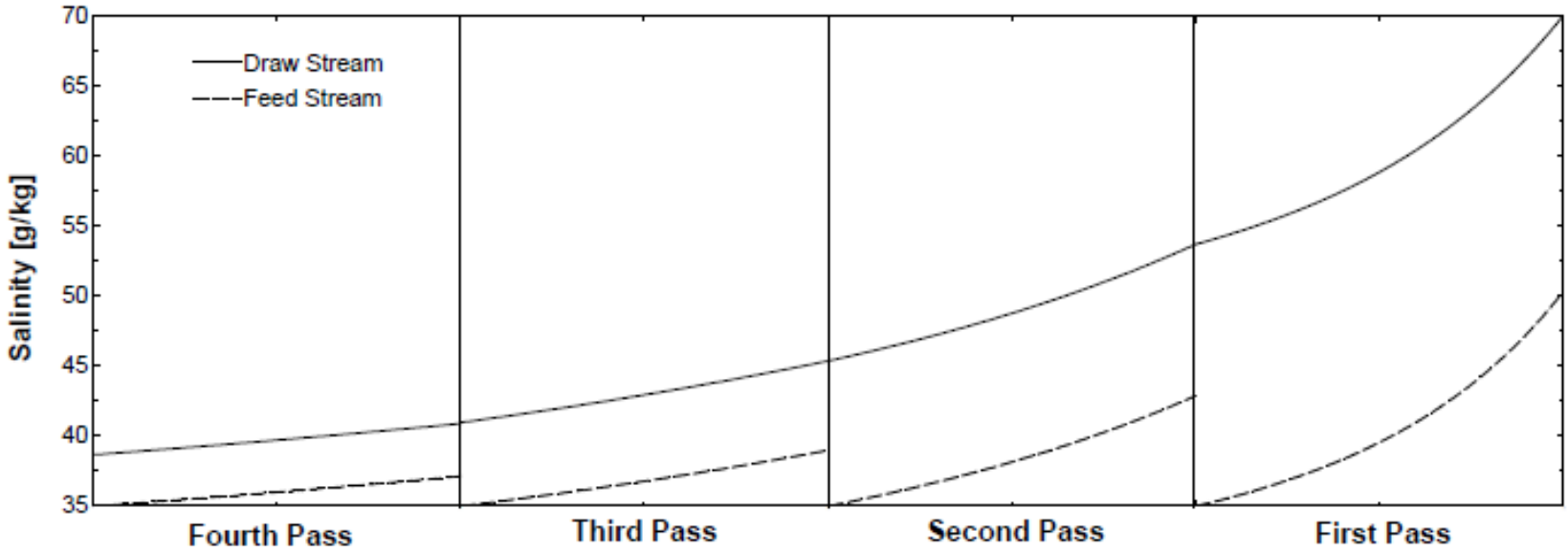

Figure 5.14: Salinity variation along the membrane for four passes PRO system, without CP

The power produced from each turbine, power consumed in pump and total accumulated net power, without considering the concentration polarization, for four passes PRO system is shown in Figure 5.15.The total power produces from the four passes PRO system is 8.31 kW or 0.654 kJ/kg of draw stream. This total produced power is 58 % more than the power produced using single unit PRO system.

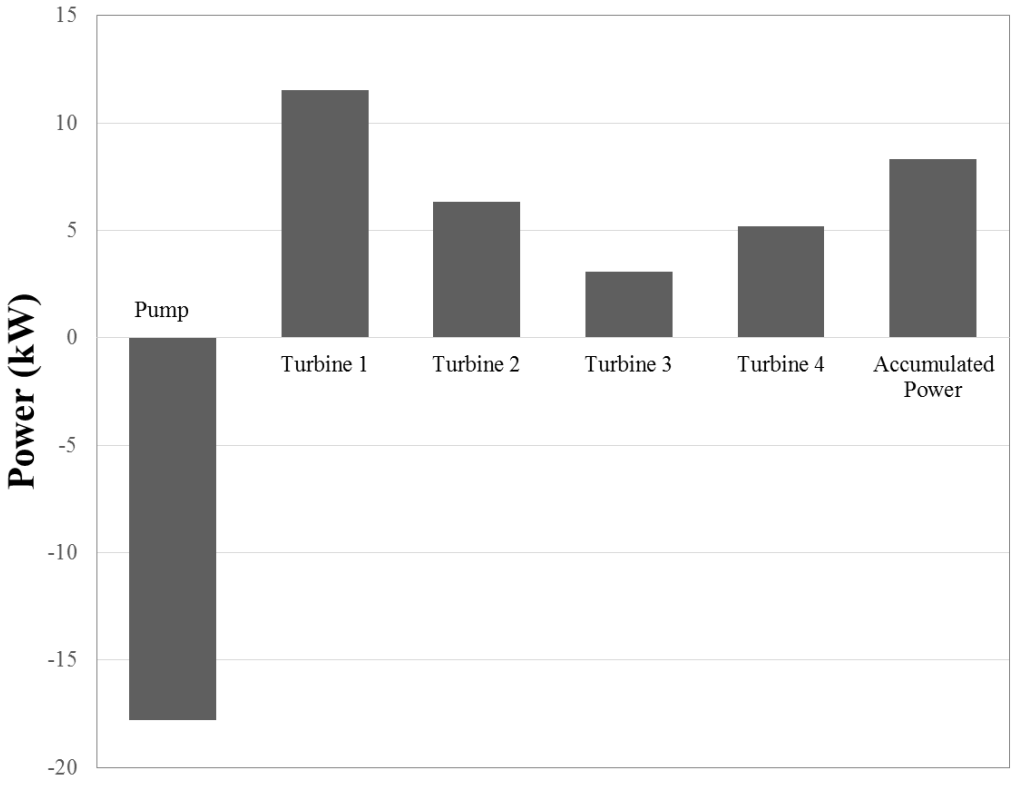

Figure 5.15: Power produced in four passes PRO system, without CP

5.3.3.2 With Concentration Polarization (CP)

The results for multi-pass PRO system including the effect of concentration polarization are shown in Figure 5.16 to Figure 5.18. The hydraulic and osmotic pressure difference variation along the membrane for five passes PRO system are shown in Figure 5.17 which also include the representation of pressure drop in turbine to produce power. Figure 5.18 represents the salinity variation for five passes PRO system.

The exit draw stream of first unit leaves at a salinity of 60.5 g/kg which after depressurizing through hydro turbine, up to the optimum hydraulic pressure (1101 kPa) of second unit, enters to second unit as intake draw solution.

The exit draw stream after the addition of permeate from the feed solution leaves the second unit with salt concentration of 54.4 g/kg and enters the third unit as an intake draw solution. Between the two units the draw stream is depressurized from 1101 kPa to 801 kPa, which is the optimum hydraulic pressure required for third unit.

Similarly like the previous units the salinity of draw stream decreases to the 50.2 g/kg when it leaves the third unit. This stream is depressurized through hydro turbine until it reaches the required hydraulic pressure (671 kPa) of fourth unit and then enter as input draw stream to the fourth unit.

After the addition of permeate in fourth unit, the salinity of draw stream reduces to 47.2 g/kg and it is depressurized to the optimum hydraulic pressure (561 kPa) of fifth unit and then enters the fifth unit as an intake draw stream, where the more water permeate

adds to the draw stream from feed stream and then depressurized completely to the atmospheric pressure using hydro turbine.

The power produced from each turbine, power consumed in pump and total accumulated net power, including the effect of concentration polarization, for five passes PRO system is shown in Figure 5.16. The total power produces using five passes PRO system is 6.21 kW 0.489 kJ/kg, which is 132 % more than the power produced using single unit PRO system for the fixed amount of intake draw stream.

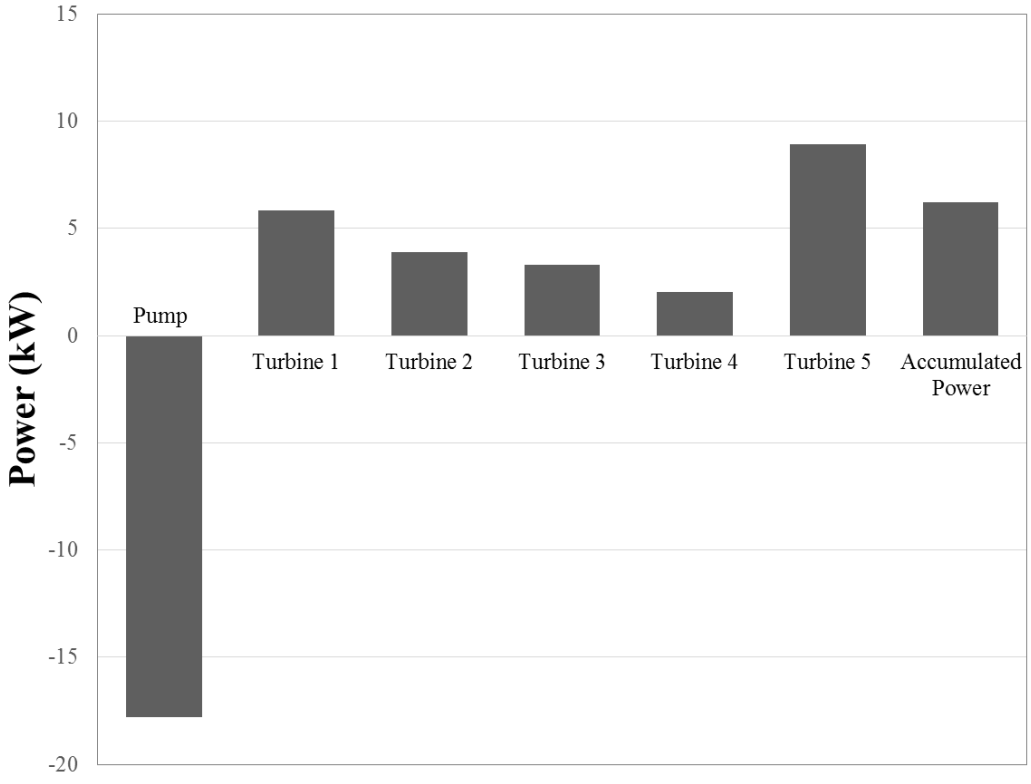

Figure 5.16: Power produced in five passes PRO system, with CP

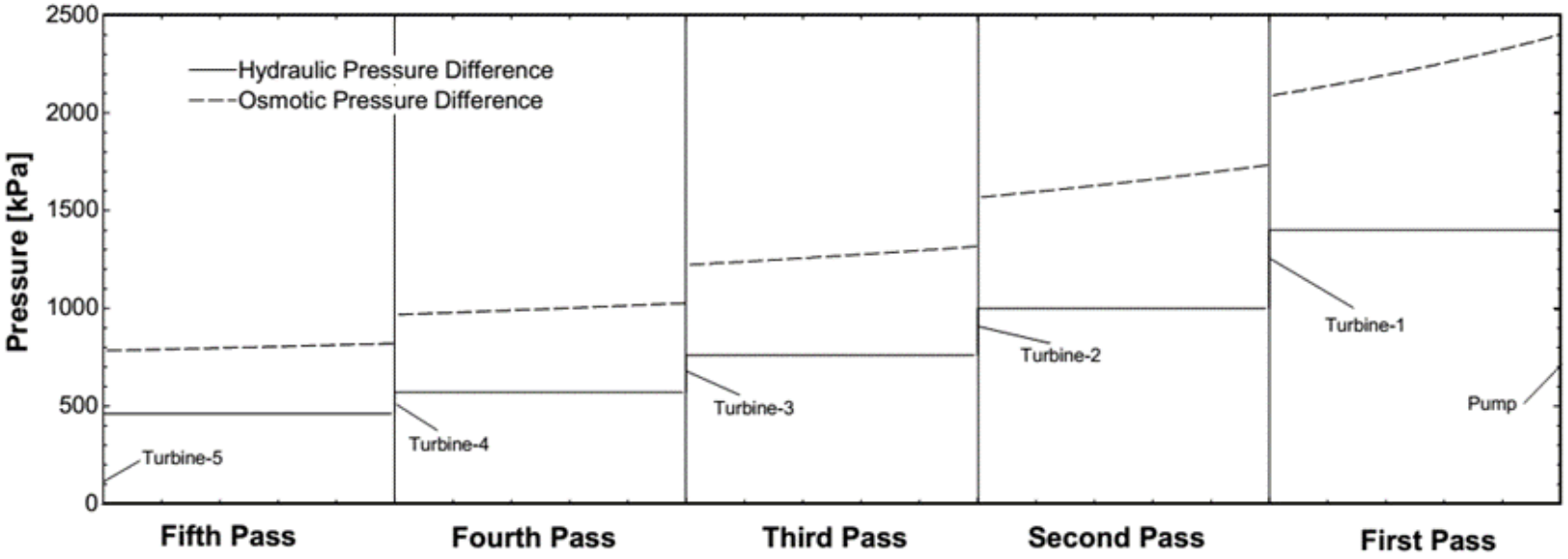

Figure 5.17: Hydraulic and osmotic pressure difference variation along the membrane for five passes PRO system, with CP

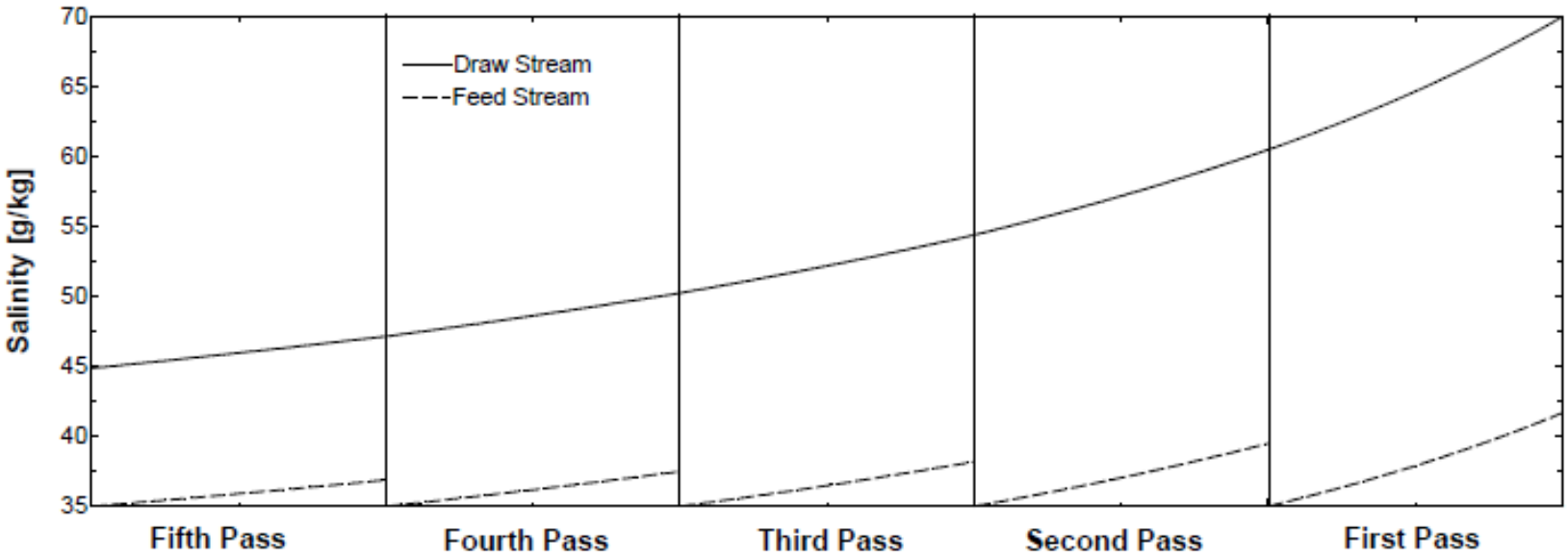

Figure 5.18: Salinity variation along the membrane for five passes PRO system, with CP

CHAPTER 6

CONCLUSIONS AND RECOMMENDATIONS

A detailed steady state model for energy and exergy analyses of multistage flash (MSF) desalination was developed and validated. A one dimensional mathematical model to predict the performance of pressure retarded osmosis (PRO) was also developed and validated. The exergy analysis of Jubail MSF desalination plant was performed. Moreover, various studies were conducted using this developed model for PRO. The following conclusions are made from the thesis work:

- The exergy analysis of Jubail MSF desalination plant was performed and the results indicated that the plant has a second law efficiency of 7.11%.
- The exergy analysis was also performed for every component of MSF desalination plant and found out that the largest exergy destruction occurs during the flashing (71%), while brine heater accounts for 12% of total exergy destruction. The pumps constitute 5% while during discharge of cooling water to sea 4.8% exergy loss occur.

- The detailed analysis of flashing stages was performed. Each flashing stage was divided into three components brine pool, distillate tray and condenser. The results indicated that the total exergy destruction in first stage is higher from the second stage of heat recovery section, the exergy destruction increased gradually and sharply in heat rejection stages. Moreover, from the three components of flashing stage, the share of exergy destruction was higher in condenser tubes.
- The developed detailed exergy analysis model identified the components which are responsible for the greatest losses in the system.
- From the comparative study of parallel flow and counter flow configuration PRO systems. It is found out that the power density obtained is higher in counter flow configuration than in the parallel flow configuration at same hydraulic pressure.
- In parallel flow configuration, the membrane area cannot be exceed a certain value otherwise the osmotic pressure difference becomes less than the applied hydraulic pressure and flux reversal occurs.
- The performance analysis of PRO system was performed by varying various operating parameters and membrane characteristics.
    - Concentration polarization (CP) has significant effect in reducing effective osmotic pressure difference which reduces the permeate flow transfer and ultimately power density. CP has even more severe effect and higher salinities.

  - With the increase of hydraulic pressure increases and reaches maximum at the half of the osmotic and pressure decreases and then decreased and until reaches zero at flux reversal point.
  - With the increase of membrane area, power increase but the power density decreases.
  - With the increase of mixing ratio, permeate transferred decreases which results in the decrease of power.
  - The membrane properties is major limitation in achieving higher power density, with the increase of water permeability the power density significantly increase while with the increase of salt permeability it decreases slightly.
  - With the increase of temperature of the streams, the power density increases.

- PRO was used as an energy recovery device (ERD) for disposed brine of MSF desalination plant. The total power produced is very small as compared to the pumping power required for the MSF desalination plant, therefore it is suggested PRO should not be used as an ERD for MSF desalination plant.
- PRO was also used as an ERD for RO desalination plant and found out that it produced 9 kW (18kW without CP) more power than if petlon wheel or any other device is used for recovering energy from disposed brine.
- Different feed and draw concentrations were used to estimate the potential of power production using PRO system. Maximum potential power can be achieved

if brine is used with fresh water, it is not practical for Saudi Arabia as there is shortage for fresh water. Apart from fresh water the maximum power can be achieved using brine with waste water in PRO system.

- New PRO configurations are proposed for maximizing the power production using a fixed amount of input draw stream, which are multi-stage and multi-pass PRO configurations,
- By using multi-stage PRO system, a 4% (18% without CP) more power is obtained compared with single stage PRO system.
- By using multi-pass PRO system, a 132% (58% without CP) more power is achieved compared with the single unit PRO system.
- In the future, the developed model can be modified by incorporating the fouling effect in membranes.

NOMENCLATURE

Symbol	Description	Unit
A	water permeability	m/s-kPa
A_m	membrane area	m^2
B	salt permeability	m/s
BPE	boiling point elevation	^oC
C_d	weir friction coefficient	
d_i	tube inside diameter	m
d_o	tube outside diameter	m
e	specific flow exergy	kJ/kg
$\dot{E}$	flow exergy	kW
f	friction factor	
GH	gate height	m
h	specific enthalpy	kJ/kg
H	brine pool height	m
h_{fg}	latent heat of vaporization	kJ/kg
j	number of heat rejection stages	
J_w	water flux	m/s
J_s	salt flux	m/s
k_m	mass transfer coefficient	m/s
k_s	solute resistivity	s/m
L	length of stage	m
m	mass flow rate	kg/s
n	total number of stages	
NEA	non equilibrium allowance	^oC
P	pressure	kPa

PR	performance ratio	
Q	volume flow rate	m^3/s
Q_p	permeate volume flow rate	m^3/s
Re	reynolds's number	
s	specific entropy	kJ/kg.K
sM_{cw}	specific cooling water flow rate	
T	temperature	^oC
TBT	top brine temperature	^oC
V_b	brine mass flow rate per stage width	kg/m.s
V_v	vapor velocity	m/s
w	seawater salinity	g/kg
W	width of flashing chamber	m
$\dot{W}_{min}$	minimum work of separation	kW
ΔP	pressure difference	kPa
ΔT_b	temperature drop across each stage	^oC
ΔT_d	temperature drop due to demister	^oC
*	dead state condition	

Greek Symbols

$\Delta\pi$	osmotic pressure differential	kPa
ϵ	roughness	m
π	osmotic pressure	kPa
ρ	density	kg/m^3
μ	chemical potential	kJ/kg
ν	kinematic viscosity	m^2/s
η_{pump}	pump efficiency	
η_{II}	second law efficiency	

Subscripts

1,2,….,n	stage number

b	brine
bh	brine heater
BP	brine pump
bpool	brine pool
cond	condenser
cw	cooling water
d	distillate or draw solution
D36esal	Complete desalination plant
DP	distillate pump
DT	distillate tray
f	feed sea water inside the condenser tubes or feed solution
FS	flashing stage
g	gaseous form
i	ith stage or number of meshes
l	liquid
n	nth stage
r	brine recycle
RP	recirculating brine pump
S	steam
SP	seawater pump
TV	throttle valve
v	vapor

REFERENCES

[1] OECD, 2012, "OECD Environmental Outlook to 2050: The Consequences of Inaction."

[2] DesalData, G. W. I., 2014, "Worldwide Desalting Plant Inventory Database," www.desaldata.com.

[3] Papapetrou, M., and Et, A., 2008, ADIRA Handbook, A guide to desalination system concepts, Euro-Mediterranean Regional Program for Water Management (MEDA).

[4] IEA-ETSAP, and IRENA, 2012, Water Desalination Using Renewable Energy - Technology Brief.

[5] International Energy Agency (IEA), 2009, World Energy Outlook 2009.

[6] Glueckstern, P., and Priel, M., 1997, "Optimized brackish water desalination plants with minimum impact on the environment," Desalination, **108**(1-3), pp. 19–26.

[7] Mohamed, A. M. O., Maraqa, M., and Al Handhaly, J., 2005, "Impact of land disposal of reject brine from desalination plants on soil and groundwater," Desalination, **182**(1-3), pp. 411–433.

[8] Dawoud, M. A., 2012, "Environmental Impacts of Seawater Desalination: Arabian Gulf Case Study," Int. J. Environ. Sustain. (IJES); Vol 1, No 3 Spec. Issue 2nd Ajman Int. Environ. Conf.

[9] International Energy Agency, 2012, Key World Energy Statistics.

[10] U.S. Energy Information Administration, 2011, International Energy Outlook 2011, U.S. Energy Information Administration, DOE/EIA-0484(2011), http://www.eia.doe.gov/oiaf/ieo/index.html.

[11] PATTLE, R. E., 1954, "Production of Electric Power by mixing Fresh and Salt Water in the Hydroelectric Pile," Nature, **174**, p. 660.

[12] Achilli, A., and Childress, A., 2010, "Pressure retarded osmosis: From the vision of Sidney Loeb to the first prototype installation—Review," Desalination, **261**(3), pp. 205–211.

[13] Loeb, S., and Norman, R. S., 1975, "Osmotic Power Plant," Science (80-.)., **189**, pp. 654–655.

[14] Kahraman, N., and Cengel, Y. A., 2005, "Exergy analysis of a MSF distillation plant," Energy Convers. Manag., **46**(15-16), pp. 2625–2636.

[15] Hisham T. El-Dessouky and Hisham M. Ettouney, 2002, Fundamental of Sea water Desalination, Elsevier.

[16] Achilli, A., Cath, T., and Childress, A., 2009, "Power generation with pressure retarded osmosis: An experimental and theoretical investigation," J. Memb. Sci., **343**, pp. 42–52.

[17] Darwish, M., 1991, "Thermal analysis of multi-stage flash desalting systems," Desalination, **85**, pp. 59–79.

[18] El-Dessouky, H., Shaban, H., and Al-Ramadan, H., 1995, "Steady-state analysis of multi-stage flash desalination process," Desalination, **103**, pp. 271–287.

[19] Rosso, M., Beltramini, A., Mazzotti, M., and Morbidelli, M., 1996, "Modeling multistage flash desalination plants," Desalination, **108**, pp. 365–374.

[20] Husain, A., Woldai, A., AI-Radif, A., Kesou, A., Borsani, R., Sultan, H., and Deshpande, P. B., 1994, "Modelling and simulation of a multistage flash (MSF) desalination plant," Desalination, **97**, pp. 555–566.

[21] Baig, H., Antar, M., and Zubair, S., 2011, "Performance evaluation of a once-through multi-stage flash distillation system: Impact of brine heater fouling," Energy Convers. Manag., **52**(2), pp. 1414–1425.

[22] ElMoudir, W., ElBousiffi, M., and Al-Hengari, S., 2008, "Process modelling in desalination plant operations," Desalination, **222**, pp. 431–440.

[23] Abdel-Jabbar, N. M., Qiblawey, H. M., Mjalli, F. S., and Ettouney, H., 2007, "Simulation of large capacity MSF brine circulation plants," Desalination, **204**(1-3), pp. 501–514.

[24] Soliman, M. A., 1981, "A mathematical model for multi-stage flash desalination plants," J. Eng. Sci.

[25] Al-Mutaz, I. S., and Soliman, M. A., 1989, "Simulation of MSF desalination plants," Desalination, **74**, pp. 317–326.

[26] Pantelides, C. C., 1988, "SpeedUp—recent advances in process simulation," Comput. Chem. Eng., **12**(7), pp. 745–755.

[27] Khan, A. H., 1986, Desalination Processes and Multi-stage Flash Distillation Practice, Elsevier Science Ltd, Amsterdam.

[28] Rouzbeh Shafaghat, Hoda Shafaghat, Fatemeh Ghanbari, P. S. R. and R. E., 2012, "Design of a MSF Desalination Plant to be supplied by a New Specific 42 MW Power Plant Located in Iran," World Acad. Sci. Eng. Technol., **6**.

[29] Darwish, M. A., El-Refaee, M. M., and Abdel-Jawad, M., 1995, "Developments in the multi-stage flash desalting system," Desalination, **100**(1-3), pp. 35–64.

[30] El-Dessouky, H., Ettouney, H., and Al-Roumi, Y., 1999, "Multi-stage flash desalination: present and future outlook," Chem. Eng. J., **73**(February).

[31] Helal, A., and Odeh, M., 2004, "The once-through MSF design. Feasibility for future large capacity desalination plants," Desalination, **166**, pp. 25–39.

[32] Hawaidi, E., and Mujtaba, I., 2010, "Simulation and optimization of MSF desalination process for fixed freshwater demand: Impact of brine heater fouling," Chem. Eng. J., **165**(2), pp. 545–553.

[33] Abduljawad, M., and Ezzeghni, U., 2010, "Optimization of Tajoura MSF desalination plant," Desalination, **254**(1-3), pp. 23–28.

[34] Helal, A., 2003, "Uprating of Umm Al Nar East 4–6 MSF desalination plants," Desalination, **159**, pp. 43–60.

[35] Marcovecchio, M. G., Mussati, S. F., Scenna, N. J., and Aguirre, P. A., 2005, "Optimization of hybrid desalination processes including multi stage flash and reverse osmosis systems," **182**(May), pp. 111–122.

[36] Sharqawy, M., Lienhard V, J. H., and Zubair, S. M., 2010, "Thermophysical properties of seawater: A review of existing correlations and data," Desalin. Water Treat., **16**, pp. 354–380.

[37] R. Kempton, D. Maccioni, S. M. M. and G. L., 2010, "Thermodynamic efficiencies and GHG emissions of alternative desalination processes," Water Sci. Technol. Water Supply, **10**(3), pp. 416–427.

[38] Mistry, K., and Lienhard, J., 2013, "Generalized Least Energy of Separation for Desalination and Other Chemical Separation Processes," Entropy, **15**(6), pp. 2046–2080.

[39] Al-Sulaiman, F., and Ismail, B., 1995, "Exergy analysis of major recirculating multi-stage flash desalting plants in Saudi Arabia," Desalination, **103**, pp. 265–270.

[40] Hamed, O., Al-Sofi, M., and Imam, M., 2000, "Thermal performance of multi-stage flash distillation plants in Saudi Arabia," Desalination, **I**, pp. 281–292.

[41] Cerci, Y., 2002, "Exergy analysis of a reverse osmosis desalination plant in California," Desalination, **142**(3), pp. 257–266.

[42] Sharqawy, M. H., Lienhard V, J. H., and Zubair, S. M., 2011, "On exergy calculations of seawater with applications in desalination systems," Int. J. Therm. Sci., **50**, pp. 187–196.

[43] Nafey, A. S., Fath, H. E. S., and Mabrouk, A. A., 2006, "Exergy and thermoeconomic evaluation of MSF process using a new visual package," Desalination, **201**(1-3), pp. 224–240.

[44] Al-Weshahi, M. a., Anderson, A., and Tian, G., 2013, "Exergy efficiency enhancement of MSF desalination by heat recovery from hot distillate water stages," Appl. Therm. Eng., **53**(2), pp. 226–233.

[45] SimTech, 2005, "IPSEpro-Desalination Process Library Manual."

[46] Lior, N., 1986, "Formulas for calculating the approach to equilibrium in open channel flash evaporators for saline water," Desalination, **60**(3), pp. 223–249.

[47] Bergman, T. L., and Incropera, F. P., 2011, Fundamentals of Heat and Mass Transfer, Wiley.

[48] Klein, S. A., "Engineering Equation Solver. Academic Professional, Version 9. http://www.fchart.com/ees/ees.shtml."

[49] Narayan, G. P., Sharqawy, M. H., Lienhard V., J. H., and Zubair, S. M., 2010, "Thermodynamic analysis of humidification–dehumidification desalination cycles," Desalin. Water Treat., **1078**(c), pp. 339–353.

[50] Mehta, G. D., and Loeb, S., 1978, "Internal polarization in the porous substructure of a semipermeable membrane under pressure-retarded osmosis," J. Memb. Sci., **4**, pp. 261–265.

[51] Ahmad, M., and Williams, P., 2009, "Application of salinity gradient power for brines disposal and energy utilisation," Desalin. Water Treat., **10**, pp. 220–228.

[52] Forgacs, C., 1982, "Recent developments in the utilization of salinity power," Desalination, **40**(1-2), pp. 191–195.

[53] Loeb, S., 1998, "Energy production at the Dead Sea by pressure-retarded osmosis: challenge or chimera?," Desalination, **120**, pp. 247–262.

[54] Loeb, S., 2002, "Large-scale power production by pressure-retarded osmosis, using river water and sea water passing through spiral modules," Desalination, **143**(2), pp. 115–122.

[55] Panyor, L., 2006, "Renewable energy from dilution of salt water with fresh water: pressure retarded osmosis," Desalination, **199**, pp. 408–410.

[56] Sharqawy, M. H., Zubair, S. M., and Lienhard, J. H., 2011, "Second law analysis of reverse osmosis desalination plants: An alternative design using pressure retarded osmosis," Energy, **36**(11), pp. 6617–6626.

[57] Skilhagen, S., Dugstad, J., and Aaberg, R., 2008, "Osmotic power—power production based on the osmotic pressure difference between waters with varying salt gradients," Desalination, **220**, pp. 476–482.

[58] Enomoto, H., Fujitsuka, M., Hasegawa, T., Kuwada, M., Tanioka, A., and Minagawa, M., 2010, "A feasibility study of pressure-retarded osmosis power generation system based on measuring permeation volume using reverse osmosis membrane," Electr. Eng. Japan, **173**(2), pp. 8–20.

[59] Lee, K. L., Baker, R. W., and Lonsdale, H. K., 1981, "Membrane for Power generation by pressure retarded osmosis," J. Memb. Sci., **8**, pp. 141–171.

[60] Thorsen, T., and Holt, T., 2009, "The potential for power production from salinity gradients by pressure retarded osmosis," J. Memb. Sci., **335**, pp. 103–110.

[61] Zwan, S. Van Der, and Pothof, I., 2011, "Feasibility of osmotic power from a hydrodynamic analysis at module and plant scale," J. Memb. Sci., **389**, pp. 324–333.

[62] Xu, Y., Peng, X., Tang, C., Fu, Q., and Nie, S., 2010, "Effect of draw solution concentration and operating conditions on forward osmosis and pressure retarded osmosis performance in a spiral wound module," J. Memb. Sci., **348**, pp. 298–309.

[63] Sharqawy, M. H., Banchik, L. D., and Lienhard, J. H., 2013, "Effectiveness–mass transfer units (ε–MTU) model of an ideal pressure retarded osmosis membrane mass exchanger," J. Memb. Sci., **445**, pp. 211–219.

[64] Chou, S., Wang, R., Shi, L., She, Q., Tang, C., and Fane, A. G., 2012, "Thin-film composite hollow fiber membranes for pressure retarded osmosis (PRO) process with high power density," J. Memb. Sci., **389**, pp. 25–33.

[65] Han, G., Zhang, S., Li, X., and Chung, T., 2013, "High performance thin film composite pressure retarded osmosis (PRO) membranes for renewable salinity-gradient energy generation," J. Memb. Sci., **440**, pp. 108–121.

[66] Chou, S., Wang, R., and Fane, A. G., 2013, "Robust and High performance hollow fiber membranes for energy harvesting from salinity gradients by pressure retarded osmosis," J. Memb. Sci., **448**, pp. 44–54.

[67] Sivertsen, E., Holt, T., Thelin, W., and Brekke, G., 2013, "Pressure retarded osmosis efficiency for different hollow fibre membrane module flow configurations," Desalination, **312**, pp. 107–123.

[68] Gerstandt, K., Peinemann, K., Skilhagen, S., Thorsen, T., and Holt, T., 2008, "Membrane processes in energy supply for an osmotic power plant," Desalination, **224**, pp. 64–70.

[69] Helfer, F., Lemckert, C., and Anissimov, Y. G., 2014, "Osmotic power with Pressure Retarded Osmosis: Theory, performance and trends – A review," J. Memb. Sci., **453**, pp. 337–358.

[70] SWC5 1640 Hydranautics Membrane, "http://www.pure-aqua.com/swc-5-1640-hydranautics-membrane.html," Accessed 2nd Oct. 2012 [Online]. Available: http://www.pure-aqua.com/swc-5-1640-hydranautics-membrane.html. [Accessed: 02-Oct-2012].

[71] Mabrouk, A., Nafey, A., and Fath, H., 2007, "Thermoeconomic analysis of some existing desalination processes," Desalination, **205**(May 2006), pp. 354–373.

[72] Y.Hancok, N., Slepowron, M. S. N., and Marchewka, L. S., 2013, "Application of Forward Osmosis Based Membrane Brine Concentrators for Produced Water," The

International Desalination Association World Congress on Desalination and Water Reuse, Tianjin, China.

[73] Skilhagen, S. E., Brekke, J. W., Machenbach, I., Havskjold, M., Nielsen, W. K., and Guldberg, S., 2013, "Competitiveness of Osmotic Power in the Renewable Energy Market," The International Desalination Association World Congress on Desalination and Water Reuse, Tianjin, China.

Appendix A

Table A. 1: Brine Flowing Through Flashing Chamber Parameters

Stage	**Temperature**	**Pressure**	**Salinity**	**Specific flow Exergy**	**Mass flow rate**	**Total Exergy**
n	**T_b (°C)**	**P_b (kPa)**	**w_b (g/kg)**	**e_b (kJ/kg)**	**m_b (kg/s)**	**E_b (kW)**
0	90.8	152.4	64.8	17.9	3583	64053
1	88.6	64.1	65.0	16.5	3570	59025
2	86.5	59.0	65.3	15.3	3557	54478
3	84.3	54.2	65.5	14.1	3544	50116
4	82.2	49.7	65.7	13.0	3531	45939
5	80.0	45.6	66.0	11.9	3518	41946
6	77.9	41.7	66.2	10.9	3505	38139
7	75.7	38.2	66.5	9.9	3493	34515
8	73.5	34.9	66.7	8.9	3480	31076
9	71.4	31.8	66.9	8.0	3468	27822
10	69.2	29.0	67.2	7.2	3455	24753
11	67.1	26.3	67.4	6.4	3443	21868
12	64.9	23.9	67.7	5.6	3430	19169
13	62.7	21.7	67.9	4.9	3418	16656
14	60.6	19.7	68.1	4.2	3406	14328
15	58.4	17.8	68.4	3.6	3394	12188
16	56.3	16.1	68.6	3.0	3382	10234
17	54.1	14.5	68.9	2.5	3370	8469
18	51.9	13.0	69.1	2.1	3358	6892
19	49.8	11.7	69.4	1.6	3346	5505
20	47.6	10.5	69.6	1.3	3335	4308
21	45.5	9.4	69.9	0.99	3323	3302
22	43.3	8.4	70.1	0.75	3311	2488

Table A. 2: Brine Flowing in Condenser Tubes Parameters

Stage	Temperature	Pressure	Salinity	Specific flow Exergy	Mass flow rate	Total Exergy
n	**T_f (°C)**	**P_f (kPa)**	**w (g/kg)**	**e_f (kJ/kg)**	**m (kg/s)**	**E_f (kW)**
0	84.6	182.9	64.8	14.4	3583	51601
1	82.4	206.6	64.8	13.3	3583	47559
2	80.2	230.3	64.8	12.2	3583	43712
3	78.1	254.0	64.8	11.2	3583	40021
4	75.9	277.7	64.8	10.2	3583	36488
5	73.7	301.5	64.8	9.2	3583	33116
6	71.6	325.2	64.8	8.3	3583	29907
7	69.4	348.9	64.8	7.5	3583	26864
8	67.2	372.6	64.8	6.7	3583	23989
9	65.1	396.4	64.8	5.9	3583	21285
10	62.9	420.1	64.8	5.2	3583	18754
11	60.7	443.9	64.8	4.6	3583	16401
12	58.5	467.7	64.8	4.0	3583	14227
13	56.4	491.5	64.8	3.4	3583	12235
14	54.2	515.4	64.8	2.9	3583	10430
15	52.0	539.2	64.8	2.5	3583	8813
16	49.8	563.1	64.8	2.1	3583	7390
17	47.7	587.0	64.8	1.7	3583	6162
18	45.5	611.0	64.8	1.4	3583	5134
19	43.3	635.0	64.8	1.2	3583	1160
20	40.5	116.1	46.5	0.20	2770.1	563
21	37.8	142.0	46.5	0.08	2770.1	234
22	35.0	168.0	46.5	0.06	2770.1	179.5

Table A. 3: Distillate Product Flowing Through Distillate Tray Parameters

Stage	Temperature	Pressure	Salinity	Specific flow Exergy	Mass flow rate	Total Exergy
n	**T_d (°C)**	**P (kPa)**	**w (g/kg)**	**e_d (kJ/kg)**	**m_d (kg/s)**	**E_d (kW)**
1	87.3	64.1	0	20.6	13.3	274
2	85.2	59.0	0	19.3	26.3	509
3	83.0	54.2	0	18.1	39.3	710
4	80.8	49.7	0	16.9	52.2	881
5	78.7	45.6	0	15.7	65.1	1022
6	76.5	41.7	0	14.6	77.8	1136
7	74.3	38.2	0	13.5	90.5	1226
8	72.1	34.9	0	12.5	103.1	1293
9	70.0	31.8	0	11.6	115.7	1340
10	67.8	29.0	0	10.7	128.2	1369
11	65.6	26.3	0	9.8	140.6	1381
12	63.4	23.9	0	9.0	152.9	1380
13	61.2	21.7	0	8.3	165.1	1368
14	59.0	19.7	0	7.6	177.3	1346
15	56.8	17.8	0	7.0	189.4	1318
16	54.6	16.1	0	6.4	201.4	1285
17	52.4	14.5	0	5.9	213.4	1250
18	50.2	13.0	0	5.4	225.2	1215
19	48.0	11.7	0	5.0	237.0	1182
20	45.7	10.5	0	4.6	248.8	1155
21	43.5	9.4	0	4.4	260.4	1135
22	41.3	8.4	0	4.1	272.0	1127

Table A. 4: Flashing Vapors Parameters

Stage	Temperature	Pressure	Salinity	Specific flow Exergy	Mass flow rate	Total Exergy
n	**T_v (°C)**	**P (kPa)**	**w (g/kg)**	**e_v (kJ/kg)**	**m_d (kg/s)**	**E_v (kW)**
1	87.3	64.1	0	348.80	13.26	4627
2	85.2	59.0	0	336.50	13.06	4395
3	83.0	54.2	0	323.90	12.99	4207
4	80.8	49.7	0	311.20	12.91	4019
5	78.7	45.6	0	298.30	12.84	3831
6	76.5	41.7	0	285.30	12.77	3642
7	74.3	38.2	0	272.10	12.69	3453
8	72.1	34.9	0	258.60	12.62	3264
9	70.0	31.8	0	245.00	12.54	3074
10	67.8	29.0	0	231.20	12.47	2883
11	65.6	26.3	0	217.20	12.40	2693
12	63.4	23.9	0	203.00	12.32	2502
13	61.2	21.7	0	188.60	12.25	2310
14	59.0	19.7	0	174.00	12.17	2118
15	56.8	17.8	0	159.10	12.10	1925
16	54.6	16.1	0	144.00	12.02	1731
17	52.4	14.5	0	128.60	11.95	1537
18	50.2	13.0	0	113.00	11.87	1342
19	48.0	11.7	0	97.16	11.80	1146
20	45.7	10.5	0	81.02	11.72	950
21	43.5	9.4	0	64.58	11.65	752
22	41.3	8.4	0	48.09	11.58	557

Table A. 5: Distillate Condensate Parameters

Stage	Temperature	Pressure	Salinity	Specific flow Exergy	Mass flow rate	Total Exergy
n	**T_d (°C)**	**P (kPa)**	**w (g/kg)**	**m_d (kg/s)**	**m (kg/s)**	**E_d (kW)**
1	87.34	64.08	0	20.61	13.26	273.5
2	85.17	58.95	0	19.32	13.06	252.3
3	83	54.17	0	18.06	12.99	234.6
4	80.83	49.72	0	16.86	12.91	217.7
5	78.66	45.57	0	15.71	12.84	201.7
6	76.48	41.73	0	14.6	12.77	186.4
7	74.31	38.16	0	13.54	12.69	171.9
8	72.13	34.85	0	12.54	12.62	158.2
9	69.95	31.78	0	11.58	12.54	145.3
10	67.76	28.95	0	10.68	12.47	133.2
11	65.58	26.34	0	9.829	12.4	121.8
12	63.39	23.92	0	9.03	12.32	111.3
13	61.2	21.7	0	8.285	12.25	101.5
14	59	19.66	0	7.594	12.17	92.44
15	56.8	17.78	0	6.958	12.1	84.19
16	54.6	16.05	0	6.379	12.02	76.7
17	52.39	14.48	0	5.856	11.95	69.98
18	50.18	13.03	0	5.392	11.87	64.03
19	47.96	11.71	0	4.987	11.8	58.84
20	45.74	10.51	0	4.642	11.72	54.43
21	43.5	9.417	0	4.36	11.65	50.79
22	41.3	8.421	0	4.143	11.58	47.99

Appendix B

Table B. 1: Results for Single Stage/Unit PRO System, with and without considering Concentration Polarization (CP)

Single Stage/Unit PRO							
without Concentration Polarization (CP)							
ΔP	**w_{di}**	**w_{do}**	**w_{fi}**	**w_{fo}**	**Q_p**	**Power**	
kPa	**g/kg**	**g/kg**	**g/kg**	**g/kg**	**m^3/s**	**kW**	**kJ/kg**
1400	70	53.7	35	50.3	0.0038	5.26	**0.414**
including the effect of Concentration Polarization (CP)							
1400	70	60.5	35	41.7	0.0019	2.67	**0.210**

Table B. 2: Results for Multi Stage PRO System, without considering CP

without considering Concentration Polarization (CP)								
Stage	**ΔP**	**w_{di}**	**w_{do}**	**w_{fi}**	**w_{fo}**	**Q_p**	**$Q_{f,out}$**	**Power**
	kPa	**g/kg**	**g/kg**	**g/kg**	**g/kg**	**m3/s**	**m3/s**	**kW**
1st	1400	70	53.7	35	50.3	0.0038	0.0089	5.26
2nd	600	50.3	43.6	35	41.4	0.0014	0.0076	0.825
3rd	238	41.4	38.4	35	38	0.0006	0.0070	0.135
							Total	**6.22**
Total Power = 6.22 kW or 0.49 kJ/kg of draw solution								

Table B. 3: Results for Multi Stage PRO System, with considering CP

including the effect of Concentration Polarization (CP)								
Stage	**ΔP**	**w_{di}**	**w_{do}**	**w_{fi}**	**w_{fo}**	**Q_p**	**$Q_{f,out}$**	**Power**
	kPa	**g/kg**	**g/kg**	**g/kg**	**g/kg**	**m3/s**	**m3/s**	**kW**
1st	1400	70	60.5	35	41.7	0.0019	0.0108	2.67
2nd	250	41.7	40.1	35	36.5	0.0004	0.0104	0.104
							Total	**2.78**
Total Power = 2.78 kW or 0.219 kJ/kg of draw solution								

Table B. 4: Results for Multi Pass PRO System, without considering CP

without considering Concentration Polarization (CP)									
Pass	**ΔP**	**w_{di}**	**w_{do}**	**w_{fi}**	**w_{fo}**	**Q_p**	**$Q_{d,out}$**	**$P_{d,in}$**	**Power**
	kPa	**g/kg**	**g/kg**	**g/kg**	**g/kg**	**m3/s**	**m3/s**	**kPa**	**kW**
1st	1400	70	53.7	35	50.3	0.0038	0.0165	1501	-6.27
2nd	700	53.7	45.1	35	43.3	0.0030	0.0194	801	6.31
3rd	375	45.1	40.9	35	39	0.0019	0.0213	476	3.09
4th	230	40.9	36.7	35	37.1	0.0012	0.0225	331	5.18
								Total	**8.31**
Total Power = 8.31 kW or 0.654 kJ/kg of draw solution									

Table B. 5: Results for Multi Pass PRO System, with considering CP

including the effect of Concentration Polarization (CP)									
Pass	**ΔP**	**w_{di}**	**w_{do}**	**w_{fi}**	**w_{fo}**	**Q_p**	**$Q_{d,out}$**	**$P_{d,in}$**	**Power**
	kPa	**g/kg**	**g/kg**	**g/kg**	**g/kg**	**m3/s**	**m3/s**	**kPa**	**kW**
1st	1400	70	60.5	35	41.7	0.0019	0.0146	1501	-11.94
2nd	1000	60.5	54.4	35	39.5	0.0016	0.0162	1101	3.88
3rd	760	54.4	50.2	35	38.2	0.0013	0.0174	861	3.31
4th	570	50.2	47.2	35	37.5	0.0011	0.0185	671	2.04
5th	460	47.2	44.9	35	36.9	0.0009	0.0194	561	8.92
								Total	**6.21**
Total Power = 6.21 kW or 0.489 kJ/kg of draw solution									

VITAE

Name: Waqas Akram

Date of Birth: May 21, 1985

Present Address: P.O. Box 8119, King Fahd University of Petroleum and Minerals, Dhahran 31261, Saudi Arabia

Permanent Address: House No. 6, Farzand Street No. 15 Ichhra, Lahore, Pakistan

Email Address: waqasam@gmail.com

Educational Qualification:

M.S (Mechanical Engineering)
May, 2014
King Fahd University of Petroleum & Minerals,
Dhahran, Saudi Arabia.

B.Sc. (Mechanical Engineering)
July, 2009
University of Engineering and Technology,
Lahore, Pakistan.

Research Publications:

- Waqas A. Akram, Mostafa H. Sharqawy, John H. Lienhard V, *Multistage Pressure Retarded Osmosis System*, **In Progress**

- W. Akram, M.H. Sharqawy, J.H. Lienhard V, *Energy utilization of brine from an MSF desalination plant by pressure retarded osmosis*, IDA World Congress, Tianjin, China, 2013.

- W. Akram, M.H. Sharqawy, *Power generation with Pressure retarded osmosis*, ASME International Mechanical Engineering Congress and Exhibition, Sand Diego, CA, USA, 2013.